FACULTAD DE FARMACIA

DEPARTAMENTO DE CIENCIAS FARMACÉUTICAS

Cytinus hypocistis (L.) L. — an edible parasitic plant with skin anti-ageing potential

DOCTORAL THESIS

Ana Rita Santos Silva

Supervisors

Dr. Lillian Bouçada de Barros
Dr. Pablo Anselmo García García

Salamanca, 2023

Pablo Anselmo García García, Profesor Titular de Farmacia de la Universidad de Salamanca (España) y Lillian Bouçada de Barros, Investigadora del Centro de Investigação de Montanha del Instituto Politécnico de Bragança (Portugal), directores del trabajo " *Cytinus hypocistis* (L.) L. — an edible parasitic plant with skin anti-ageing potential", realizado por Ana Rita Santos Silva para optar al Grado de Doctor con Mención Doctorado Internacional, AUTORIZAN la a presentación de este trabajo al considerar que se han alcanzado los objetivos inicialmente previstos

Salamanca, 6 de noviembre de 2023

_____   _____
Lillian Bouçada de Barros   Pablo Anselmo García García

TABLE OF CONTENTS

ACKNOWLEDGEMENTS

Aos meus primeiros amores, os meus Irmãos. Se pudesse proteger-vos do mundo para sempre, fá-lo-ia. O amor verdadeiro aprendi-o com vocês, aquele que gosta por igual, de forma incondicional e que vibra com cada uma das vossas conquistas. E que conquistas!!!! Obrigada pelo Amor e pelas horas infindáveis de cafunés e abracinhos. Mimir vocês.

Aos meus amores emprestados, Joana e Catarina. Confiei-vos a minha maior riqueza e vivo em paz porque sei que quando eu não estou para os defender do mundo, vocês estão. Obrigada! Para nós, vocês são família.

À minha alma metade, ao meu Amor Manuel. Foram precisas umas quantas voltas ao sol para que as voltas da vida nos cruzassem, mas valeu a pena a espera. Viver contigo é aconchego. Ensinaste-me a simplicidade do descomplicar, do viver a dançar. Um dia disseste-me que só sabemos qual é o nosso lugar quando lá chegamos. É verdade! Obrigada por seres o meu lugar favorito. Amo-te.

"Para ser grande, sê inteiro: nada
Teu exagera ou exclui.
Sê todo em cada coisa. Põe quanto és
No mínimo que fazes.
Assim em cada lago a lua toda
Brilha, porque alta vive"

Fernando Pessoa

ABSTRACT

The skin undergoes visible changes over time, reflecting the combined effects of intrinsic and extrinsic insults. Intrinsic ageing primarily results from natural physiological changes. Conversely, external factors, such as pollution, lifestyle habits, and exposure to ultraviolet radiation (UVR), play a significant role in extrinsic ageing. From all the insults, UVR is considered the primary contributor to skin ageing, accounting for 80% of its visible signs. Despite the highly effective barrier the skin layers provide, UVR can induce oxidative stress in human skin.

When the load of reactive species in this organ is high, several pathways are activated, culminating in the degradation of extracellular matrix proteins such as collagen and elastin by the upregulation of metalloproteinases (MMPs) and other enzymes. Neutrophil elastase is considered one of the most destructive enzymes in this process due to its ability to degrade almost all extracellular matrix components by directly activating MMPs (pro- and active forms), facilitating their progression, and inactivating their activity regulators.

The interplay of intrinsic and extrinsic factors shapes phenotypically distinct clinical manifestations. Chronological ageing leads to skin changes such as thinning, pallor, fine surface wrinkles, and reduced elasticity. In contrast, prolonged exposure to UVR results in more severe manifestations, including pronounced wrinkles, loss of elasticity, thickening, coarsening, dryness, telangiectasias, and uneven pigmentation.

Hydrolysable tannins are recognised for their skin anti-ageing properties, particularly their strong antioxidant effects and their ability to inhibit elastolytic enzyme precursors. The genus *Cytinus*, described as one of the most enigmatic in the plant kingdom, has garnered attention for its potential as a source of bioactive compounds. While its properties were ascribed to its hydrolysable tannin content, the chemical composition of *Cytinus hypocistis* (L.) L. had not undergone thorough characterisation, and its active constituents remained undisclosed prior to the research conducted in the present thesis.

Therefore, the primary objective of this work was to valorise the underexplored parasitic species *Cytinus hypocistis* (L.) L. subsp. *macranthus* Wettst by conducting its comprehensive characterisation, followed by a more detailed investigation of its skin anti-ageing properties.

The chemical and bioactive characterisation (**Chapter 3**) was performed by analysing the nutritional and phytochemical profile of *C. hypocistis* and evaluating its bioactive properties. To the author's best knowledge, there are no studies on this edible plant's nutritional characterisation. The whole plant and its nectar revealed being nutritionally balanced, shedding light on its significance as famine food in the past. Its nectar proved to be a good source of protein and unsaturated fatty acids, approximately 2-fold higher than the whole plant. The phytochemical profile and bioactive properties of the whole plant, its petals, stalks, and nectar were also evaluated. Seventeen phenolic compounds were identified in all samples. Galloyl-bis-HHDP-glucose was the most abundant, with no significant difference in concentration between the petals and the whole plant. All extracts exhibited antidiabetic, anti-tyrosinase, antibacterial, and cytotoxicity against four tested tumour cell lines, with no toxicity observed on a non-tumour cell line. The antioxidant capacity was the most prominent among the assessed activities, with no significant differences between the petals and the whole plant.

The results from Chapter 3 suggested a relationship between phenolic compound concentration and *C. hypocistis* bioactive properties, rendering it necessary to investigate whether there is a phenolic compound exchange between the host and the parasite (**Chapter 4**). To the authors' best knowledge, this work was the first to compare the phenolic profile and bioactive properties of the parasite *C. hypocistis* and its host, *Halimium lasianthum* subsp. *alyssoides* (Lam.) Greuter. Except for one compound, trigalloyl-HHDP-glucoside, the phenolic profile of the host (both non-parasited and parasited) was different from that of the parasite, which possibly indicates the existence of a proper pathway of compound biosynthesis in the parasite. This hypothesis was supported by the PCA analysis, where three defined groups were identified: root extracts from *H. lasianthum*, aerial extracts from *H.*

lasianthum, and *C. hypocistis* extracts. This work also highlighted the correlation between *C. hypocistis* hydrolysable tannin content and its antioxidant and anti-tyrosinase activities.

C. hypocistis' biological properties were potentially correlated with its high content in hydrolysable tannins; thus, studying their extraction optimisation would give comprehensive clues for recovering these high-added-value bioactive compounds (**Chapter 5**). This work applied Response Surface Methodology to optimise tannin extraction using Heat-Assisted (HAE) and Ultrasound-Assisted (UAE) methods. Two three-factor Rotatable Central Composite Designs were used to assess the independent variables' linear, quadratic, and interactive effects on the target responses. The results from both extraction systems revealed high ethanol percentages as the critical factor in increasing tannin content, with UAE being selected as the best technique for the recovery.

The skin anti-ageing properties of *C. hypocistis* optimal extracts from three distinct years were assessed, followed by a biochemometric approach to identify the discriminant metabolites associated with the most relevant properties (**Chapter 6**). Among the studied bioactivities, the anti-elastase results exhibited a significant variation among the samples from different years. A bioassay-guided fractionation was performed to identify the discriminant features responsible for this variation, followed by its purification and structural elucidation. Remarkably, one of the purified subfractions exhibited a tenfold improvement in neutrophil elastase inhibition efficacy compared to the crude extract; its effectiveness fell within the same range as SPCK, a potent irreversible elastase inhibitor. Overall, this subfraction also presented better antioxidant and enzyme inhibitory properties (collagenase and tyrosinase) than the crude extract and the positive controls, with no phototoxicity and cytotoxicity against different skin cell lines. Upon NMR structural clarification, this subfraction was elucidated as a galloyl glucose congener as indicated by characteristic spectral resonances of pedunculagin. However, the purified fraction seems to remain a mixture of isomers with differences in glucose, which might indicate that the anti-ageing compound found in *C. hypocistis* could be pedunculagin configurational isomers.

The work developed in the present thesis comprehensively characterised the unexploited species *C. hypocistis*, offering insights into its use as famine food in the past and as a source of compounds with a broad spectrum of bioactive properties. Furthermore, it was possible to identify the compound class of utmost relevance for its bioactivities, validate its exclusive biosynthesis within the parasite, and maximise its recovery. Finally, *C. hypocistis* confirmed its potential as a source of anti-ageing compounds, revealing excellent antioxidant and enzyme-inhibitory properties, particularly its anti-neutrophil elastase activity.

RESUMEN

La piel experimenta cambios visibles con el tiempo, reflejando los efectos combinados de factores intrínsecos y extrínsecos. El envejecimiento intrínseco se debe principalmente a cambios fisiológicos naturales, mientras que la contaminación, hábitos de vida y la exposición a radiación ultravioleta (UVR) desempeñan un papel significativo en el envejecimiento extrínseco. De todas las agresiones que experimenta la piel, se considera que la UVR es la principal contribuyente a su envejecimiento, representando el 80% de sus signos visibles. A pesar de la barrera altamente efectiva que proporcionan las diferentes capas, la UVR puede inducir estrés oxidativo en la piel humana.

Cuando la carga de especies reactivas en este órgano es alta, se activan varias vías que culminan en la degradación de proteínas de la matriz extracelular, como el colágeno y la elastina, mediante la sobreexpresión de metaloproteinasas (MMP) y otras enzimas. La elastasa de neutrófilos se considera una de las enzimas más destructivas en este proceso debido a su capacidad para degradar casi todos los componentes de la matriz extracelular mediante la activación directa de MMPs (formas proactivas y activas), facilitando su progresión e inactivando sus reguladores de actividad. La interacción de factores intrínsecos y extrínsecos da forma a manifestaciones clínicas fenotípicamente distintas. El envejecimiento cronológico conduce a cambios en la piel, como adelgazamiento, palidez, arrugas finas en la superficie y reducción de la elasticidad. En contraste, la exposición prolongada a la UVR resulta en manifestaciones más severas, que incluyen arrugas pronunciadas, pérdida de elasticidad, engrosamiento, rugosidad, sequedad, telangiectasias y pigmentación desigual.

Los taninos hidrolizables son reconocidos por sus propiedades antienvejecimiento en la piel, especialmente por sus fuertes efectos antioxidantes y su capacidad para inhibir los precursores de enzimas elastolíticas. El género *Cytinus* (Cytinaceae), descrito como uno de los más enigmáticos en el reino vegetal, ha llamado la atención por su potencial como fuente de compuestos bioactivos. Aunque sus propiedades se atribuyeron a su contenido de taninos hidrolizables, la composición química de

Cytinus hypocistis (L.) L. no había sido todavía caracterizada a fondo, y sus constituyentes activos permanecían sin revelar antes de la investigación realizada en la presente tesis.

Por lo tanto, el objetivo principal de este trabajo ha sido el de valorizar la especie parasitaria poco explorada *Cytinus hypocistis* (L.) L. subsp. *macranthus* Wettst mediante una caracterización química integral, seguida de una investigación más detallada de sus propiedades antienvejecimiento en la piel.

La caracterización química y bioactiva (Capítulo 3) fue realizada a través del análisis del perfil nutricional y fitoquímico de *C. hypocistis*, así como con la evaluación de sus propiedades bioactivas. Hasta donde el autor sabe, este es el primer trabajo que estudia la caracterización nutricional de esta planta comestible. Toda la planta y su néctar demostraron ser equilibrados desde el punto de vista nutricional, arrojando luz sobre su importancia como alimento en tiempos de hambruna en el pasado. Se demostró que su néctar es una buena fuente de proteínas y ácidos grasos insaturados, aproximadamente el doble que toda la planta. También se evaluó el perfil fitoquímico y las propiedades bioactivas de toda la planta, sus pétalos, tallos y néctar. Se identificaron diecisiete compuestos fenólicos en todas las muestras. El galato-bis-HHDP-glucosa fue el más abundante, sin mostrar una diferencia significativa de concentración entre los pétalos y toda la planta. Todos los extractos mostraron actividad antidiabética, anti-tirosinasa, antibacteriana y citotoxicidad frente a las cuatro líneas celulares tumorales ensayadas sin observar toxicidad en una línea celular no tumoral. La capacidad antioxidante fue la más destacada entre las actividades evaluadas, también sin diferencias significativas entre los pétalos y toda la planta.

Los resultados del Capítulo 3 sugirieron una relación entre la concentración de compuestos fenólicos y las propiedades bioactivas de *C. hypocistis*, haciendo necesario investigar si hay un intercambio de compuestos fenólicos entre el huésped y la planta parásita (Capítulo 4). Según el conocimiento de los autores, este trabajo también fue el primero en comparar el perfil fenólico y las propiedades bioactivas del parásito *C. hypocistis* y su huésped, *Halimium lasianthum* subsp. *alyssoides* (Lam.) Greuter (Cistaceae).

Excepto por un compuesto, el trigaloyl-HHDP-glucósido, el perfil fenólico del huésped (tanto no parasitado como parasitado) fue diferente al del parásito, lo que posiblemente indica la existencia de una vía adecuada de biosíntesis de compuestos en el parásito. Esta hipótesis fue respaldada por el análisis de PCA, donde se identificaron tres grupos definidos: extractos de raíces de *H. lasianthum*, extractos aéreos de *H. lasianthum* y extractos de *C. hypocistis*. Este trabajo también destacó la correlación entre el contenido de taninos hidrolizables de *C. hypocistis* y sus actividades antioxidantes y anti-tirosinasa.

Las propiedades biológicas de *C. hypocistis* estuvieron potencialmente correlacionadas con su alto contenido de taninos hidrolizables; por lo tanto, estudiar la optimización de su extracción proporcionaría pistas completas para recuperar estos compuestos bioactivos de alto valor añadido (Capítulo 5). Este trabajo aplicó la Metodología de Superficie de Respuesta para optimizar la extracción de taninos utilizando los métodos de Asistencia Térmica (HAE) y Asistencia Ultrasónica (UAE). Se aplicó un diseño compuesto central y rotativo para la optimización, que constaba de tres factores para evaluar los efectos lineales, cuadráticos e interactivos de las variables independientes en las respuestas objetivo. Los resultados de ambos sistemas de extracción revelaron altos porcentajes de etanol como el factor crítico para aumentar el contenido de taninos, y se seleccionó UAE como la mejor técnica para la recuperación de los mismos.

Se evaluaron las propiedades antienvejecimiento en la piel de los extractos óptimos de muestras de *C. hypocistis* recogidas en tres años distintos, seguidas de un enfoque bioquimiométrico para identificar los metabolitos discriminantes asociados con las propiedades más relevantes (Capítulo 6). Entre las bioactividades estudiadas, los resultados anti-elastasa mostraron una variación significativa entre las muestras de diferentes años, por lo que se realizó un fraccionamiento guiado por ensayos biológicos para identificar las características discriminantes responsables de esta variación, seguido de la purificación y elucidación estructural del compuesto responsable. Notablemente, una de las subfracciones purificadas mostró una mejora diez veces mayor en la eficacia de inhibición de la

elastasa de neutrófilos en comparación con el extracto crudo; su efectividad se encontró dentro del mismo rango que SPCK, un potente inhibidor irreversible de elastasa. En general, esta subfracción también presentó mejores propiedades antioxidantes e inhibidoras de enzimas (colagenasa y tirosinasa) que el extracto crudo sin mostrar fototoxicidad y citotoxicidad contra diferentes líneas celulares de la piel. Tras la validación estructural mediante RMN, esta subfracción se elucidó como un compuesto formado por una base de glucogalina, que muestra resonancias espectrales características similares a las de la pedunculagina. Sin embargo, la fracción purificada parece tener una mezcla de isómeros con diferencias en la glucosa, lo que podría indicar que el compuesto antienvejecimiento encontrado en *C. hypocistis* podrían ser isómeros configuracionales de la pedunculagina.

El trabajo desarrollado en la presente tesis caracterizó de manera integral la especie poco explorada *C. hypocistis*, ofreciendo perspectivas sobre su uso como alimento en tiempos de hambruna en el pasado y como fuente de compuestos con un amplio espectro de propiedades bioactivas. Además, fue posible identificar la clase de compuestos de máxima relevancia para sus bioactividades, validar su biosíntesis exclusiva dentro del parásito y maximizar su recuperación. Finalmente, *C. hypocistis* confirmó su potencial como fuente de compuestos antienvejecimiento, revelando excelentes propiedades antioxidantes e inhibidoras de enzimas, especialmente su actividad anti-elastasa de neutrófilos.

LIST OF PUBLICATIONS

The studies developed during this Ph.D. thesis led to the following communications.

Articles within this Thesis

1. **A.R. Silva**, Â. Fernandes, P.A. García, L. Barros, I.C.F.R. Ferreira, *Cytinus hypocistis* (L.) L. subsp. *macranthus* Wettst.: Nutritional Characterization, Molecules. 24 (2019) 1111. https://doi.org/10.3390/molecules24061111.

2. **A.R. Silva**, J. Pinela, M.I. Dias, R.C. Calhelha, M.J. Alves, A. Mocan, P.A. García, L. Barros, I.C.F.R. Ferreira, Exploring the phytochemical profile of *Cytinus hypocistis* (L.) L. as a source of health-promoting biomolecules behind its in vitro bioactive and enzyme inhibitory properties, Food and Chemical Toxicology. 136 (2020) 111071. https://doi.org/10.1016/j.fct.2019.111071.

3. **A.R. Silva**, J. Pinela, P.A. García, I.C.F.R. Ferreira, L. Barros, *Cytinus hypocistis* (L.) L.: Optimised heat/ultrasound-assisted extraction of tannins by response surface methodology, Separation and Purification Technology 276 (2021) 119358. https://doi.org/10.1016/j.seppur.2021.119358.

4. **A.R. Silva**, M. Ayuso, C. Pereira, M.I. Dias, M. Kostić, R.C. Calhelha, M. Soković, P.A. García, I.C.F.R. Ferreira, L. Barros, Evaluation of parasite and host phenolic composition and bioactivities − The Practical Case of *Cytinus hypocistis* (L.) L. and *Halimium lasianthum* (Lam.) Greuter, Industrial Crops Production. 176 (2022) 114343. https://doi.org/10.1016/J.INDCROP.2021.114343.

Other articles

1. I.G de Araujo, J.R. Pattaro-Júnior, C.G. Barbosa, G.S. Philippsen, **A.R. Silva**, R.S. Ioshino, C.B. Moraes, L.H Freitas-Junior, L. Barros, R.M. Peralta, M.A. Fernandez, F.A.V. Seixas, Potential of plant extracts in targeting SARS-CoV-2 main protease: an *in vitro* and *in silico* study. Journal of Biomolecular Structure and Dynamics. (2023) 1–10. https://doi.org/10.1080/07391102.2023.2166589.

2. C. Medeiros, **A.R. Silva**, T. Ferreira, L. Barros, M.J. Neuparth, F. Peixoto, M.M.S.M. Bastos, R. Medeiros, R.M. Gil da Costa, M.J. Pires, A.I. Faustino-Rocha, P.A. Oliveira, *Cytinus hypocistis* (L.) L. Extract Effects in an Animal Model of Papillomavirus-Induced Neoplasia. Veterinarska stanica, 54 (2023) 637–653, https://doi.org/10.46419/vs.54.6.9.

3. V.G. Correa, J.A.A. Garcia-Manieri, **A.R. Silva**, E. Backes, R.C.G. Corrêa; L. Barros, A. Bracht, R.M. Peralta, Exploring the *α*-amylase-inhibitory properties of tannin-rich extracts of *Cytinus hypocistis* on starch digestion. Food Research International.173 (2023) 113260. https://doi.org/10.1016/J.FOODRES.2023.113260.

Oral communications

1. **A.R. Silva***, M. I. Dias, P.A. García, L. Barros, I.C.F.R. Ferreira (2018), "*Cytinus hypocistis* (L.) L. plant as a source of phenolic compounds with anti-lipid peroxidation activity", XXIX Encontro Luso-Galego de Química. Porto, **Portugal**, November 21st-23rd.

2. **A.R. Silva**, T. Oludemi*, J. Pinela, M. I. Dias, R.C. Calhelha, M.J. Alves, A. Mocan, P. A. García, L. Barros, I.C.F.R. Ferreira (2019), "*Cytinus hypocistis* (L.) L. extract as a source of anti-ageing cosmeceutical ingredients", 11º Congresso Nacional de Cromatografia. Caparica, **Portugal**, December 9th-12th.

3. **A.R. Silva***, J. Pinela, I.C.F.R. Ferreira, Pablo A. García, Lillian Barros (2021), "Optimisation of a tannin-rich extract using response surface methodology", Natural products application: Health, Cosmetic, and Food. February 5th, **Online edition (International congress)**.

4. **A.R. Silva***, Pablo A. García, I.C.F.R. Ferreira, Lillian Barros (2022), "*Cytinus hypocistis* (L.) L. and its great bioactive potential", 1st Novel Food Webinar: Novel foods based on new ingredients, materials, and processes. January 21st, **Online (Invited Talk - International)**.

5. **A.R. Silva***, M. Ayuso, O. Taofiq, P.A. García, R. Edrada-EbeL, L. Barros (2023), "A Metabolic Approach to assess *Cytinus Hypocistis* (L.) L. Cosmeceutical Properties", 5th International Conference on Natural Products Utilization: From Plants to Pharmacy Shelf. Varna, **Bulgaria**, 30th May to 2nd June. – **Best Oral Presentation Award**

Poster communications

1. **A.R. Silva**, A. Fernandes, P.A. García, L. Barros, I.C.F.R. Ferreira (2018), "Nutritional characterization of *Cytinus hypocistis* (L.) L.", XXIX Encontro Luso-Galego de Química. Porto, **Portugal**, November 21st-23rd

2. **A.R. Silva**, C. Pereira, R.C. Calhelha, P.A. García, I.C.F.R. Ferreira, L. Barros (2021), "Comparative Analysis on Parasite and Host Bioactive Properties - A *Cytinus hypocistis* (L.) L. Case Study", Encontro Ciência '21. **Online edition (National)**, June 28th-30th.

3. **A.R. Silva**, M. Ayuso, M.I. Dias, P.A. García, I.C.F. Ferreira, L. Barros (2022), "Evaluation of Parasite and Host Phenolic Composition – *Cytinus hypocistis* and *Halimium lasianthum*", Encontro Ciência '22. Lisboa, **Portugal**, May 16th-18th.

4. **A.R. Silva**, M. Ayuso, P.A. García, L. Barros, R. Edrada-EbeL (2022), "Metabolomic approach to assess the effect of the foraging year on the anti-elastase activity of *Cytinus hypocistis* (L.) L.", Scottish Metabolomics Network Annual Symposium. Aberdeen, **Scotland**, November 3rd-4th.

ABBREVIATIONS AND ACRONYMS

AAPH	2,2'-azobis-(2-methyl-propanimidamide) dihydrochloride
AGEs	Advanced glycation end products
AGS	Human gastric adenocarcinoma
ANOVA	Analysis of variance
AOAC	Official Methods of Analysis of AOAC INTERNATIONAL
AP-1	Activator protein-1
ATCC	American Type Culture Collection
BALB/3T3	A31 mouse embryo cell line
CAA	Cellular antioxidant activity
Caco-2	Human colorectal adenocarcinoma
CCD	Central Composite Designs
CFU	Colony forming unit
CH	*C. hypocistis* extract
CLS	Cell Lines Service
COX-2	Cyclooxygenase-2
DAD	Diode-array detection
DCFH-DA	2',7'-Dichlorodihydrofluorescein diacetate
DEJ	dermal-epidermal junction
DMEM	Dulbecco's Modified Eagle Medium
DMSO	Dimethyl sulfoxide
DNA	Deoxyribonucleic acid
DOPA	Dihydroxyphenylalanine
DPPH	2,2-Diphenyl-1-picrylhydrazyl
dw	Dry weight
ECACC	European Collection of Authenticated Cell Cultures
ECM	Extracellular matrix
EGF	Epidermal growth factor
ERK	Extracellular signal-regulated kinase
FBS	Foetal bovine serum
FID	Flame ionisation detection
GC-FID	Gas-liquid chromatography
GDP	Guanosine diphosphate
GTP	Guanosine-5'-triphosphate
HaCaT	Spontaneously immortalized keratinocyte cell line
HAE	Heat-assisted extraction
HBSS	Hank's Balanced Salt Solution
HeLa	Cervical carcinoma
HepG2	Hepatocellular carcinoma
HFF-1	Human foreskin fibroblasts
HHDP	Hexahydroxydiphenoyl
HLAP	Non-parasited *H. lasianthum* aerial extract
HLR	Non-parasited *H. lasianthum* roots extract
HPLC	High-performance liquid chromatography
HPLC-RI	HPLC Refractive Index Detector
IFN-g	Interferon-gamma
IL	Interleukins
IL	Interleukin
iNOS	Inducible Nitric oxide synthase
IκB	Inhibitor of kappa B
JNK	c-Jun NH_2-terminal kinase
LC-HRMS	Liquid chromatography-high resolution mass spectrometry
λ_{max}	Wavelength (nm) of maximum absorption
LOD	Limit of detection
LOQ	Limit of quantification

LPS	Lipopolysaccharides
MAPK	Mitogen-activated protein kinase
MBC	Minimum bactericidal concentration
MCF-7	Breast adenocarcinoma
MDA	Malondialdehyde
MFC	Minimal fungicidal concentration
MIC	Minimal inhibitory concentration
MITF	Microphthalmia-associated transcription factor
MMP	Matrix metalloproteinases
MPE	Mean photo effect
MPLC	Medium-pressure liquid chromatography
MRSA	Methicillin-resistant Staphylococcus aureus
MS	Mass spectrometry
MS^2	Fragment ions generated in MS^2 spectra
MUFA	Monounsaturated fatty acids
MW	Molecular weight
NADPH	Nicotinamide adenine dinucleotide phosphate oxidase
NCH	*C. hypocistis* nectar extract
NCI-H460	Non-small cell lung cancer
NF-κB	Nuclear factor κB
NFκB	nuclear factor kappa-light-chain-enhancer of activated B cells
NMR	Nuclear Magnetic Resonance
NO	Nitric oxide
ns	Non-significant
O_2^-	Superoxide anion
OECD	Organisation for Economic Co-operation and Development
OH^-	Hydroxyl ion
$OH^{\bullet}$	Hydroxyl radical
OPLS	Orthogonal partial least squares discriminant analysis
OxHLIA	Oxidative Haemolysis Inhibition
P	Ultrasonic power
$p16^{INK4a}$	Cyclin-dependent kinase inhibitor 2A
$p21^{(WAF1)}$	Cyclin-dependent kinase inhibitor 1
p38	p38 kinase
p53	Tumor protein p53
PBS	Phosphate buffered saline
PC	Principal components
PCA	Principal component analysis
PCH	*C. hypocistis* petals extract
PGE2	Prostaglandin E2
pH	Potential of Hydrogen
PHLAP	Parasited *H. lasianthum* aerial extract
PHLR	Parasited *H. lasianthum* roots extract
PIF	Photo irritation factor
PLP2	freshly harvested porcine liver cell line
PLS-DA	Partial least squares discriminant analysis
pRB	Retinoblastoma protein
PTP	Protein tyrosine phosphatase
PUFA	Polyunsaturated fatty acids
r	Radial distance
$R^{\bullet}$	Carbon-centred alkyl radical
R^2	Coefficient of determination
R^2_{adj}	Adjusted coefficient of determination
Rac	GTP-binding protein Rac
RAGE	Receptor for advanced glycation end products
RCCD	Rotatable Central Composite Design
RFU	Relative fluorescence units
RNA	Ribonucleic acid
RNS	Reactive nitrogen species
$ROO^{\bullet}$	Lipid peroxyl radical

ROOH	Lipid hydroperoxide
ROS	Reactive oxygen species
RS	Reactive species
RSM	Response Surface Methodology
Rt	Retention time
S	Solvent
S/L	Solid/liquid ratio
SASP	Senescence-associated secretory phenotype
SCH	*C. hypocistis* stalks extract
SEM	Standard error of the mean
SFA	Saturated fatty acids
SPCK	MeOSuc-Ala-Ala-Pro-Val-chloromethylketone
SRB	Sulforhodamine B
t	Time
T	Temperature in ºC
TBA	Thiobarbituric acid
TBARS	Thiobarbituric Acid Reactive Substances
tc	Traces
TCA	Trichloroacetic acid
TGF-β	Transforming growth factor β
TIMP	Tissue inhibitors of metalloproteinases
TNF-α	Tumor necrosis factor-α
Trolox	6-Hydroxy-2,5,7,8-tetramethylchroman-2-carboxylic acid
UAE	Ultrasound-assisted extraction
UFA	Unsaturated fatty acids
UFLC	Ultra-fast liquid chromatography
UPLC-ESI-QTOF-MS^2	Liquid chromatography coupled to electrospray ionisation quadrupole
UVA	Ultraviolet A
UVB	Ultraviolet B
UVC	Ultraviolet C
UVR	Ultraviolet radiation
VERO	Kidney epithelial cell line of an African green monkey

THESIS LAYOUT

Thesis organisation

The present thesis is organised into three main parts, which are subdivided into eight chapters. The following scheme provides an illustrative overview of the thesis's organisation.
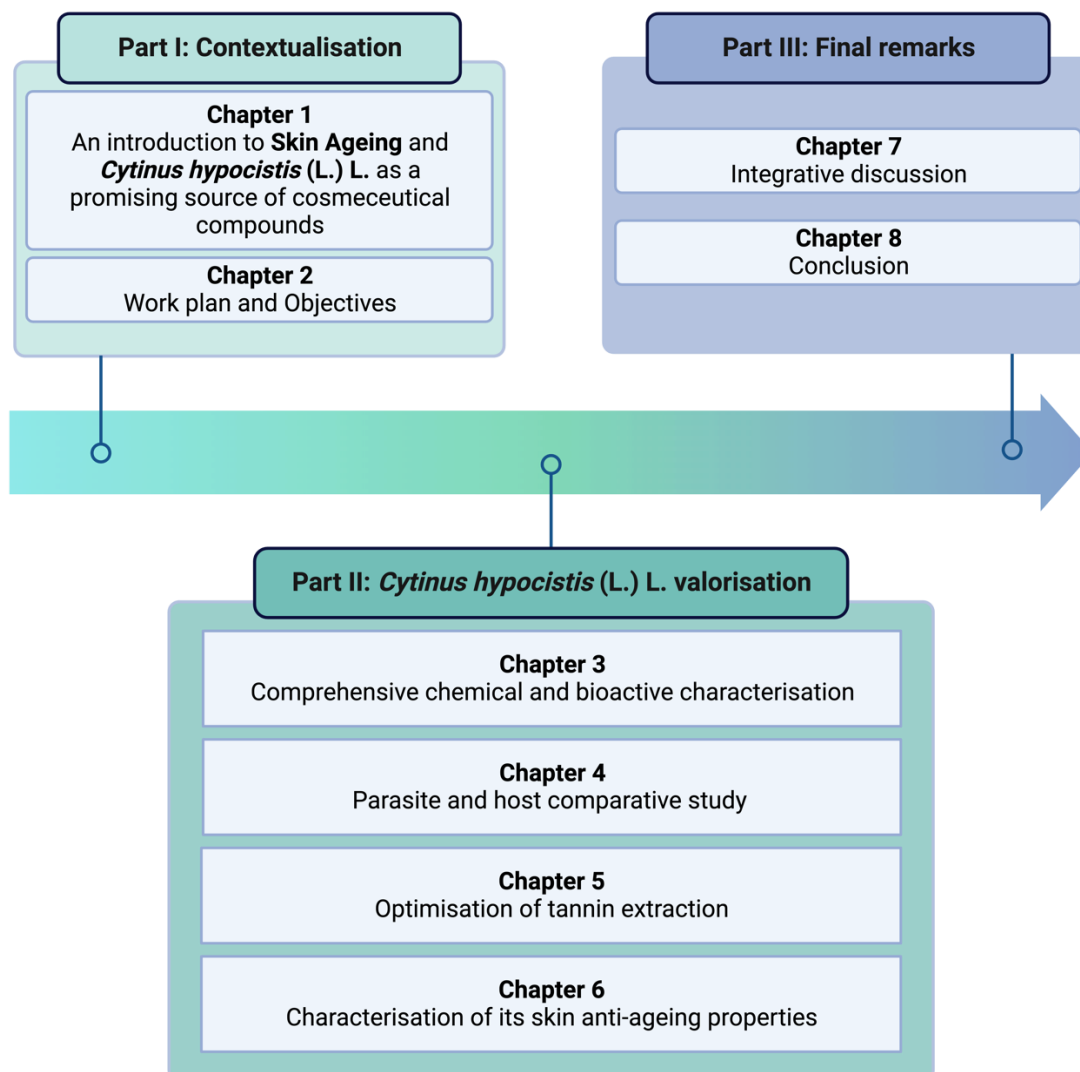
Part I is composed of two chapters. **Chapter 1** presents a literature review on skin ageing and the species *Cytinus hypocistis* (L.) L. as a promising source of bioactive compounds. **Chapter 2** corresponds to the work plan and objectives of the present thesis.

Part II, chapters 3 to 6, encompasses the experimental work to valorise this unexploited plant. **Chapter 3** describes the results of this species' comprehensive chemical and bioactive characterisation. This work is followed by **Chapter 4**, which explores the potential phytochemical exchange between this parasitic plant and its host, *Halimium lasianthum* subsp. *alyssoides* (Lam.) Greuter. **Chapter 5** presents the extraction optimisation of the phenolic class more correlated to its bioactive properties and finally, **Chapter 6** identifies the metabolites responsible for its most notable skin anti-ageing properties using a biochemometric approach.

Part III includes two chapters. **Chapter 7** provides an overall synthesis and interpretation of the thesis findings. The final chapter, **Chapter 8**, summarises this work's final remarks.

Figures and Tables

The Tables and Figures in this thesis are systematically numbered to facilitate easy reference. Each number is composed of two parts: the first indicates the chapter, and the second signifies the sequential order of the figure or table within that chapter. For instance, Figure 1.1 corresponds to the initial figure in Chapter 1.1.

PART I

Introduction

Chapter 1: An introduction to Skin ageing and *Cytinus hypocistis* (L.) L. as a promising source of cosmeceutical compounds

The information presented in this chapter is currently being prepared for publication.

EN ESTA VERSIÓN DE LA TESIS NO SE MUESTRA
EL CAPITULO 1 POR CONFLICTO CON UNA
POSIBLE PUBLICACIÓN FUTURA

Chapter 2: Work Plan and Objectives

The primary objective of this thesis was to valorise the underexplored parasitic species *Cytinus hypocistis* (L.) L. subsp. *macranthus* Wettst by conducting its comprehensive characterisation, followed by a more detailed investigation of its skin anti-ageing properties. According to this, the following specific objectives were established, **each corresponding to a different Chapter in the present thesis.**

Specific objectives:

1) **Chemical and bioactive characterisation**: Analyse the nutritional and phytochemical profile of *C. hypocistis* and evaluate its bioactive properties. ⇒ **Chapter 3**

2) **Comparative study between host and parasite**: Investigate a possible phytochemical exchange between the host (*Halimium lasianthum* subsp. *alyssoides* (Lam.) Greuter) and the parasite (*C. hypocistis*). ⇒ **Chapter 4**

3) **Optimisation of hydrolysable tannin extraction**: Apply Response Surface Methodology (RSM) to optimise tannin extraction using Heat-Assisted and Ultrasound-Assisted methods. ⇒ **Chapter 5**

4) **Investigate *Cytinus hypocistis* skin anti-ageing properties**: Identify the compounds responsible for the skin anti-ageing potential of *C. hypocistis* using a biochemometric approach.⇒ **Chapter 6**

Each of the four chapters follows a defined structure, beginning with the contextualisation and scope of the experimental work, followed by a graphical abstract, a material and methods section, and a detailed discussion of the results and conclusion.

PART II

Cytinus hypocistis (L.) L. valorisation

Chapter 3: Comprehensive chemical and bioactive characterisation

    I.   **Nutritional value**

   II.   **Phytochemical profile and bioactive properties**

The information presented in this chapter was published in the following two publications:

- **A.R. Silva**, Â. Fernandes, P.A. García, L. Barros, I.C.F.R. Ferreira, *Cytinus hypocistis* (L.) L. subsp. *macranthus* Wettst.: Nutritional Characterization, Molecules. 24 (2019) 1111. https://doi.org/10.3390/molecules24061111.

- **A.R. Silva**, J. Pinela, M.I. Dias, R.C. Calhelha, M.J. Alves, A. Mocan, P.A. García, L. Barros, I.C.F.R. Ferreira, Exploring the phytochemical profile of *Cytinus hypocistis* (L.) L. as a source of health-promoting biomolecules behind its in vitro bioactive and enzyme inhibitory properties, Food and Chemical Toxicology. 136 (2020) 111071. https://doi.org/10.1016/j.fct.2019.111071.

I. Nutritional value

Contextualisation and Scope

Wild edible plants have been a critical source of nutrition for humans since ancient times. Many species now considered weeds were used as food substitutes, especially during times of scarcity and famine across various cultures [175–177]. Indeed, all the early studies on the use of wild food plants in Europe, beginning in the 19th century to approximately the 1960s, captured the history of famine and the use of wild plants as a means of basic survival [177]. Despite agricultural societies' primary dependence on crop plants, the tradition of eating wild plants has not completely disappeared [171,178–180]. An example is the parasitic plant *Cytinus hypocistis* (L.) L. [159,171]. At least three studies on wild plants traditionally used for human consumption in Portugal and Spain quoted *C. hypocistis* as famine food, especially its sweet nectar eaten or spread on rye bread during the working day to avoid hunger pains [171,180,181]. Interestingly, according to a semi-quantitative approach comparing the cultural importance of ninety-seven wild edible plant species of the Iberian Peninsula, *C. hypocistis* occupies 44 in the ranking [171].

Approximately 1% of flowering plants are parasitic [161,182,183], and *Cytinus* is one of the most extreme manifestations of this type of parasitism [159,184]. From a nutritional perspective, flowers can be divided into three major components: pollen, nectar, and petals [185]. The nectar is the second most important component; it is usually a sweetish liquid which contains a balanced mixture of sugars, proteins, lipids, and organic acids, among others [186]. Despite the cultural relevance of this plant, its chemical characterisation is mainly unknown [159,172,173], and to the author's best knowledge, its nutritional composition is not yet identified. Therefore, *Cytinus hypocistis* subsp. *macranthus* Wettst. was nutritionally characterised based on its protein, fat, ash, fibre, and carbohydrate content, following which its energetic value was calculated. Furthermore, its sugar, organic, and fatty acids content was also determined.

Graphical abstract

Nutritional characterisation

Organic Acids	Soluble sugars/Tocopherols	Nutritional value
		Protein (AOAC 978.04)
		Fat (AOAC 920.85)
		Ash (AOAC 923.03)
		Carbohydrates = 100 - ($g_{proteins}$ + $g_{carbohydrates}$ + g_{fat})
UPLC-DAD	HPLC-RI	Energy (Kcal) = 4 × ($g_{proteins}$ + $g_{carbohydrates}$) + 9 × g_{fat}
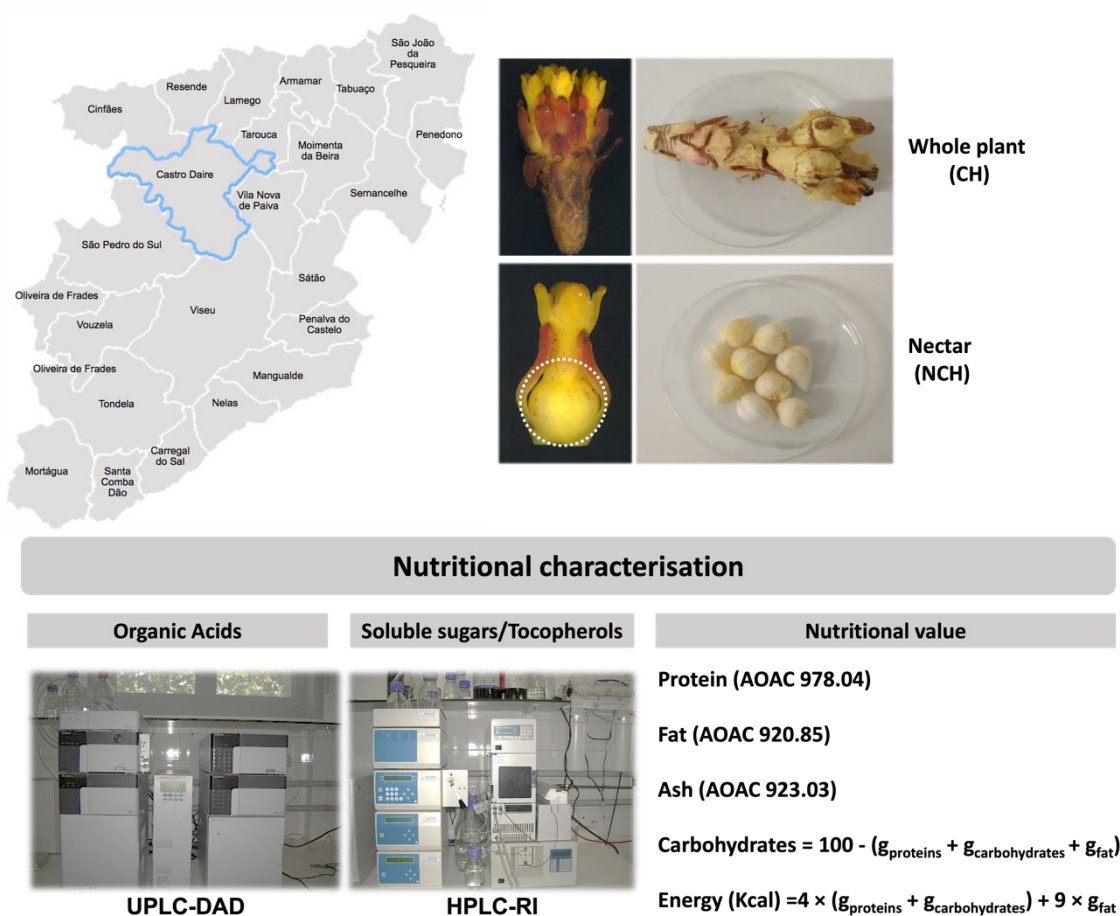
Material and Methods

Plant collection and processing

Cytinus hypocistis (L.) L. subsp. *macranthus* Wettst plants were collected in July 2018 from the host species *Halimium lasianthum* subsp. *alyssoides* (Lam.) Greuter at three different locations in Castro Daire, Portugal. Plant identification was conducted by a botanical specialist. The fresh material was thoroughly cleaned with deionised water to remove all soil, drained on absorbent tissue, and frozen at -30 °C. After lyophilisation (FreeZone 4.5 model 7750031, Labconco, Kansas, USA), as shown in **Figure 3.1**, dried plants were separated into two different samples, whole plant (CH) and nectar (NCH). The plant material was reduced to a fine-dried powder (20 mesh) and stored at room temperature (protected from light) until further analysis.
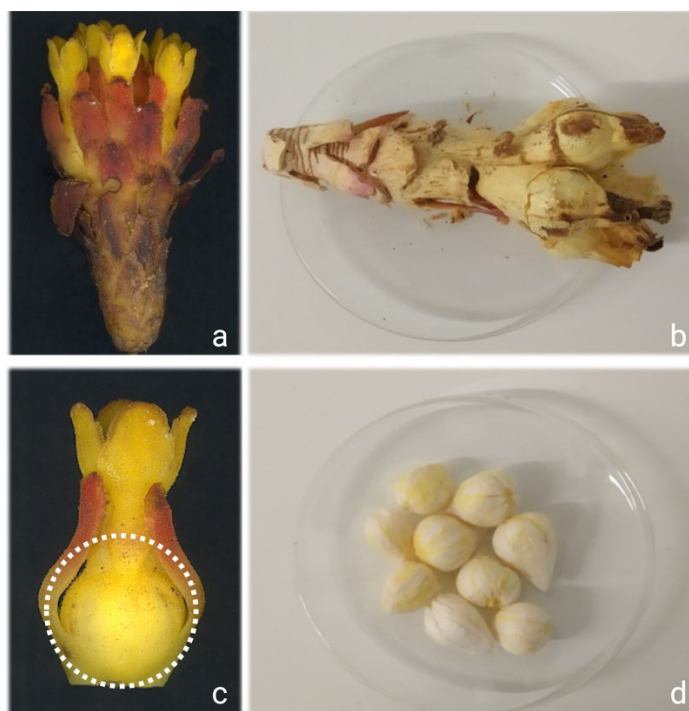
Figure 3.1. *Cytinus hypocistis* subsp. *macranthus* Wettst. (L.) L.: **(a)** fresh plant; **(b)** lyophilised plant; **(c)** fresh flower; and **(d)** lyophilised nectar.

Nutritional value of C. hypocistis

The proximate composition (i.e., proteins, fat, ash, fibre, and carbohydrates) and energetic value of CH and NCH were evaluated following official procedures. The crude protein content of the samples was determined following the macro-Kjeldahl method [N × 6.25, AOAC (Official Methods of Analysis of AOAC INTERNATIONAL) 991.02], the total fat using a Soxhlet apparatus with petroleum ether as the extraction solvent (AOAC 989.05), and the ash content by sample incineration at 550 ± 15 °C (AOAC 935.42) [187]. The fibre content was determined based on the solubilisation of non-cellulosic compounds using sulfuric acid and potassium hydroxide solutions (FIWE Fibre Analyzers). Total available carbohydrates were calculated by difference, using the following equation: Total carbohydrates (g/100 g) $= 100 - (g_{fat} + g_{protein} + g_{ash} + g_{fibre})$. The total energy was calculated according to the following equation: Energy (kcal/100 g) $= 4 \times (g_{proteins} + g_{carbohydrates}) + 9 \times (g_{fat}) + 2 \times (g_{fibre})$.

Soluble Sugars

To determine soluble sugar composition, 1 g of each sample (CH and NCH) was mixed with melezitose (internal standard - IS, 25 mg/mL) and extracted with 40 mL of 80% aqueous ethanol at 80 °C, followed by solvent evaporation and fat removal with consecutive ethyl ether washes as previously described by Pinela and colleagues [188]. High-performance liquid chromatography (Knauer, Smartline system 1000, Berlin, Germany) coupled to a refractive index detector (HPLC-RI) was the chosen methodology; the data were analysed using Clarity 2.4 Software (DataApex, Prague, Czech Republic). HPLC consisted of integrated equipment with a pump (Knauer, Smartline system 1000, Berlin, Germany), a degasser (Smartline manager 5000), an auto-sampler (AS-2057 Jasco, Easton, MD, USA), and an RI detector (Knauer Smartline 2300). The chromatographic separation was achieved with a Eurospher 100-5 NH_2 column (4.6 × 250 mm, 5 µm, Knauer) operating at 30 °C (7971 R Graceoven). The mobile phase was acetonitrile/deionised water (70:30, *v/v*) at a 1 mL/min flow rate. The compounds were identified by chromatographic comparisons with standards, and the quantifications were performed using the internal standard method. Soluble sugars were expressed in g per 100 g dry weight (dw).

Organic Acids

Metaphosphoric acid (4.5%) was added to 1 g of each sample; the mixture was then protected from light and incubated (with agitation) for 20 min at room temperature. After sample filtration, organic acids were determined using a Shimadzu 20A series UFLC (Shimadzu Corporation, Kyoto, Japan) coupled to a photodiode array detector (PDA) [189]. Separation was achieved on a SphereClone (Phenomenex, Torrance, CA, USA) reverse phase C_{18} column (5 µm, 250 mm × 4.6 mm) at 35 °C. The elution was performed with sulphuric acid (3.6 mM) using a flow rate of 0.8 mL/min. Detection was carried out in a PDA using 215 and 245 nm (for ascorbic acid) as preferred wavelengths. For the quantitative analysis, calibration curves with known concentrations of commercial standards were

constructed, and the organic acids present in the two samples were determined by peak area

comparison at 215 nm and 245 nm (for ascorbic acid). The results were expressed in g per 100 g dw.

Fatty Acids

Fatty acid content was investigated after trans-esterification of the lipid fraction obtained through

Soxhlet extraction, as described by Pinela and colleagues [188]. The samples were filtered with a 0.2

μm nylon filter (Whatman) and analysed by gas-liquid chromatography (DANI 1000, Contone,

Switzerland) with flame ionisation detection (GC-FID)/capillary column. The analysis was carried out

with a split/splitless injector, an FID at 260 °C, and a Zebron-Kame column (30 m × 0.25 mm i.d. ×

0.20 μm df, Phenomenex, Torrance, California, USA). The oven temperature program was as follows:

the initial temperature of the column (100 °C) was held for 2 min, then a 10 °C/min ramp to 140 °C, 3

°C/min ramp to 190 °C, 30 °C/min ramp to 260 °C, held for 2 min. The carrier gas (hydrogen) flow

rate was 1.1 mL/min, measured at 100 °C. Split injection (1:50) was performed at 250 °C. Fatty acid

identification and quantification were achieved by comparing the relative retention times of the fatty

acids methyl ester peaks with standards. The results were recorded and processed using CSW 1.7

software (DataApex 1.7) and expressed in the relative percentage for each fatty acid.

Tocopherols

Hexane solutions of butyl-hydroxy-toluene (10 mg/mL; 100 μL) and tocol (internal standard, 400 μL

at 50 μg/mL) were added to 500 mg of the sample before extraction, as formerly described [188]. The

combination was then homogenised with 4 mL of methanol by vortex mixing (1 min), followed by 4

mL of hexane (mixing for 1 min). After sample homogenisation, a saturated NaCl aqueous solution (2

mL) was added, the mixture was combined (vortex mixed for 1 min), centrifuged (5 min, 4000 *g*), and

the clear upper layer carefully transferred to a vial. Sample extraction with hexane was performed three

times. The combined extracts (i.e., the clear layer) were dried under a nitrogen stream, dissolved in 2

mL of *n*-hexane, dehydrated with anhydrous sodium sulphate, filtered through a 0.2 μm nylon filter

(Whatman), transferred into a dark injection vial, and analysed by HPLC (Knauer, Smartline system

1000, Berlin, Germany) coupled to a fluorescence detector (FP-2020; Jasco, Easton, MD, USA) [38]. The chromatographic separation was achieved with a Polyamide II (250 mm × 4.6 mm i.d.) normal-phase column from YMC Waters operating at 30 °C. The mobile phase was a mixture of *n*-hexane and ethyl acetate (70:30, *v/v*) at a flow rate of 1 mL/min; the injection volume was 20 μL. The fluorescence detector was programmed for excitation at 290 nm and emission at 330 nm. The compounds were identified by chromatographic comparisons with standards. Quantification was based on calibration curves obtained from commercial standards of each compound using the internal standard method. The results were expressed in μg/100 g dw.

Statistical Analysis

CH and NCH samples were used for all assays performed in triplicate, and the results were expressed as mean values and standard deviations (SD). The results were analysed using a Student's *t*-test to determine the significant difference between two samples with a 5% significance level (IBM SPSS Statistics, version 22.0. SPSS, Armonk, NY, USA).

Results and Discussion

The nutritional characterisation of *Cytinus hypocistis* was performed for the whole plant and its nectar. While the nectar is more frequently mentioned as edible, there is also data suggesting the consumption of its shoots [159,172]. For a more comprehensive discussion, and since *C. hypocistis* nectar accounts for 70 ± 0.5% of its flower weight, the authors compared the obtained data with published results from other studies on different edible flowers.

The nutritional profiles of the whole plant (CH) and its nectar (NCH) are shown in **Table 3.1** and fall within the typical documented range for edible flowers. The humidity contents of CH and NCH were 78% and 25%, respectively. Protein (9.4 versus 4.90 g/100 g dw) and fat (1.4 versus 0.67 g/100 g dw) values were approximately 2-fold higher in NCH than in CH. Unlike ash (2.87 g/100 g dw for CH and 3.05 g/100 g dw for NCH) and carbohydrates (86.8 g/100 g dw for CH and 85.1 g/100 g dw for NCH), where the content in both samples was very similar, crude fibre was 4.6-fold higher in CH compared

to NCH (4.76 versus 1.03 g/100 g dw). Altogether, these factors contributed to a similar energetic value for both samples (382.4 kcal/100 g dw for CH and 392.9 kcal g/100 g dw for NCH).

The soluble sugar composition of the two samples is also displayed in **Table 3.1**. Both samples presented two reducing (i.e., fructose and glucose) and two non-reducing (i.e., sucrose and trehalose) sugars. Fructose is known to be the sweetest of all naturally occurring carbohydrates [190] and was the main sugar present in CH, almost 9-fold higher (6.3 g/100 g dw) than in NCH (0.71 g/100 g dw). Glucose was also almost 9-fold more elevated in CH (1.92 g/100 g dw) than in NCH (0.22 g/100 g dw). Although sucrose was the main soluble sugar in NCH, its concentration was almost 2-fold lower (0.85 g/100 g dw) than in CH (1.37 g/100 g dw). Contrary to the other three sugars, trehalose content was similar for both samples, 0.95 g/100 g dw in CH and 0.80 g/100 g dw in NCH. The total sugar content was 4-fold higher in the whole plant (10.5 g/100 g dw versus 2.58 g/100 g dw), mainly due to the contribution of fructose. The literature describes plant nectar as containing a well-balanced sugar composition [185]. This characterisation was confirmed for NCH, which revealed a similar content of fructose, sucrose, and trehalose.

Three different organic acids were identified in both samples (CH and NCH): oxalic (0.030 g/100 g dw versus traces), malic (0.40 g/100 g dw versus 0.45 g/100 g dw), and citric acid (0.41 g/100 g dw versus 1.48 g/100 g dw). Contrarily, ascorbic acid and traces of shikimic acid were only detected in NCH (0.180 g/100 g dw) and CH, respectively. The total organic acid content was 2.48-fold higher in NCH (2.11 g/100 g dw) than CH (0.85 g/100 g dw). Similarly, to the data published in the literature for edible flowers, water is its main constituent (*CH*: 78% vs literature: 70 to 95%), and carbohydrates its most abundant macronutrient (*CH*: 86.8 /100 g dw vs literature: 42.4 to 90.2 g/100 g dw) [191]. Regarding tocopherol content, only traces of the α-tocopherol isoform were detected in the whole plant (CH).

Table 3.1. *Cytinus hypocistis* whole plant (CH) and nectar (NCH) nutritional value, soluble sugars, and organic acids composition. Mean ± SD.

Moisture (%)	CH	NCH	*p*-value
	78 ± 1	25 ± 1	<0.001
Nutritional value	**g/100 g dw**		
Fat	0.67 ± 0.03	1.4 ± 0.1	<0.001
Proteins	4.90 ± 0.07	9.4 ± 0.3	<0.001
Ash	2.87 ± 0.02	3.05 ± 0.05	0.005
Fibre	4.8 ± 0.1	1.03 ± 0.05	<0.001
Carbohydrates	86.8 ± 0.2	85.1 ± 0.4	0.002
Energy (kcal/100 g dw)	382.4 ± 0.1	392.9 ± 0.1	<0.001
Soluble sugars	**g/100 g dw**		
Fructose	6.3 ± 0.1	0.71 ± 0.01	<0.001
Glucose	1.92 ± 0.05	0.22 ± 0.02	<0.001
Sucrose	1.37 ± 0.05	0.85 ± 0.01	<0.001
Trehalose	0.95 ± 0.02	0.80 ± 0.04	0.001
Total	10.5 ± 0.2	2.58 ± 0.07	<0.001
Organic acids	**g/100 g dw**		
Oxalic acid	0.030 ± 0.001	tr.	-
Malic acid	0.40 ± 0.01	0.45 ± 0.02	0.007
Shikimic acid	tr.	nd.	-
Ascorbic acid	nd.	0.180 ± 0.002	-
Citric acid	0.41 ± 0.01	1.48 ± 0.01	<0.001
Total	0.85 ± 0.02	2.11 ± 0.03	<0.001

dw: Dry weight basis, **tr.**: Traces, and **nd.**: not detected.

The results regarding the fatty acids composition of CH and NCH are given in **Table 3.2**. The fatty acids profile showed twenty-five compounds for CH and twenty-six for NCH. Polyunsaturated fatty acids (PUFA) were the major group, followed by saturated fatty acids (SFA) and monounsaturated fatty acids (MUFA). PUFA corresponded to 46.95% of the fatty acids in CH and 49% in NCH, mainly due to the high linoleic acid content in both samples (40.08% and 39.90%, respectively). The body can produce most fatty acids, but two, known as essential fatty acids, cannot be synthesised by humans. These essential fatty acids are α-linolenic acid (*n*-3 PUFA) and linoleic acid (*n*-6 PUFA). While humans can convert dietary α-linolenic acid into longer chain *n*-3 PUFAs like eicosapentaenoic acid and docosahexaenoic acid, this process may not meet the body's requirements [192]. Therefore, it is

recommended to include good dietary sources of these fatty acids. High percentages of linoleic and *α*-linolenic acids can be found in some edible flowers, including *Calendula officinalis* L. and *Trifolium angustifolium* L [193]. Similarly, CH and NCH presented 42.14% and 43.62%, respectively. SFA is the second group of fatty acids with similar predominance in CH (35.56%) and NCH (35.36%), largely due to the high content of palmitic acid (24.12 and 24.76%, respectively). Palmitic acid is one of the most common SFAs found in edible plants. Although SFAs are associated with an increased risk of developing cardiovascular diseases [194], oxidative DNA damage, DNA strand breakage, necrosis, and apoptosis in human cells *in vitro* [195,196], when consumed with other fatty acids, like PUFAs, SFA are unlikely to have any significant impact on human health [193,196,197]. CH and NCH also contain other saturated fatty acids in lower concentrations, such as stearic (CH: 5.19%, NCH: 4.79%), arachidic (CH: 1.87%, NCH: 1.453%), and behenic acids (CH: 1.86%, NCH: 1.57%). MUFA makes up the smallest contribution to the fatty acids content in CH (17.5%) and NCH (15.31%), mainly due to the presence of oleic acid (CH: 15.4%, NCH: 13.70%). Both samples presented small percentages of palmitoleic (CH: 0.662%, NCH: 0.628%), elaidic (CH: 1.10%, NCH: 0.861%), and eicosanoic acids (CH: 0.366%, NCH: 0.121%). The well-known hypotensive effect of olive oil is induced by oleic acid, and according to Fernandes and colleagues, one of the highest percentages of this fatty acid present in edible flowers was found in *Gundelia tournefortii* L. buds (28.5%) [193,198]. Due to the significant contributions of linoleic and palmitic acids, PUFA and SFA are the predominant fatty acids in both samples (**Table 3.2**). However, unsaturated fatty acids (UFA) prevail over SFA (64.44% versus 35.56% in CH and 6.9% versus 35.36% in NCH). According to the literature, with the exception observed in calendula flowers (23.3%), unsaturated fatty acids predominate over saturated ones for edible flowers, usually higher than 53% [199].

Most edible flowers studied have shown ratios above 0.45 of PUFA/SFA, which can help reduce the risk of cardiovascular diseases [197]. *C. hypocistis* was no exception, with PUFA/SFA ratios for CH and NCH of 1.32 and 1.37, respectively.

Table 3.2. *Cytinus hypocistis* fatty acids composition (Mean ± SD).

Fatty Acids (Relative Percentage; %)	CH	NCH	*p*-value
Caproic acid (C6:0)	nd.	0.100 ± 0.001	-
Caprilic acid (C8:0)	0.030 ± 0.003	0.033 ± 0.001	0.178
Capric acid (C10:0)	0.037 ± 0.003	0.036 ± 0.001	0.011
Undecylic acid (C11:0)	0.016 ± 0.001	0.042 ± 0.001	<0.001
Lauric acid (C12:0)	0.315 ± 0.002	0.268± 0.001	<0.001
Myristic acid (C14:0)	0.425 ± 0.001	0.384 ± 0.001	<0.001
Pentadecylic acid (C15:0)	0.15 ± 0.01	0.13 ± 0.01	0.001
Palmitic acid (C16:0)	24.12 ± 0.07	24.76 ± 0.02	<0.001
Palmitoleic acid (C16:1)	0.662 ± 0.001	0.628± 0.001	<0.001
Margaric acid (C17:0)	0.311 ± 0.004	0.305 ± 0.001	<0.001
Stearic acid (C18:0)	5.19 ± 0.04	4.79 ± 0.01	<0.001
Elaidic acid (C18:1n9t)	1.10 ± 0.02	0.86 ± 0.01	<0.001
Oleic acid (C18:1n9c)	15.4 ± 0.1	13.7 ± 0.1	<0.001
γ-Linolenic acid (C18:3n6)	2.16 ± 0.01	1.88 ± 0.01	0.001
α-Linolenic acid (C18:3n3)	40.08 ± 0.02	39.90 ± 0.03	<0.001
γ-Linolenic acid (C18:3n6)	1.088 ± 0.001	0.940 ± 0.005	<0.001
α-Linolenic acid (C18:3n3)	2.07 ± 0.06	3.72 ± 0.02	<0.001
Arachidic acid (C20:0)	1.87 ± 0.01	1.45 ± 0.01	<0.001
Eicosanoic acid (C20:1)	0.366 ± 0.004	0.121 ± 0.004	<0.001
cis-11,14-Eicosadienoic acid (C20:2)	1.471 ± 0.005	1.273 ± 0.001	0.001
Heneicosanoic acid (C21:0)	0.22 ± 0.01	0.25 ± 0.01	0.001
Arachidonic acid (C20:4n6)	0.028 ± 0.001	0.034 ± 0.002	<0.001
Behenic acid (C22:0)	1.86 ± 0.06	1.57 ± 0.01	0.001
cis-13,16-Docosadienoic acid (C22:2)	0.058 ± 0.001	0.037 ± 0.001	<0.001
Tricosanoic acid (C23:0)	0.182 ± 0.003	0.191 ± 0.004	0.003
Lignoceric acid (C24:0)	0.83 ± 0.03	2.60 ± 0.02	<0.001
SFA	35.56 ± 0.09	35.36 ± 0.02	0.006
MUFA	17.5 ± 0.1	15.3 ± 0.1	<0.001
PUFA	46.95 ± 0.04	49 ± 1	0.022
UFA	64.4 ± 0.1	63.8 ± 0.8	0.282
PUFA/SFA	1.32 ± 0.01	1.37 ± 0.02	0.015

dw: Dry weight basis; **nd.**: not detected; **SFA**: saturated fatty acids; **MUFA**: monounsaturated fatty acids; **PUFA**: polyunsaturated fatty acids; and **UFA**: unsaturated fatty acids.

Conclusions

This study offered novel insights into the nutritional and chemical properties of the edible parasitic plant *C. hypocistis*, shedding light on its historical significance as food during famine. Especially its nectar, which proved to be a good source of protein and unsaturated fatty acids, approximately 2-fold higher than the whole plant.

II. Phytochemical profile and bioactive properties

Contextualisation and Scope

For thousands of years, humans have harnessed the healing properties of medicinal plants, starting with rudimentary forms like teas, tinctures, and poultices [200]. As technology has advanced, the understanding of complex natural profiles has expanded, leading to the emergence of numerous blockbuster drugs through the isolation or chemical synthesis of natural product lead compounds [201]. Phenolic compounds are the largest and the most widespread group of secondary metabolites in plants and have been reported to have multiple biological effects [202]. In addition to their fundamental activities, such as binding to proteins, large molecular compounds, and metallic ions, tannins chemical, biological, and pharmacological actions include superoxide anion scavenging, apoptosis, antitumor, anti-Epstein–Barr virus, anti-MRSA (Methicillin-resistant *Staphylococcus aureus*), and anti-plasmin inhibitory activities [203]. Galloyl moieties have been identified as the most bioactive components of tannin-rich plants, playing multiple functional roles such as antimicrobial, anti-inflammatory, antidiabetic, and antioxidant activities [158]. Its anti-tyrosinase properties have been attributed to its strong copper chelation properties, which can inhibit tyrosinase competitively by mimicking its substrate [204]. *C. hypocistis* extracts were reported as having cytotoxic, antimicrobial, antioxidant, anti-inflammatory, and enzyme-inhibitory properties [159,172,173]. Although its biological properties were potentially attributed to its hydrolysable tannin content, to the author's best knowledge, its chemical composition is largely unknown, and active biomolecules have not yet been identified [158,159,172]. Therefore, the present work aimed to determine *C. hypocistis* phytochemical profile and perform a bioactive screening of different properties.

Graphical abstract

Phytochemical profile

Hydroethanolic extracts

CH

SCH

NCH

PCH

HPLC-DAD/ESI-MS^n

CH

SCH

NCH

PCH

Cytotoxic and Anti-inflammatory activities

Sulforodamine B

Cytotoxic activity

Tumour cell lines
HeLa (cervical carcinoma)
HepG-2 (hepatocellular carcinoma)
MCF-7 (breast adenocarcinoma)
NCI-H460 (large cell lung cancer)

Non-tumour cell lines
PLP2 (porcine liver primary culture)

Anti-inflammatory activity

Macrophage cells RAW 264.7

Griess reagent

Antioxidant activity

Oxidative hemolysis inhibition (OxHLIA)

AAPH: 2,2′-azobis(2-methylpropionamidine) dihydrochloride

AAPH

Thiobarbituric acid reactive substances (TBARS)

Pig brain Extracts

Iron sulphate
Ascorbic acid
Malondialdehyde
Thiobarbituric acid

Antidiabetic activity

Yeast α-glucosidase

p-nitrophenyl-α-D-glucopyranoside (colourless)

D-glucose

p-nitrophenol
λ_{max} = 405 nm
(yellow)

Anti-tyrosinase activity

λ 475 nm

L-DOPA

Mushroom Tyrosinase

Dopaquinone

L-DOPA: substrate

Dopaquinone: oxidation product

Antibacterial activity

● Growth
○ No growth

Growth (control)

No growth

No growth
MBC

Growth
MIC

63

Material and methods

Plant collection and extract preparation

Cytinus hypocistis (L.) L. subsp. *macranthus* Wettst plants were collected in July 2018 from the host species *Halimium lasianthum* subsp. *alyssoides* (Lam.) Greuter at three different locations in Castro Daire, Portugal. Plant identification and preparation were conducted as previously described [205]. **Figure 3.2** shows how lyophilised plants were separated into four different samples: whole plant (CH), petals (PCH), stalks (SCH) and nectar (NCH). Hydroethanolic extracts of the four samples were prepared using an ethanol:water solvent (80:20, *v/v*), as described by Bessada and colleagues [206].
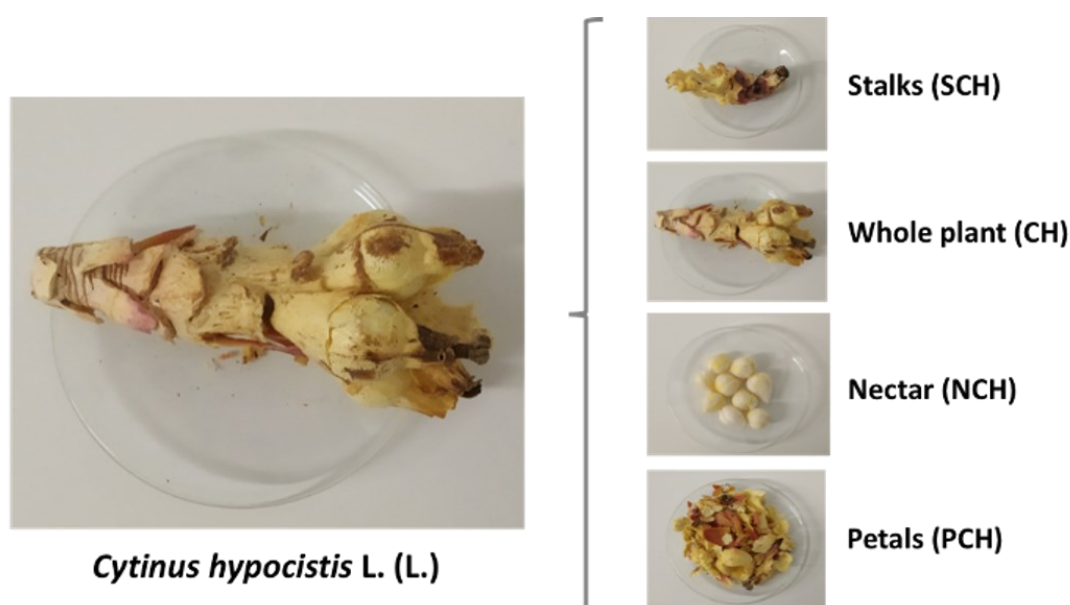
Figure 3.2. Graphical representation of the four *C. hypocistis* studied samples.

Phenolic compounds characterisation

After preparation, the dry extracts (20 mg) were dissolved in a mixture of ethanol:water (20:80 *v/v*, 2 mL) and filtered through a 0.2 μm nylon filter (Whatman). Phenolic compounds were determined by HPLC-DAD-ESI/MS^n (Dionex Ultimate 3000 UPLC, Thermo Scientific, San Jose, CA, USA) as previously described [206]. Detection was carried out in the diode array detector (DAD) using 280 nm, 330 nm, and 370 nm as the preferred wavelengths and a mass spectrometer connected to the HPLC

system. Mass spectrometric detection was performed using a Linear Ion Trap LTQ XL (Thermo Finnigan, San Jose, CA, USA) equipped with an ESI source. The spectrums were recorded in negative ion mode (m/z 100 – 1700). The phenolic compounds were identified according to their UV spectra, fragmentation pattern, retention times, and comparison with available standards. For quantification, calibration curves were obtained from commercial standards: gallic acid (y = 131538x + 292163; R2 = 0.9998; LOD = 0.68 µg/mL; LOQ = 1.61 µg/mL); catechin (y = 84950x + 23200; R2= 0.9999; LOD = 0.17 µg/mL; LOQ = 0.68 µg/mL); ellagic acid (y = 26719x – 317255; R2 = 0.9996; LOD = 0.10 µg/mL; LOQ = 0.48 µg/mL). The results were expressed in mg/g of extract.

Bioactive properties characterisation

Cytotoxic activity. MCF-7 (breast adenocarcinoma), NCI-H460 (non-small cell lung carcinoma), HeLa (cervical carcinoma), and HepG2 (hepatocellular carcinoma) were the tested human tumour cell lines. A cell culture previously prepared from a freshly harvested porcine liver (PLP2) was used as the non-tumour cell line [207]. The cell lines were treated with different concentrations (0.125-0.4 mg/mL) of the samples dissolved in a mixture of ethanol:water (20:80 *v/v*, 2 mL). Cell density following incubation with *C. hypocistis* extracts was conducted using the sulforhodamine B method described by Guimarães and colleagues [207]. The cells were sub-cultured and plated in 96-well plates (density of 1.0×10^4 cells/well). Dulbecco's modified eagle's medium (DMEM) was supplemented with 10% fetal bovine serum (FBS), 100 U/mL of penicillin, and 100 µg/mL of streptomycin. Ellipticine was used as the positive control, and the results were expressed as the sample concentrations required to inhibit 50% of the cell growth (GI_{50}: µg/mL). All results were confirmed using a phase-contrast microscope.

Anti-inflammatory activity. The nitrite concentration produced by lipopolysaccharide (LPS)-stimulation was tested in a murine macrophage RAW 264.7 cell line. Cells were treated with different concentrations (0.125-0.4 mg/mL) of the samples dissolved in a mixture of ethanol:water (20:80 *v/v*, 2 mL), and the production of nitric oxide (NO) was measured using the Griess Reagent System kit as

formerly described [208]. Dexamethasone was used as the positive control. The results were expressed as IC_{50} values (μg/mL), corresponding to the extract concentration inhibiting 50% of NO.

Antioxidant activity. The Oxidative Haemolysis Inhibition (OxHLIA) and Thiobarbituric Acid Reactive Substances (TBARS) formation assays were conducted using methodologies previously described by Lockowandt and colleagues [209]. Trolox was used as the positive control for both assays. OxHLIA assay: In a flat bottom 48-well microplate, 200 μL of erythrocytes in PBS (2.8% *w/v*) were mixed with 400 μL of the samples (0.0625-2 μg/mL in PBS); PBS was used as control and milli-Q water for complete haemolysis. After pre-incubation at 37 °C for 10 min with shaking, AAPH (200 μL, 160 mM in PBS) was added, and the optical density (690 nm) was measured every 10 min in a microplate reader (Bio-Tek Instruments, ELX800) until complete haemolysis. The results were given as IC_{50} values, i.e., extract concentration (ng/mL) required to protect 50% of the erythrocyte population from oxidative haemolysis (Δt of 60 min and 120 min).

TBARS assay: A porcine brain cell mixture (1:2, *w/v*; 0.1 mL) was incubated with 0.2 mL of the samples (0.0625-2 μg/), $FeSO_4$ (10 μM; 0.1 mL), and ascorbic acid (0.1 mM; 0.1 mL) at 37 °C for 1 h. Then, trichloroacetic (28% *w/v*, 0.5 mL) and thiobarbituric (TBA, 2%, *w/v*, 0.38 mL) acids were added, and the mixture was heated at 80 °C for 20 min. After centrifugation at 3000 g for 10 min, the malondialdehyde (MDA)-TBA complexes formed in the supernatant were monitored at 532 nm (Specord 200 spectrophotometer, Analytik Jena, Jena, Germany). The results were expressed as IC_{50} values, i.e., extract concentration (ng/mL) providing 50% antioxidant protection.

Antidiabetic assay. The α-glycosidase inhibitory assay was adapted from a previously described methodology [210,211]. The assay was conducted in a 96-well microplate with a reaction mixture containing 50 μL of extract diluted in 50 μL of 100 mM-phosphate buffer (pH 6.8) and 50 μL yeast α-glucosidase (2 U/mL in the same buffer). The reaction mixture was then incubated for 10 min, and 50 μL substrate (5 mM, *p*-nitrophenyl-α-D-glucopyranoside prepared in the same buffer) was added. After

20 min of incubation, the release of p-nitrophenol was spectrophotometrically measured at 405 nm. Acarbose was used as the positive control. The results were expressed as IC_{50} values (mg/mL), calculated using the formula: Inhibition (%) = [(Abs$_{control}$- Abs$_{sample}$)/Abs$_{control}$]x100.

Tyrosinase inhibitory activity. Tyrosinase inhibitory activity of the extracts was determined as previously described [212], using a SPECTROstar Nano Multi-Detection Microplate Reader and 96-well plates (BMG Labtech, Ortenberg, Germany). Each sample was dissolved in a 5% DMSO solution. Four wells were prepared for each sample: (A) 120 µL of 66 mM PBS (pH 6.8) and 40 µL of mushroom tyrosinase in PBS (46 U/mL); (B) 160 µL PBS; (C) 80 µL PBS, 40 µL tyrosinase and 40 µL sample; and (D) 120 µL PBS and 40 µL sample. After incubation (10 min at room temperature), 40 µL of 2.5 mM L-DOPA dissolved in PBS was added to each well, and the mixtures were incubated at room temperature for 20 min. The absorbance of each well was measured at 475 nm, and the inhibition percentage of the tyrosinase activity was calculated using the equation: Inhibition (%) = ((A-B)-(C-D))/((A-B)) x 100. Kojic acid (0.10 mg/mL) was used as the positive control. IC_{50} values (mg/mL) were then calculated from the obtained inhibition percentage values.

Antibacterial activity. The extracts were tested against microbial strains isolated from patients hospitalised at the Hospital Center of Trás-os-Montes and Alto Douro (Vila Real, Portugal). Five Gram-negative bacteria (*Escherichia coli*, *Proteus mirabilis*, *Klebsiella pneumoniae*, *Pseudomonas aeruginosa*, and *Morganella morganii*) and four Gram-positive bacteria (*Enterococcus faecalis*, *Listeria monocytogenes*, and methicillin-sensitive *Staphylococcus aureus* (MRSA) were incubated at 37 ºC (24 h) in suitable fresh medium before further analysis. The minimum inhibitory concentration (MIC) was determined using the microdilution method and the rapid p-iodonitrotetrazolium chloride (INT) colourimetric assay, following the methodology previously described [213,214]. The extracts were dissolved in Tryptic Soy Broth (TSB) at a final concentration of 100 mg/mL. The subsequent dilutions (10–60 mg/mL for Gram-negative bacteria and 1.25–20 mg/mL for Gram-positive bacteria) were prepared directly in the well. The lowest extract concentration that prevented colour change

(yellow to pink) by inhibiting bacterial growth is described as MIC. Positive controls ampicillin (20 mg/mL) and imipenem (1 mg/mL) were used on Gram-negative bacteria, while ampicillin and vancomycin (1 mg/mL) were used on Gram-positive bacteria. The microplates were covered and incubated at 37 °C for 24 h. MIC was detected by adding 40 μL (0.2 mg/mL) of p-iodonitrotetrazolium chloride and incubating the mixture at 37 °C for 30 min. For minimum bactericidal concentration (MBC) determination, 50 μL of the different well mixtures (no colour change) were plated and incubated at 37 °C for 24 h. The lowest concentration showing no bacteria growth was defined as MBC.

Statistical analysis

All assays were carried out in triplicate. The results were expressed as mean values ± standard deviation (SD). Statistical analysis was conducted using SPSS v. 23.0 (IBM Corp., Armonk, NY, USA). Data were evaluated by a variance analysis (ANOVA) and a Turkey HSD test ($\alpha = 0.05$). The results were analysed by t-Student test to determine the significant differences between the two samples, with $p = 0.05$.

Results and discussion

Phenolic compounds characterisation

The phenolic compounds' peak characteristics and tentative identities are presented in **Table 3.3,** and the quantification is presented in **Table 3.4**. An example (petals: PCH) of *C. hypocistis* phenolic profile recorded at 280 nm is shown in **Figure 3.3**.

Peaks 1-3 and 5-17 showed UV spectra consistent with hydrolysable tannins, and its galloyl and hexahydroxydiphenoyl (HHDP) derivatives. According to the literature, the main characteristics in the mass spectra of these compounds are the losses of a proton [M-H]⁻, one or more ellagic acids (302 u), gallic acids (170 u), and/or galloyl groups (152 u) [215].

Peaks 1 and 2 were tentatively identified as galloyl-glucose and digalloyl-glucose due to the loss of a galloyl moiety characterised by a typical MS² fragment at *m/z* 331. The elimination of a glucose moiety

[162 u] and, subsequently, the formation of a deprotonated gallic acid at *m/z* 169 were also observed. The deprotonated gallic acid underwent decarboxylation with a mass loss of 44 to form a trihydroxyphenol moiety at *m/z* 125 [216]. Peaks 3 and 5 were tentatively deduced as trigalloyl-glucose, with [M-H]⁻ at *m/z* 635, and a typical MS^2 fragment at *m/z* 483, indicating the loss of one galloyl group (152 u). Product ions at *m/z* 465 and 313, usually found on the fragmentation scheme of gallotannins, were also observed [216,217]. Peak 6 ([M-H]⁻ at *m/z* 937; fragment ions at *m/z* 767, 637, 467 and 301) was coherent with trigalloyl-HHDP-glucose isomers [215].

Table 3.3. Phenolic compounds identified in *C. hypocistis* extracts.

Peak	Rt (min)	λ$_{max}$ (nm)	[M-H]⁻ (*m/z*)	MS^2 (*m/z*)	Tentative identification	Ref.
1	4.42	275	331	169(100), 125(9)	Galloyl-glucose	[216]
2	4.83	275	483	331(100), 169(50), 125(9)	Digalloyl-glucose	[216]
3	6.28	275	635	483(22), 465(100), 421(6), 313(5), 169(38), 125(5)	Trigalloyl-glucose	[216,217]
4	7.03	280	289	245(100), 203 (10), 137(5)	(+)-Catechin	[215]
5	9.25	275	635	483(17), 465(100), 421(5), 313(5), 169(25), 125(5)	Trigalloyl-glucose	[216,217]
6	14.83	275	937	787(36), 767(100), 637(22), 467(41), 301(38)	Trigalloyl-HHDP-glucose	[215]
7	15.46	275	787	635(26), 617(100), 465(5)	Tetragalloyl-glucoside	[218]
8	16.7	278	783	765(65), 597(100), 301(15)	Pedunculagin (bis-HHDP-glucose)	[219,220]
9	19.14	275	939	787(100), 769(70), 617(5), 601(5), 599(46), 465(5), 301(4)	Pentagalloyl-glucose	[217,221]
10	19.43	278	935	783(100), 765(13), 633(5), 301(5)	Galloyl-bis-HHDP-glucose	[215]
11	20.79	275	939	787(100), 769(5), 465(8), 301(3)	Pentagalloyl-glucose	[217,221]
12	21.8	278	935	783(100), 765(15), 633(8), 301(7)	Galloyl-bis-HHDP-glucose	[215]
13	22.63	278	1087	935(100), 783(20), 633(3), 301(11)	Digalloyl-bis-HHDP-glucose	[222,223]
14	24.11	277	1087	935(100), 783(18), 633(5), 301(14)	Digalloyl-bis-HHDP-glucose	[222,223]
15	25.2	277	1087	935(100), 783(18), 633(5), 301(14)	Digalloyl-bis-HHDP-glucose	[222,223]
16	26.56	276	1259	1087(100), 935(66), 783(15), 633(5), 301(12)	Trigalloyl-bis-HHDP-glucose	[222,223]
17	27.75	276	1259	1087(100), 935(55), 783(13), 633(5), 301(10)	Trigalloyl-bis-HHDP-glucose	[222,223]

Rt: Retention time in minutes; **λ$_{max}$**: wavelength (nm) of maximum absorption in the UV–visible region; **[M-H]⁻**: deprotonated ion (negative ion mode); **MS^2**: fragment ions generated in MS^2 spectra and relative abundance in brackets.

Peak 7 (tetragalloyl-glucoside; *m/z* 787) presented a characteristic MS^2 fragment at *m/z* 635 (trigalloyl-glucose), correspondent to the loss of one galloyl group (152 u), and product ions at *m/z* of 617 and 465, consistent with the loss of a gallate moiety (*m/z* 170), H$_2$O (*m/z* 18), and galloyl (*m/z* 152), respectively [218]. Peak 8 presented a singly charged pseudo-molecular ion [M-H]⁻ at *m/z* 783 and,

together with daughter ions at *m/z* 765, 597, and 301 allowed its identification as pedunculagin (*i.e.,* bis-HHDP-glucose) isomers [219,220]. The UV spectra of peak 9 showed a precursor ion at *m/z* 939 and product ions at *m/z* 787 and 769, attributed to the loss of a galloyl group [M-152-H]⁻ and a water molecule [M-152-18-H]⁻, respectively. This ion fragment (*m/z* 769) underwent the loss of a galloyl and a water molecule, originating *m/z* fragments of 617 and 599, respectively. Although with the absence of two MS² fragments (*m/z* at 617 and 599) present in the UV spectra of peak 9, peak 11 was also identified as pentagalloyl-glucose (*m/z* 939) due to the characteristic product ions at *m/z* 787, 769, and 465, which unveil the presence of homologous series of galloylglucose [217,221]. Peaks 10 and 12 ([M-H]⁻ at *m/z* 935) presented the same pseudomolecular ion and MS² product ions at *m/z* 783, 765, 633, and 301, likely due to the loss of a water molecule, HHDP, and galloyl-glucose moieties, respectively; thus being consistent with galloyl-bis-HHDP-glucose isomers [215]. The fragment ions at *m/z* 1087, 935, and 783 present in the UV spectra of peaks 13-17, show the consecutive loss of two galloyl moieties; that, together with pseudomolecular ions at 1087 and 1259 *m/z* allowed its identification as digalloyl-bis-HHDP-glucopyranose and trigalloyl-bis-HHDP-glucopyranose [223–225].
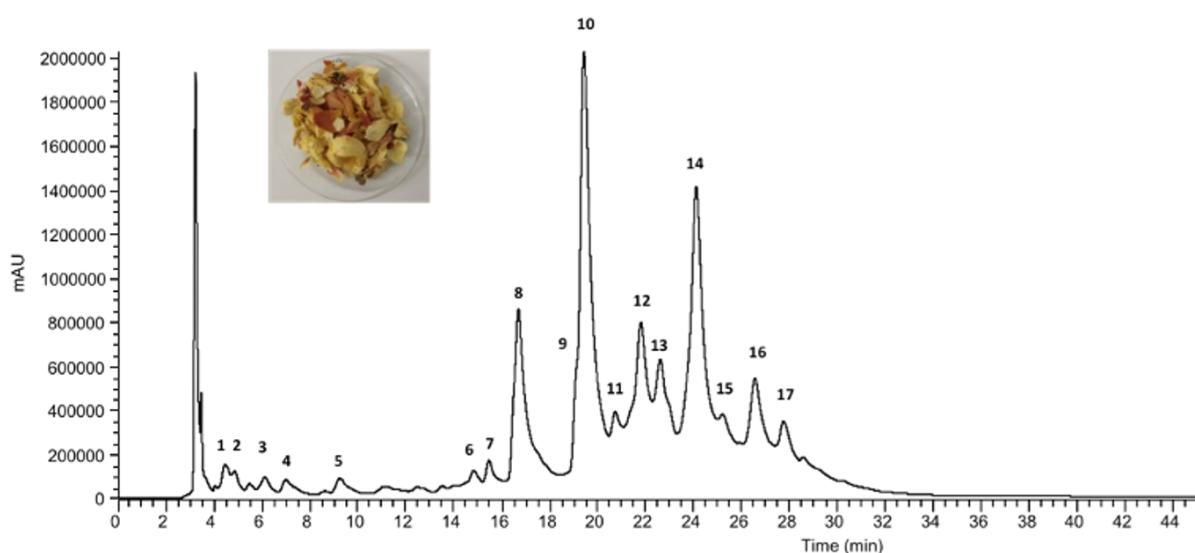
Figure 3.3. Phenolic profile of *C. hypocistis* petals extract (PCH) recorded at 280 nm.

Regarding falvan-3-ols, (+)-catechin (peak 4: [M-H]$^-$ at *m/z* 289) was the only detected compound, being identified based on the characteristic MS^2 fragments at *m/z* 245 (loss of CO_2), and 203 (cleavage of the A-ring of flavan-3-ol) [215].

Seventeen phenolic compounds were identified in all four samples, with galloyl-bis-HHDP-glucose identified as the main compound. PCH showed the highest concentrations of phenolic compounds, while NCH had the lowest (**Table 3.4**).

Table 3.4. Phenolic compounds quantification in *C. hypocistis* extracts.

Peak	Tentative identification	Content (mg/g extract)			
		CH	PCH	SCH	NCH
1	Galloyl-glucose[1]	0.81 ± 0.01^c	1.9 ± 0.05^a	1.19 ± 0.08^b	0.77 ± 0.05^c
2	Digalloyl-glucose[1]	0.99 ± 0.01^b	1.68 ± 0.03^a	0.335 ± 0.004^d	0.65 ± 0.02^c
3	Trigalloyl-glucose[1]	1.47 ± 0.04^a	0.46 ± 0.04^b	1.49 ± 0.07^a	0.146 ± 0.003^c
4	(+)-Catechin[2]	1.83 ± 0.04^c	2.9 ± 0.1^a	2.17 ± 0.06^b	1.69 ± 0.03^d
5	Trigalloyl-glucose[1]	1.09 ± 0.03^b	1.41 ± 0.06^a	0.64 ± 0.03^c	tr
6	Trigalloyl-HHDP-glucose[1]	1.26 ± 0.04^c	1.88 ± 0.03^b	2.52 ± 0.08^a	0.29 ± 0.01^d
7	Tetragalloyl-glucoside[1]	1.907 ± 0.004^b	1.13 ± 0.02^c	2.7 ± 0.1^a	0.114 ± 0.005^d
8	Pedunculagin (bis-HHDP-glucose)[3]	2.23 ± 0.03^b	3.34 ± 0.05^a	1.63 ± 0.04^c	tr
9	Pentagalloyl-glucose[1]	5.10 ± 0.04^a	5.3 ± 0.2^a	3.7 ± 0.2^b	1.43 ± 0.06^c
10	Galloyl-bis-HHDP-glucose[3]	42 ± 1^a	41 ± 1^a	34 ± 1^b	5.43 ± 0.05^c
11	Pentagalloyl-glucose[1]	0.85 ± 0.03^b	2.80 ± 0.01^a	0.14 ± 0.01^c	0.114 ± 0.004^c
12	Galloyl-bis-HHDP-glucose[3]	9.60 ± 0.05^b	11.1 ± 0.3^a	6.8 ± 0.3^c	2.1 ± 0.1^d
13	Digalloyl-bis-HHDP-glucos[3]	6.45 ± 0.0^a	6.5 ± 0.2^a	5.1 ± 0.1^b	1.74 ± 0.02^c
14	Digalloyl-bis-HHDP-glucose[3]	18.3 ± 0.4^b	27.2 ± 0.1^a	11.4 ± 0.2^c	3.64 ± 0.02^d
15	Digalloyl-bis-HHDP-glucose[3]	5.4 ± 0.1^b	7.7 ± 0.1^a	1.65 ± 0.02^c	1.78 ± 0.02^c
16	Trigalloyl-bis-HHDP-glucose[3]	2.58 ± 0.02^c	13.1 ± 0.7^a	4.2 ± 0.1^b	1.30 ± 0.01^d
17	Trigalloyl-bis-HHDP-glucose[3]	nd	7.4 ± 0.3*	2.35 ± 0.01*	nd
	Σ Phenolic compounds	102.0 ± 0.6^b	137 ± 2^a	82 ± 2^c	21.2 ± 0.2^d

CH: whole plant extract; **PCH**: petals extract; **SCH**: stalks extract; **NCH**: nectar extract. Standard calibration curves recorded at 280 nm: ([1])- Gallic acid (y = 131538x + 292163; R^2 = 0.9998; LOD = 0.68 µg/mL; LOQ = 1.61 µg/mL); ([2])- catechin (y = 84950x + 23200; R^2 = 0.9999; LOD = 0.17 µg/mL; LOQ = 0.68 µg/mL); ([3])- Ellagic acid (y = 26719x - 317255; R^2 = 0.9996; LOD = 0.10 µg/mL; LOQ = 0.48 µg/mL). Different letters correspond to significant differences ($p < 0.05$). *Means statistical differences obtained by a *t*-student test.

Bioactive properties characterisation

Cytotoxic activity. Modern chemotherapy employs various plant-derived compounds with cytotoxic properties, working through diverse mechanisms, including induction of apoptosis, DNA damage, and inhibition of cell growth and topoisomerases I and II [226]. The sulforhodamine B colourimetric assay was applied to determine the inhibitory growth activity of *C. hypocistis* hydroethanolic extracts on four human tumour cell lines (NCI-H460, HeLa, HepG2 and MCF-7) and one non-tumour cell line (PLP2). **Table 3.5** presents the results as GI_{50}, i.e., the concentration of *C. hypocistis* extracts required to inhibit 50% cell growth. CH, PCH, and SCH presented good cytotoxic effects against all tumour cell lines, while the nectar (NCH) showed the least effective results. To the authors' best knowledge, there are only two studies on the cytotoxic activity of *C. hypocistis* extracts [159,172]. The data from the present study agree with that reported by Magiatis and colleagues, who found that the methanolic extracts of three Greek *Cytinus* species exhibited cytotoxic activity against several cancer cell lines [172]. These results led the authors to the fractionation of the methanolic extracts by medium-pressure liquid chromatography (MPLC), obtaining an inactive fraction (GI_{50} >400), containing mainly sugars and a fraction with increased cytotoxicity when compared to the total methanolic extracts. For the two species of *C. hypocistis* studied by Magiatis and co-workers, the methanolic extracts exhibited GI_{50} of 100 and 98 μg/mL for human mammary adenocarcinoma (MDA-MB-231), in contrast with GI_{50} of 75 and 77 μg/mL for the cytotoxic active fraction. Similar results were obtained for human bladder transitional cell carcinoma (BC3c), 110 and 105 μg/mL, in contrast with 71 and 67 μg/mL for the active fraction [172]. The authors attributed this cytotoxic activity to hydrolysable tannins without apparent dependence on their molecular weights. Although different cell lines were used in the present work, both studies exhibited a similar range of GI_{50}s.

Table 3.5. Enzyme inhibitory, cytotoxic, and anti-inflammatory properties of *C. hypocistis* extracts and positive controls.

	CH	PCH	SCH	NCH	Positive control
	Antidiabetic activity (IC$_{50}$, µg/mL)				Acarbose
α-Glucosidase	40 ± 1^a	46 ± 4^a	39 ± 1^a	214 ± 5^b	830 ± 20^c
	Tyrosinase inhibition activity (IC$_{50}$, µg/mL)				Kojic acid
Tyrosinase	200 ± 10^d	190 ± 10^c	90 ± 20^b	>500	78 ± 1^a
	Cytotoxic activity (GI$_{50}$, µg/mL)				Ellipticine*
HeLa	80 ± 7^a	71 ± 2^a	68 ± 4^a	159 ± 5^b	1.91 ± 0.06
NCI-H460	102 ± 4^a	93 ± 8^a	100 ± 6^a	175 ± 13^b	1.03 ± 0.09
MCF-7	117 ± 6^a	103 ± 7^a	98 ± 4^a	206 ± 11^b	1.1 ± 0.2
HepG2	80 ± 2^b	90 ± 6^b	77 ± 2^a	110 ± 3^c	1.1 ± 0.2
PLP2	>400	>400	>400	>400	3.2 ± 0.7
	Anti-inflammatory activity (IC$_{50}$, µg/mL)				Dexamethasone*
RAW 264.7	136 ± 11^b	127 ± 8^a	127 ± 12^a	277 ± 14^c	16 ± 1

CH: whole plant extract; **PCH**: petals extract; **SCH**: stalks extract; **NCH**: nectar extract. The results are presented as mean ± standard deviation and expressed as **IC$_{50}$** (extract concentration in mg/mL responsible for 50% enzyme inhibition), **GI$_{50}$** (extract concentration in µg/mL responsible for 50% of growth inhibition in human tumour cell lines and a liver primary cell culture) or **IC$_{50}$** (extract concentration in µg/mL responsible for 50% inhibition in NO production) values. Different letters correspond to significant differences ($p < 0.05$). *The positive control differs significantly from the plant extracts ($p < 0.05$).

Anti-inflammatory activity. Macrophages play an essential role in the anti-inflammatory process and can be activated by interferon-gamma (IFN-γ), interleukins (IL-4, IL-10, IL-13), transforming growth factor beta (TGF-β), and some structures from pathogenic microorganisms such as lipopolysaccharides (LPS) [227]. During pathogen invasion, immunocytes secrete inflammatory mediators, such as nitric oxide (NO) and prostaglandin E2 (PGE2), via the inducible nitric oxide synthase (iNOS) and cyclooxygenase-2 (COX-2). iNOS and COX-2 are involved in tumour progression through various mechanisms, including inhibition of apoptosis, stimulation of angiogenesis, and promotion of tumour cell proliferation [228]. All four *C. hypocistis* extracts successfully reduced the anti-inflammatory enzyme iNOS activity in LPS-activated murine macrophages. NO reduction was measured employing a Griess reagent system kit and expressed as lower IC$_{50}$ values (**Table 3.5**). Among all extracts, the petals (PCH) and stalks (SCH) showed the highest inhibitory effects in NO production by LPS-

stimulated RAW264.7 cells, with an IC_{50} of 127 μg/mL, followed by CH (IC_{50} = 136 μg/mL) and NCH (IC_{50} = 277 μg/mL). To the authors' best knowledge, this is a novel study regarding the anti-inflammatory activity of *C. hypocistis,* and thus, no comparisons could be performed.

Antioxidant activity. Lipid peroxidation is a sequence of destructive reactions in cell membranes. This autoxidation process is initiated when reactive species abstract an allylic H from a methylene group in the acyl chain of phospholipids. This leads to the rearrangement of double bonds into a conjugated diene form while simultaneously producing a carbon-centred alkyl radical ($R^{\bullet}$) [229]. This highly reactive radical will then react with paramagnetic molecular oxygen to form a lipid peroxyl radical ($ROO^{\bullet}$). If not neutralised by antioxidant defences, $ROO^{\bullet}$ reacts with another lipid molecule to generate $R^{\bullet}$ and lipid hydroperoxide (ROOH), which can easily be decomposed to form new $ROO^{\bullet}$ radicals, starting a process known as the chain propagation reaction [230]. The lipid peroxyl radicals and their non-radical intermediates (lipid hydroperoxides) can undergo cyclisation and cleavage, forming secondary products such as malondialdehyde (MDA), known for its mutagenic and toxic effects [231]. The TBARS assay is an easy and low-cost method to screen lipid peroxidation. During this assay, MDA reacts with thiobarbituric acid (TBA) in acidic conditions and forms a characteristic pink chromogenic product, [MDA-(TBA)$_2$], which is produced at high temperatures and spectrophotometrically detected at 532nm [232]. OxHLIA is a cellular antioxidant assay that assesses the ability of a sample to inhibit membrane damage in sheep erythrocytes induced by free radicals. During the thermal decomposition of AAPH, hydrophilic radicals are generated, which damage erythrocyte membranes and produce lipophilic radicals through lipid peroxidation. Since erythrocytes have no nucleus or mitochondria, they can be used as a simplified biological model [230]. The results of the antioxidant activity assays are presented in **Table 3.6**. Data are expressed as IC_{50} values, meaning the concentration of extract able to provide 50% of antioxidant activity (TBARS) or to protect 50% of the erythrocyte population from haemolysis caused by an oxidising agent (OxHLIA). The IC_{50} values in the OxHLIA assay were obtained at different times (Δt 60 min and Δt 120 min). In both assays, the

lower the IC_{50} values, the higher the antioxidant capacity of the extracts. All four tested extracts showed high antioxidant capacity and a lower IC_{50} than the tested positive control, trolox, a water-soluble analogue of vitamin E. Concerning the OxHLIA assay, all the IC_{50} values of the tested extracts were approximately 30 to 73 times lower, and for TBARS around 9 to 16 times inferior to trolox. The petals obtained the lowest IC_{50} for both assays, 0.279 µg/mL (Δt = 60 min) for OxHLIA and 0.342 µg/mL for TBARS. The only published study on the antioxidant activity of *C. hypocistis*, demonstrated the good antioxidant activity of its ethanolic extracts (DPPH: 6.8 µg/mL) [158].

Table 3.6. Antioxidant activity of *C. hypocistis* extracts.

	OxHLIA (IC_{50}, µg/mL)		TBARS (IC_{50}, µg/mL)
	Δt = 60 min	Δt = 120 min	
CH	0.285 ± 0.004^{bc}	0.406 ± 0.005^{a}	0.413 ± 0.009^{b}
PCH	0.279 ± 0.005^{ab}	0.384 ± 0.009^{a}	0.342 ± 0.002^{a}
SCH	0.306 ± 0.002^{c}	0.458 ± 0.004^{b}	0.634 ± 0.012^{d}
NCH	0.672 ± 0.015^{d}	1.032 ± 0.028^{c}	0.551 ± 0.013^{c}
Trolox*	20.4 ± 0.4	44.2 ± 1.5	5.4 ± 0.3

CH: whole plant extract; **PCH**: petals extract; **SCH**: stalks extract; **NCH**: nectar extract. The results are presented as mean ± standard deviation and expressed as IC_{50} values, which correspond to the extract concentration in µg/mL required to protect 50% of the erythrocyte population from haemolysis for Δt of 60 min and 120 min or to provide 50% of antioxidant activity in the OxHLIA and TBARS assays, respectively. Different letters correspond to significant differences ($p < 0.05$). *Trolox differs significantly from the plant extracts ($p < 0.05$).

Antidiabetic activity. α-Glucosidase breaks down glycosidic bonds of complex carbohydrates into absorbable monosaccharides; thus, α-glucosidase inhibitors display advantageous anti-hyperglycaemic effects and can be an important strategy in the management of hyperglycaemia linked to type 2 diabetes [233]. The discovery of potent α-glucosidase inhibitors from natural sources has received great attention due to the highly abundant compounds in nature and their promising biological activities [234]. **Table 3.5** shows the resulting IC_{50} values for the different extracts. SCH, CH, and PCH exhibited similar α-glucosidase inhibition, with IC_{50} values of 39 µg/mL, 40 µg/mL, and 46 µg/mL, respectively. NCH was less effective, with an IC_{50} value of 214 µg/mL. SCH, PCH, and CH IC_{50} values were approximately 18 to 21 times better than the positive control acarbose, a commonly

used medication for managing type 2 diabetes mellitus. To the authors' best knowledge, this is the first report evaluating the anti-glucosidase activity of *C. hypocistis* extracts; therefore, no comparisons could be performed.

Anti-tyrosinase activity. Tyrosinase is widely distributed in microorganisms, animals, and plants. It is involved in the biosynthesis of melanin, catalysing the ortho-hydroxylation of tyrosine to DOPA and the subsequent oxidation of DOPA to dopaquinone. Dopaquinone can be further converted into melanin through enzymatic and nonenzymatic reactions [235]. Products containing ingredients such as hydroquinone, kojic acid, and retinoids have been utilised to suppress the severity of hyperpigmentation; however, long-term exposure to these ingredients has been reported to cause cytotoxic, irritating, and mutagenic effects on the skin [236]. Therefore, the discovery of novel tyrosinase inhibitors is in great need for the pharmaceutical industry. Tyrosinase inhibition was determined using a mushroom-purified enzyme and expressed as IC_{50} values (**Table 3.5**), the extract concentration required to inhibit 50% enzyme activity. To the authors' best knowledge, this is the second study reporting a quantitative analysis of *C. hypocistis* anti-tyrosinase activity [158]. Although to different extents, all *C. hypocistis* ethanolic extracts were able to inhibit tyrosinase activity, with the stalks presenting the best result (SCH: 90 µg/mL), followed by the petals (PCH: 190 µg/mL) and whole plant (CH: 200 µg/mL). At the maximum tested concentration (500 µg/mL), the IC_{50} for NCH could not be determined. SCH was the extract exhibiting the closest IC_{50} (90 µg/mL) value compared to the positive control, kojic acid (78 µg/mL), one of the most intensively studied tyrosinase inhibitors [237]. *C. hypocistis* whole plant displayed a better IC_{50} (9.8 µg/mL) in a 2019 study [158]. Although both studies tested the capacity of the extracts to inhibit tyrosinase activity, the plant material from the other study was previously resuspended in cyclohexane, the collected supernatant lyophilised, and later subjected to a second extraction with ethanol. The pre-extraction step reported by Maisetta and coworkers and the different environmental conditions the plants were exposed to might also be accountable for the obtained MIC values due to differences in phenolic compound concentration.

Antibacterial activity. In recent years, antibiotic resistance has sparked increased interest in exploring plant-derived compounds as novel antibacterial agents [238]. The four hydroethanolic extracts (CH, PCH, SCH and NCH) of *C. hypocistis* were evaluated for their antibacterial potential against three Gram-positive bacteria (*E. feacalis, L. monocytogenes,* and MRSA) and five Gram-negative (*E. coli, P. mirabilis*, *K. pneumoniae*, *P. aeruginosa*, and *M. morganii*). All four *C. hypocistis* extracts were more effective against three Gram-negative bacteria than ampicillin, a beta-lactam antibiotic widely used to destroy Gram-positive and Gram-negative bacteria [158]. Considering *K. pneumoniae*, the extracts were 2 to 8-fold more effective, while for *P. aeruginosa* and *M. morganii,* they were 8 to 16-fold more effective than ampicillin. MBC values were not obtained for any tested extracts (values > 20 mg/mL). The MIC values shown in **Table 3.7** indicate that the extracts were active against Gram-negative and Gram-positive bacteria, being the former more sensitive to all the plant extracts. In general, the hydroethanolic extracts from the stalks were the most (SCH MIC = 0.625 - 2.5 mg/mL) and the nectar the least (NCH MIC = 2.5 - 10 mg/mL) effective to inhibit the growth of both Gram-positive and Gram-negative bacteria. For three tested microorganisms (MRSA, *K. pneumoniae*, and *P. aeruginosa*), *C. hypocistis* ethanolic extracts displayed better MICs in a recent study [158]. This could be due to the use of clinical isolates in the present study, which might exhibit a higher resistance profile when compared with the ATCC strains tested by Maisetta and co-workers.

Similarly, to the anti-tyrosinase activity, this could also be due to the pre-extraction step performed by Maisetta and colleagues or the different conditions to which the plants were exposed. Previous studies investigating the antimicrobial activity of tannin-rich plant extracts have attributed growth inhibition to their content in gallotannins and related compounds, which mainly act on the membranes of the bacteria and/or their ability to complex metal ions. Several studies have also shown that Gram-negative bacteria are more resistant to plant-derived biomolecules due to the strong repulsive negative charge of its lipopolysaccharides. Contrarily, in the present work, the extracts were more effective in inhibiting Gram-negative bacteria.

Table 3.7. Antibacterial activity of *C. hypocistis* extracts.

	CH		PCH		SCH		NCH		Ampicillin		Imipenem		Vancomycin	
	MIC	MBC	MIC	MBC	MIC	MBC	MIC	MBC	MIC	MBC	MIC	MBC	MIC	MBC
Gram-negative														
Escherichia coli	1.25	>20	1.25	>20	0.625	>20	2.5	>20	<0.15	<0.15	<0.0078	<0.0078	n.t.	n.t.
Klebsiella pneumoniae	1.25	>20	1.25	>20	1.25	>20	5	>20	10	20	<0.0078	<0.0078	n.t.	n.t.
Morganella morganii	1.25	>20	2.5	>20	1.25	>20	2.5	20	20	>20	<0.0078	<0.0078	n.t.	n.t.
Proteus mirabilis	1.25	20	1.25	20	1.25	20	5	>20	<015	<0.15	<0.0078	<0.0078	n.t.	n.t.
P. aeruginosa	2.5	>20	2.5	>20	1.25	>20	2.5	>20	>20	>20	0.5	1	n.t.	n.t.
Gram-positive														
Enterococcus faecalis	2.5	20	2.5	>20	2.5	>20	5	>20	<0.15	<0.15	n.t.	n.t.	<0.0078	<0.0078
Listeria monocytogenes	2.5	>20	2.5	>20	2.5	>20	10	>20	<0.15	<0.15	<0.0078	<0.0078	n.t.	n.t.
MRSA	1.25	>20	1.25	>20	0.625	>20	2.5	>20	<0.15	<0.15	n.t.	n.t.	0.25	0.5

CH: whole plant extract; **PCH**: petals extract; **SCH**: stalks extract; **NCH**: nectar extract; **n.t.**: not tested; **MRSA**: Methicillin Resistant *Staphylococcus aureus*; **MIC**: Minimum inhibitory concentration in mg/mL; **MBC**: Minimum bactericidal concentration in mg/mL.

Conclusions

In this study, the phytochemical profile of *Cytinus hypocistis* (L.) L. hydroethanolic extracts and their antioxidant, antibacterial, antidiabetic, anti-tyrosinase, cytotoxic, and anti-inflammatory properties were investigated.

The petals extract exhibited the highest concentration of total phenolic compounds, followed by the whole plant, stalks, and nectar. Among the seventeen identified phenolic compounds, galloyl-bis-HHDP-glucose was the most abundant, with no significant differences in its concentration in the petals and the whole plant.

The plant demonstrated excellent antioxidant and tyrosinase inhibitory effects without any observed cytotoxicity. These findings accentuate the potential, briefly mentioned in the literature, of *C. hypocistis* as a source of compounds with anti-ageing properties. Before further investigation, additional research is required to explore a potential phytochemical exchange between the host and parasite.

Chapter 4: Comparative study between host and parasite

The information presented in this chapter was published in the following publication:

- **A.R. Silva**, M. Ayuso, C. Pereira, M.I. Dias, M. Kostić, R.C. Calhelha, M. Soković, P.A. García, I.C.F.R. Ferreira, L. Barros, Evaluation of parasite and host phenolic composition and bioactivities − The Practical Case of *Cytinus hypocistis* (L.) L. and *Halimium lasianthum* (Lam.) Greuter, Industrial Crops Production. 176 (2022) 114343. https://doi.org/10.1016/J.INDCROP.2021.114343.

Contextualisation and Scope

Parasitism is an effective strategy exhibited by living organisms and an area that connects all Kingdoms of life [161]. Parasitic plants are characterised by the ability to obtain resources from another plant through a direct physical connection, invading both the roots and the shoots of the hosts via specific structures (haustorium) [161].

Cytinus hypocistis (L.) L. is an endophytic holoparasite that becomes visible during the blossoming season when it emerges through the host roots [159]. The subspecies *macranthus* Wettst, utilised in this study, is distinguished by its large, bright yellow flowers and has only been described as a parasite on plants from the *Halimium* genus [155,160,165]. *Halimium* belongs to the Cistaceae family; it comprises thirteen accepted evergreen or semi-deciduous small-to-large shrub species and occupies a specific niche in the Mediterranean biome with an increasingly appreciated ecological function. It improves water and light regimes, protects soil from erosion and desertification, and acts as a "nurse" species for tree seedlings [239]. Although, to date, most studies on plant parasitism were focused on nutrient transfer, a growing number of studies have recognised the transference of non-nutrient molecules. The transference of phytohormones, secondary metabolites, RNAs, and proteins suggests that hosts may significantly impact parasite physiology and ecology, essential processes for development and plant defence [163].

C. hypocistis high tannin content has been associated with its bioactivities, yet no studies on the host's phytochemical profile and potential metabolite exchange have been conducted. Therefore, this study aims to assess the phenolic composition and bioactive properties of *H. lasianthum* and their potential impact on the parasite *C. hypocistis* phytochemical profile. This study will bring new insights regarding host bioactive potential and parasite-host interactions.

Graphical abstract

Host and parasite phytochemical profile

C. hypocistis (CH)

Parasited H. lasianthum
Aerial parts (**PHLAP**)
Root parts (**PHLR**)
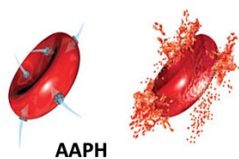
Non-parasited H. lasianthum
Aerial parts (**HLAP**)
Root parts (**HLR**)

HPLC-DAD/ESI-MS^n
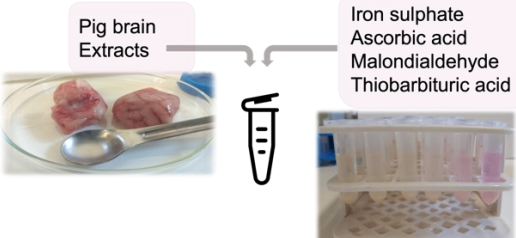
Antioxidant activity

Oxidative hemolysis inhibition (OxHLIA)

AAPH: 2,2′-azobis(2-methylpropionamidine) dihydrochloride

AAPH

Thiobarbituric acid reactive substances (TBARS)

Pig brain Extracts

Iron sulphate
Ascorbic acid
Malondialdehyde
Thiobarbituric acid

Anti-tyrosinase activity

λ 475 nm

L-DOPA → **Dopaquinone**

Mushroom Tyrosinase

L-DOPA: substrate

Dopaquinone: oxidation product

Cytotoxic and Anti-inflammatory activities

Cytotoxic activity

Sulforodamine B

Tumour cell lines
AGS (gastric adenocarcinoma)
Caco-2 (colorectal adenocarcinoma)
MCF-7 (breast adenocarcinoma)
NCI-H460 (large cell lung cancer)

Non-tumour cell lines
VERO (African green monkey)
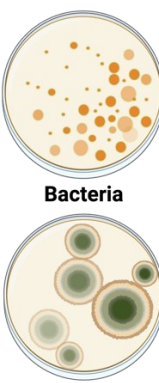
Anti-inflammatory activity

Macrophage cells RAW 264.7

Griess reagent

Antimicrobial activity
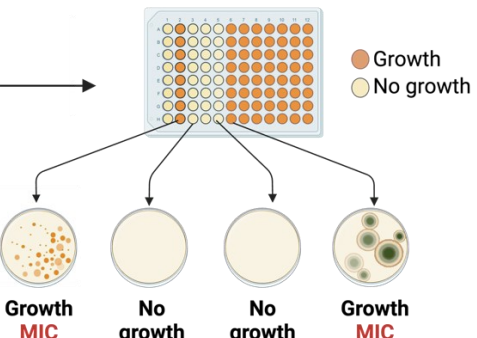
Bacteria

Fungi

● Growth
○ No growth

Growth
MIC

No growth
MBC

No growth
MFC

Growth
MIC

Material and methods

Plant collection and extract preparation

The parasitic plant *Cytinus hypocistis* (L.) L. subsp. *macranthus* Wettst and the two forms (parasited and non-parasited) of its host *Halimium lasianthum* subsp. *alyssoides* (Lam.) Greuter (**Figure 4.1**) were collected in July 2020 at three different locations in Castro Daire, Viseu, Portugal. Sample processing was conducted as formerly described [205]. The extracts were prepared using Heat-Assisted Extraction: 0.8 g of each sample was mixed with 40 mL of a hydroethanolic solution (74.3% ethanol) and extracted for 95.1 minutes at 46.4°C. A total of five hydroethanolic extracts were prepared: *C. hypocistis* (CH); parasited *H. lasianthum* aerial parts (PHLAP); parasited *H. lasianthum* roots (PHLR); non-parasited *H. lasianthum* aerial parts (HLAP); and the non-parasited *H. lasianthum* aerial roots (HLR).

Figure 4.1. (a) Multiple inflorescences of the parasitic plant *Cytinus hypocistis* (L.) L. subsp. *macranthus* Wettst growing on the roots of a single host. (b) Plant host: *Halimium lasianthum* subsp. *alyssoides* (Lam.) Greuter.

Phenolic compounds characterisation

The freeze-dried extracts were dissolved in a mixture of ethanol:water (20:80 *v/v*, 5 mg/mL) and filtered through a 0.2 µm nylon filter (Whatman). The phenolic composition was analysed by HPLC-DAD-ESI/MS^n as formerly described [206,240]. When no standards were available, the UV spectra, fragmentation pattern, and retention time were used for phenolic compound tentative identification. The commercial standards used for quantification were: gallic acid; ellagic acid; apigenin-6-*C*-

glucoside; catechin; chlorogenic acid; naringenin; quercetin-3-*O*-glucoside; taxifolin; and *p*-coumaric acid. Their calibration curve, limit of detection (LOD), and limit of quantification (LOQ) are presented in **Table 4.1**. Compound quantification was presented as mg/g extract.

Bioactive properties characterisation

Antioxidant activity. The inhibition of thiobarbituric acid reactive substances formation (TBARS) and oxidative haemolysis (OxHLIA) was evaluated as described in **Chapter 3**. The results for both methods were presented as IC_{50} (µg/mL), the extract concentration required to offer 50% antioxidant protection.

Tyrosinase inhibitory activity. Tyrosinase inhibition was evaluated using L-dihydroxyphenylalanine (L-DOPA) as substrate and mushroom tyrosinase, as described in **Chapter 3**. The $IC_{50}s$ (µg/mL) were estimated from the inhibition percentage slopes using GraphPad Prism 9 (GraphPad Prism 9.1.1 for macOS, 2021 GraphPad Software, LLC).

Cytotoxic activity. The cytotoxic activity was assessed as described in **Chapter 3** for five cell lines, including the four tumour cell cultures: AGS (gastric adenocarcinoma), Caco-2 (colorectal adenocarcinoma), MCF-7 (breast adenocarcinoma), and NCI-H460 (large cell lung cancer). Additionally, a non-tumour cell line, the kidney epithelial cell line from an African green monkey (VERO - ECACC), was included in the study. The results were expressed as the sample concentrations required to inhibit 50% of the cell growth (GI_{50}: µg/mL).

Anti-inflammatory activity. The anti-inflammatory activity was evaluated in macrophages after lipopolysaccharide (LPS)-stimulation, as described in **Chapter 3**. The results were presented as extract concentration offering 50% NO inhibition (IC_{50}: µg/mL).

Antimicrobial activity. Different concentrations (0.1-20 mg/mL) of the five extracts were tested for antibacterial and antifungal activity against several microorganisms deposited at the University of Belgrade. As previously described, three Gram+ bacteria: *Staphylococcus aureus*, *Bacillus cereus*; and

Listeria monocytogenes, and three Gram- bacteria: *Escherichia coli*, *Salmonella* Typhimurium, and *Enterobacter cloacae* were used to assess the antibacterial potential of the extracts [241]. Additionally, the activity against 6 micromycetes was also evaluated: *Aspergillus fumigatus* (human isolate), *Aspergillus niger*, *Aspergillus versicolor*, *Penicillium funiculosum*, *Penicillium verrucosum var. cyclopium*, and *Trichoderma viride* [241,242]. The positive controls for antimicrobial and antifungal activity were streptomycin and ampicillin; and ketoconazole and bifonazole, respectively. The results were presented as the minimum concentration of extract (mg/mL) required to inhibit the growth of the microbes (MIC) or to exert a bactericidal (MBC) and fungicidal (MFC) effect.

Statistical analysis

The experiments were executed in triplicate, except for the antimicrobial activity, and the results were tested to their normal distribution and homogeneity of variance. The statistical analyses were performed using GraphPad Prism (GraphPad Prism 9.1.1 for macOS, 2021 GraphPad Software, LLC.). Significant differences were evaluated by variance analysis (ANOVA) and Tukey's HSD test ($\alpha =$ 0.05). The Student's t-test was used when comparing two independent groups ($\alpha = 0.05$). Principal Component Analysis (PCA) was performed as a pattern recognition technique to distinguish samples according to their phenolic profile and bioactivities. For a better interpretation of PCA, data from antioxidant, tyrosinase inhibition, cytotoxicity against tumour cells, anti-inflammatory, and antimicrobial (average MIC for Gram+, Gram-, and Micromycetes) activities were reciprocally (inverse) transformed ($1/IC_{50}$, $1/GI_{50}$ or $1/MIC$) before analysis since in bioactivity assays a lower value means higher activity. PCA was performed on standardised data, and the principal components (PCs) selection was executed using the Kaiser rule (eigenvalues higher than 1). Two PCs were selected and plotted to improve interpretation.

Results and discussion

Phenolic compounds characterisation

Table 4.1 displays the results of the tentative identification and quantification of phenolic compounds (also referred to as peaks) for both *C. hypocistis* and *H. lasianthum* extracts. The obtained profiles encompass a range of phenolic acids, flavonoids, and hydrolysable tannins.

Phenolic acids

Two hydroxycinnamic acids were identified in *H. lasianthum* roots. The 5-*O*-caffeoylquinic acid (Peak 9) was identified in the HLR using a commercial standard and confirmed by its UV spectra and deprotonated ion (λ_{max} 325 nm; *m/z* 353) [243]. The fragmentation pattern in MS^2 gave a major ion at *m/z* 191, corresponding to the deprotonated quinic acid and a minor at *m/z* 179 [caffeic acid-H]⁻. Compound 31, present in PHLR, was tentatively identified as a *p*-coumaroyl-monotropein derivative. It occurred as a formate adduct at *m/z* 581 rather than as a molecular ion at *m/z* 535, with a minor ion at *m/z* 355, consistent with the loss of *p*-coumaric acid (−164 u) and oxygen (−16 u) [244].

Table 4.1. Phenolic compounds identification and quantification in *H. lasianthum* and *C. hypocistis* extracts.

Peak	Rt (min)	λmax (nm)	[M-H]⁻ (m/z)	MS² (m/z)	Tentative identification	Content (mg/g extract)				
						Non-parasited *H. lasianthum*		Parasited *H. lasianthum*		*C. hypocistis*
						HLR	HLAP	PHLR	PHLAP	CH
1	3.60	275	331	**169**(100), 125(9)	Galloyl-glucose[1]	nd	nd	nd	nd	0.512 ± 0.004
2	4.03	275	483	**331**(100), 169(13)	Digalloyl-glucose[1]	nd	nd	nd	nd	3.5 ± 0.2
3	4.51	259	1083	781(86), 721(21), **601**(100), 575(25)	Punicalagin isomer[2]	nd	7.4 ± 0.3	nd	7.8 ± 0.1	nd
4	5.31	259	1083	1065(5), 785(62), 763(5), 721(23), **601**(100)	Gallagyl ester[1]	nd	8.0 ± 0.3	nd	11.3 ± 0.3	nd
5	5.47	275	635	483(40), **465**(100), 421(10), 313(5)	Trigalloyl-glucoside[1]	nd	nd	nd	nd	1.77 ± 0.09
6	5.55	260	593	503(2), **473**(100), 431(2), 311(1)	Apigenin-*C*-dihexoside[3]	nd	nd	0.010 ± 0.003	nd	nd
7	6.14	278	289	**245**(100), 203 (8)	(+)-Catechin[4]	nd	nd	nd	nd	2.23 ± 0.09
8	6.20	376	1085	**781**(100), 721(13), 601(99), 575(23), 549(18)	Digalloyl-gallagyl-hexoside[1]	nd	3.2 ± 0.1	nd	3.2 ± 0.1	nd
9	6.35	325	353	**191**(100), 179(6), 173(1), 161(1), 135(0.2)	5-*O*-Caffeoylquinic acid[5]	1.87 ± 0.01	nd	nd	nd	nd
10	8.09	275	635	483(21), **465**(100), 421(1), 313(1), 169(25)	Trigalloyl-glucoside[1]	nd	nd	nd	nd	0.46 ± 0.02
11	9.33	217/317	421	403(17), 331(89), **301**(100), 259(1)	Mangiferin[6]	0.06 ± 0.02	nd	nd	nd	nd
12	11.88	352	611	593(16), **317**(100), 271(14)	Myricetin 3-*O*-arabinogalactoside[7]	nd	1.078 ± 0.004	nd	1.225 ± 0.001	nd
13	12.84	350	465	447(57), 437(68), 303(43), **285**(100), 259(32)	Taxifolin-*O*-hexoside[8]	0.25 ± 0.02	nd	0.222 ± 0.002	nd	nd
14	13.36	338	431	341(4), **311**(100), 283(3)	Apigenin-*C*-hexoside[3]	nd	nd	0.182 ± 0.004	nd	nd
15	13.90	277	937	785(64), **767**(100), 465(70), 301(94)	Trigalloyl-HHDP-glucoside[2]	nd	3.0 ± 0.1	nd	nd	5.4 ± 0.1
16	14.18	354	479	461(3), **316**(100), 317(87)	Myricetin-*O*-hexoside[7]	nd	1.23 ± 0.01	nd	1.15 ± 0.01	nd
17	14.34	275	787	635(25), **617**(100), 465(5)	Tetragalloyl-glucoside I[1]	nd	nd	nd	nd	6.6 ± 0.2
18	15.40	275	787	635(25), **617**(100), 465(5)	Tetragalloyl-glucoside II[1]	nd	nd	nd	nd	2.3 ± 0.1
19	15.64	275	787	635(25), **617**(100), 465(5)	Tetragalloyl-glucoside III[1]	nd	nd	nd	nd	8.5 ± 0.1
20	16.33	351	463	**316**(100), 317(62)	Myricetin-*O*-rhamnoside[7]	nd	4.7 ± 0.2	nd	3.829 ± 0.009	nd
21	17.22	357	463	**301**(100)	Quercetin-*O*-hexoside[7]	1.03 ± 0.02	nd	nd	nd	nd
22	17.55	352	463	317(42), 316(76), **301**(100)	Quercetin-3-*O*-glucoside[7]	1.02 ± 0.01	1.146 ± 0.002	nd	1.115 ± 0.005	nd
23	17.90	275	939	787(50), **769**(100), 617(10), 599(5)	Pentagalloyl-glucoside[1]	nd	nd	nd	nd	10.4 ± 0.5
24	18.30	278	935	**783**(100), 765(13), 633(5), 301(5)	Galloyl-bis-HHDP-glucose I[2]	nd	nd	nd	nd	26 ± 1
25	19.06	272/353	505	463(23), **301**(100)	Quercetin-*O*-acetylhexoside[7]	nd	2.495 ± 0.005	nd	1.010 ± 0.004	nd

#	Rt	λmax	[M-H]⁻	MS²	Compound	CH	PHLAP	PHLR	HLAP	HLR
26	20.03	354	433	342(2), 307(1), **301**(100)	Quercetin-*O*-pentoside[7]	nd	0.987 ± 0.002	nd	1.024 ± 0.005	nd
27	20.31	353	491	**315**(100)	Isorhamnetin-*O*-glucuronide[7]	nd	nd	nd	1.16 ± 0.01	nd
28	20.48	353	771	551(51), 533(59), 463(16), **317**(100), 265(48)	Myricetin-*O*-coumaroyl-deoxyhexoside-hexoside[7]	nd	1.000 ± 0.004	nd	nd	nd
29	20.72	278	935	**783**(100), 765(15), 633(8), 301(7)	Galloyl-bis-HHDP-glucose II[2]	nd	nd	nd	nd	9.4 ± 0.4
30	20.92	348	447	429(2), 343(1), 327(1), **301**(100), 285(5)	Quercetin-3-*O*-rhamnoside[7]	nd	1.13 ± 0.01	nd	1.204 ± 0.002	nd
31	20.98	277	581	**535** (100), 355(21)	*p*-Coumaroyl-monotropein derivative[9]	0.32 ± 0.01	nd	0.141 ± 0.007	nd	nd
32	21.44	278	1087	**935**(100), 783(20), 633(3), 301(11)	Digalloyl-bis-HHDP-glucose I[2]	nd	nd	nd	nd	7.31 ± 0.07
33	23.02	277	1087	**935**(100), 783(18), 633(5), 301(14)	Digalloyl-bis-HHDP-glucose II[2]	nd	nd	nd	nd	8.6 ± 0.1
34	23.76	278	1087	**935**(100), 783(18), 633(5), 301(14)	Digalloyl-bis-HHDP-glucose III[2]	nd	nd	nd	nd	3.32 ± 0.01
35	25.53	277	1257	**1087**(100), 935(66), 783(15), 633(5), 301(12)	Trigalloyl-bis-HHDP-glucose I[2]	nd	nd	nd	nd	5.9 ± 0.3
36	26.77	277	1257	**1087**(100), 935(55), 783(13), 633(5), 301(10)	Trigalloyl-bis-HHDP-glucose II[2]	nd	nd	nd	nd	2.9 ± 0.1
37	27.10	346	1187	901(68), 635(11), **593**(100), 447(5)	Kaempferol-coumaroyl-hexoside[7]	nd	0.976 ± 0.005	nd	0.996 ± 0.001	nd
38	31.70	269/332	593	575(1), 447(13), 327(1), 307(7), **285**(100)	Kaempferol-*O*-rhamnoside-*O*-hexoside[7] Kaempferol-coumaroyl-hexoside[7]	nd	1.122 ± 0.006	nd	1.001 ± 0.004	nd
39	31.91	270/333	593	575(1), 447(14), 327(2), 307(8), **285**(100)	Kaempferol-*O*-rhamnoside-*O*-hexoside[7] Kaempferol-coumaroyl-hexoside[7]	nd	1.057 ± 0.005	nd	0.985 ± 0.001	nd
Σ Phenolic acids						2.19 ± 0.02ᵃ	nd	0.141 ± 0.007ᵇ	nd	nd
Σ Flavonoids						2.359 ± 0.002ᶜ	16.9 ± 0.2ᵃ	0.414 ± 0.006ᵈ	14.70 ± 0.01ᵇ	2.23 ± 0.09ᶜ
Σ Hydrolysable tannins						nd	21.7 ± 0.2ᵇ	nd	22.3 ± 0.5ᵇ	103 ± 2ᵃ
Σ Phenolic compounds						4.55 ± 0.02ᶜ	38.6 ± 0.4ᵇ	0.55 ± 0.01ᵈ	37.0 ± 0.5ᵇ	105 ± 2ᵃ

Rt: Retention time in minutes; **λ$_{max}$**: wavelength (nm) of maximum absorption in the UV–visible region; **[M-H]⁻**: deprotonated ion (negative ion mode); **MS²** fragment ions generated in MS² spectra and relative abundance in brackets; **CH**: *C. hypocistis* extract; **PHLAP:** Parasited *H. lasianthum* aerial extract; **PHLR:** Parasited *H. lasianthum* roots extract**; HLAP:** Non-parasited *H. lasianthum* aerial extract; **HLR**: Non-parasited *H. lasianthum* roots extract. **nd**: not determined. Calibration curve: **compound** (equation; R^2; LOD; LOQ both expressed in µg mL⁻¹). [1]**Gallic acid** (y = 131538x + 292163; 0,9969; 8.05; 24.41); [2]**Ellagic acid** (y = 26719x - 317255; 0.9986; 41.20; 124.84); [3]**Apigenine-6-C-glucoside** (y = 107025x + 61531; 0.9989; 0.19; 0.63); [4]**Catechin** (y = 84950x - 23200; 1; 0.17; 0.68); [5]**Chlorogenic acid** (y = 312503x - 199432; 0.9999; 0.20; 0.68); [6]**Naringenin** (y = 18433x + 78903; 0.9998; 0.17; 0.81); [7]**Quercetin-3-*O*-glucoside** (y = 34843x – 160173; 0.9998; 0.21; 0.71); [8]**Taxifolin** (y = 203766x - 208383; 1; 0.67; 2.02); [9]***p*-Coumaric acid** (y = 301950x + 6966; 0.9999; 0.68; 1.61). In each row, different letters mean significant differences between samples (*p* < 0.05).

Flavonoids

A total of eighteen flavonoids were tentatively identified: four flavones (peaks 6, 11, 14, and 27), one flavan-3-ol (peak 7), one flavanonol (peak 13), and twelve flavonols (peaks 12, 16, 20 to 22, 25, 26, 28, 30, and 37 to 39). Compounds 6 and 14 were tentatively identified as apigenin derivatives (PHLR extract). Apigenin-*C*-dihexoside (Peak 6) presented a deprotonated ion at *m/z* 593 and a major peak at *m/z* 473 [M–H−120]⁻, characteristic of di-*C*-glycosyl flavones. The MS^n fragment at 311 indicated the loss of a hexosyl moiety [M–H−162]⁻ and the presence of apigenin (MW 270) as aglycone. Compound 14 gave a [M−H]⁻ ion at *m/z* 431, and its MS^n spectrum yielded ions at *m/z* 341 [M−H−90]⁻ and 311 [M−H−120]⁻, thus being identified as apigenin-*C*-hexoside [245]. Compound 11 (HLR extract) was tentatively identified as mangiferin, a *C*-glycoside of monomeric xanthones with a pseudo-molecular ion at *m/z* 421, showing two characteristic ions ([M–H–90]⁻ and [M–H–120]⁻) at *m/z* 331 and 301, corresponding to the different parts of the glucose moiety in the MS^2 analysis. The two minor ions at *m/z* 403 and 259 correspond to a typical loss of a water molecule (−18 u) and a fragment of the glucose moiety (−72 u), respectively [246]. Compound 27 was tentatively identified as isorhamnetin-*O*-glucuronide based on its deprotonated ion (*m/z* 491) and MS^2 spectra, releasing fragments corresponding to isorhamnetin (*m/z* 315) and the loss of a glucuronide moiety (−176 u) [247]. Compound 7, present in the *C. hypocistis* extract, was identified as (+)-catechin, based on its MS^2 pattern, showing two typical ions corresponding to the loss of CO_2 (major ion at *m/z* 245) and an A-ring of flavan-3-ol (minor ion at *m/z* 203) [215]. Compound 13 ([M−H]⁻ at *m/z* 465) present in the root extracts of the parasited and non-parasited *H. lasianthum* lost a fragment ion (*m/z* 303; [taxifolin−H]⁻) and a hexosyl moiety (−162 u), being identified as taxifolin-*O*-hexoside [248]. Peaks 12, 16, 20, and 28 exhibited a UV spectrum and ion fragmentation similar to myricetin glycoside derivatives. These compounds presented a typical MS^2 fragmentation of an ionised myricetin (*m/z* 317). Compound 12 (*m/z* 611), identified as myricetin 3-*O*-arabinogalactoside in the PHLAP extract, presented a fragment ion at *m/z* 317 ([myricetin−H]⁻); the difference represented the loss of the sugar moiety (arabino-

galactose; MW 312). This compound also exhibited a major fragment at *m/z* 316; however, *m/z* 317 is the fragment consistent with the cleavage into the aglycone myricetin; this anomalous fragmentation pattern has been reported previously for quercetin derivatives [249]. The minor ion at *m/z* 271 is characteristic of 3-*O*-monoglycosides [250]. Myricetin-*O*-hexoside (peak 16) and myricetin-*O*-rhamnoside (peak 20) were tentatively identified in the non-parasited (HLAP) and parasited (PHLAP) aerial extracts of *H. lasianthum*, with deprotonated ions [M−H]⁻ at *m/z* 479 and 463, respectively. Both compounds exhibited two common MS^2 fragments of myricetin (*m/z* 317 and 316) after the release of a hexosyl (−162 u) and a rhamnoside (−146 u) moiety [250–253]. Compound 28 showed [M–H]⁻ ion at *m/z* 771, and further fragmentation at *m/z* 463 [M–H–308]⁻ and *m/z* 317 [(M–H)–308+146]⁻, suggesting the losses of coumaric acid and deoxyhexoside-hexoside groups, and the presence of myricetin (MW 317) [252]. Compounds 21, 22, 25, 26, and 30 showed UV spectra and MS^2 a fragment at *m/z* 301, typical of quercetin glycoside derivatives. Compound 21 (HLR extract) was identified as quercetin-*O*-hexoside by the presence of a pseudo-molecular ion [M−H]⁻ at *m/z* 463 and a major fragment at *m/z* 301 (loss of a hexosyl residue) [254]. Compound 22 (HLR, HLAP, and PHLR extracts) was positively identified as quercetin-3-*O*-glucoside using a commercial standard. Compound 25 (PHLAP) was assigned as quercetin-*O*-acetylhexoside ([M–H]− at *m/z* 505) according to its deprotonated ion and MS^2 spectra, releasing fragments corresponding to the losses of an acetyl residue (−42 u) and a hexosyl moiety (−162 u) [254]. Quercetin-*O*-pentoside (compound 26; *m/z* 433; HLAP and PHLAP extracts) and quercetin-3-*O*-rhamnoside (compound 30; *m/z* 447; HLAP and PHLAP extracts) were identified using their deprotonated ions and MS^2 fragments, consistent with quercetin (*m/z* at 301), and the loss of pentosyl (−132 u) and rhamnosyl (−146 u) moieties, respectively [253]. Compounds 37, 38, and 39 in HLAP and PHLAP extracts exhibited a UV spectrum and a MS^2 fragmentation typical of kaempferol glycoside derivatives. Compound 37 was identified as an isomer of a kaempferol-coumaroyl-hexoside by its deprotonated ion [M−H]⁻ at *m/z* 593, artefact peak [2M−H]⁻ at *m/z* 1187, and a MS^2 fragment at m/z 447 [255]. Compounds 38 and 39 (*O*-rhamnoside-

O-hexoside and kaempferol-coumaroyl-hexoside, respectively) had a molecular ion [M−H]⁻ at *m/z* 593 that generated one minor MS² fragment at *m/z* 447 (rhamnose moiety release) and a major at 285 (release of rhamnose and hexose moieties), which is in agreement with kaempferol-*O*-rhamnoside-*O*-hexoside tentative identification [254]. Kaempferol-coumaroyl-hexoside is also a possible tentative identification for peaks 38 and 39 due to their [M-H]⁻ at *m/z* 593, a MS² minor fragment at *m/z* 447, and a major fragment at *m/z* 285 (loss of 308 u, M–coumaroyl–hexose moiety) [255]. The acylation of flavonoids increases their molecular size and changes the spatial structure of the flavonoid aglycone, as it occurs with anthocyanin compounds [256]. These structural changes decrease the polarity of the entire molecule, increasing their retention time in a reversed-phase column, as used in the present study.

Hydrolysable tannins

Gallotannins or galloylated esters of glucose show the elimination of multiple galloyl [M–H–152]⁻ and gallate [M–H–170]⁻ moieties in MSⁿ analysis. Compounds 1 ([M–H]⁻ at *m/z* 331) and 2 ([M–H]⁻ at *m/z* 483) were deduced as galloyl-glucose and digalloyl-glucose, respectively. These CH compounds exhibited the release of one and two galloyl moieties, characterised by MS² fragments at *m/z* 331 and 169 and the loss of a glucose moiety (−162 u) [216,240]. Compounds 5 and 10 were tentatively identified as trigalloyl-glucose, exhibiting a [M–H]⁻ at *m/z* 635 and a characteristic MS² fragment at *m/z* 483, denoting the release of one galloyl group (−152 u). Fragment ions at *m/z* 465 and 313, frequently found on the fragmentation pattern of gallotannins (loss of galloyl groups), were also observed [216]. Compound 3 (HLAP and PHLAP extracts) was tentatively identified as a punicalagin isomer, with a molecular ion [M−H]⁻ at *m/z* 1083 that yielded a MS² fragmentation pattern of punicalin (*m/z* 781), *m/z* 721, *m/z* 601, and *m/z* 575 [220,257]. Compound 4 (PHLAP extract) also exhibited a deprotonated molecular ion at *m/z* 1083. Still, the MS² fragmentation pattern differed from punicalagin (**Table 4.1**). The presence of a specific major daughter ion (*m/z* 601) suggested the existence of a gallagyl derivative, most probably an ester [220]. Compound 8 (HLAP extract) was tentatively

identified as digalloyl-gallagyl-hexoside, with a deprotonated ion at m/z 1085, denoting the release of two galloyls $[M–H–152+152]^-$ and the presence of a gallagyl-hexose (m/z 781). The minor MS^2 fragment at m/z 601 (gallagyl) shows the consistent mass release of a hexose (−162 u) and a water molecule (−18 u) [220]. Compound 15 (HLAP and CH) was tentatively identified as trigalloyl-HHDP-glucoside, exhibiting a $[M−H]^-$ at m/z 937 and a characteristic MS^2 at m/z 301 (ellagic acid). The product ions at m/z 767 and 465 are coherent with the release of gallic acid and hexahydroxydiphenoyl (HHDP) + gallic acid [258]. Isomers 17, 18, and 19 in the *C. hypocistis* extract were tentatively identified as tetragalloyl-glucoside I, II, and III, respectively. All compounds presented a pseudo-molecular ion at m/z 787 and a representative MS^2 fragment at m/z 635 (trigalloyl-glucose), coherent with the release of one galloyl group (−152 u). Their product ions at m/z of 617 and 465 correspond to the release of gallate (−170 u) and galloyl (−152 u) moieties, respectively [218]. Pentagalloyl-glucoside (compound 23; CH extract) was tentatively identified based on its $[M−H]^-$ at m/z 939 and fragments at m/z 787 and 769, recognised as the release of a galloyl moiety $[M–H–152]^-$ and a water molecule, respectively. The major fragment (m/z 769) experienced the release of a galloyl and a water molecule, creating m/z at 617 and 599, respectively [259]. Compounds 24 and 29 in the CH extract were tentatively identified as galloyl-bis-HHDP-glucose I and II, respectively. Both compounds presented the same deprotonated ion at m/z 935, and MS^2 fragments at m/z 783, 765, 633, and 301, possibly due to the release of a galloyl (–152 u), a water molecule (−18 u), and two HHDP moieties (–301 u), respectively [215]. Digalloyl-bis-HHDP-glucose I, II, and III (compounds 32, 33, and 34, respectively) and trigalloyl-bis-HHDP-glucose I and II (compounds 35 and 36, respectively) were tentatively identified in the CH extract. The product ions at m/z 1087 and 1257 unveil the consecutive release of two and three galloyl moieties, respectively. This and a fragmentation pattern like galloyl-bis-HHDP-glucose allowed its identification [215,240].

Among the five studied extracts, thirty-nine compounds were tentatively identified. Flavonoids were the principal group of phenolic compounds identified in the host extracts, while hydrolysable tannins

were the major group in the parasite extract. These results are consistent with the available data for *C. hypocistis* and the only published study regarding *Halimium* genus phytochemical profile [240,260]. Phenolic acids were only identified in the roots of *H. lasianthum*; the highest concentration was found in the non-parasited extract. The highest concentration of flavonoids was observed in the non-parasited *H. lasianthum* aerial parts and the lowest in the parasited *H. lasianthum* roots. CH extract exhibited the highest concentration of phenolic compounds, followed by HLAP/PHLAP, HLR, and PHLR.

Bioactive properties characterisation

Antioxidant activity. Lipid peroxidation is a sequence of damaging reactions in cell membranes. During OxHLIA, the hydrophilic radicals arise from AAPH and attack the membranes; this attack will then generate lipophilic radicals through lipid peroxidation. OxHLIA was used to evaluate the antioxidant ability of the extracts to capture radicals and, consequently, retard haemolysis in sheep erythrocytes [261]. The TBARS assay is a simple and low-cost method to screen lipid peroxidation. During this assay, malondialdehyde (MDA), a degradation product of polyunsaturated fatty acids (*Sus scrofa domesticus* brain tissue), reacts with thiobarbituric acid (TBA) and forms a characteristic [MDA-(TBA)$_2$] complex. The obtained results for both methods are presented in **Table 4.2**. Concerning OxHLIA, the CH extract (*C. hypocistis*) gave the best antioxidant effect, with an IC$_{50}$ of 7.3 µg/mL. The extracts HLAP (IC$_{50}$: 18 µg/mL) and HLR (IC$_{50}$: 14 µg/mL), both from the non-parasited *H. lasianthum*, exhibited the second-best results and a similar IC$_{50}$ to the positive control Trolox (IC$_{50}$: 21.8 µg/mL). The extracts from the parasited *H. lasianthum* were the least antioxidant, exhibiting the highest IC$_{50}$ (PHLR: 307 µg/mL and PHLAP: 63 µg/mL).

Similarly, to OxHLIA, the CH extract displayed the best result during TBARS, with an IC$_{50}$ of 1.11 µg/mL, followed by the non-parasited *H. lasianthum* roots and aerial extracts, 5.3 µg/mL and 5.7 µg/mL, respectively. The root extract of the parasited *H. lasianthum* (PHLR: 9.5 µg/mL) and the positive control (Trolox: 9.1 µg/mL) presented similar results. For both antioxidant methods, the best result was obtained by *C. hypocistis*, followed by the non-parasited and parasited *H. lasianthum*

extracts. In previous work, *C. hypocistis* presented a lower IC_{50} for OxHLIA and TBARS [240]. Harvest time/year and extraction methodologies have been suggested to affect plants' phenolic composition and concentration [262–264]. Analysing the available phenolic profiles of *C. hypocistis*, it is possible to observe a decrease/increase in the concentration of certain phenolic compounds present in the extracts [240]. Galloyl-bis-HHDP-glucose, for example, was the major compound identified in the extract, but its extracted concentrations decreased from the sample harvested in 2019 to the present work (2020). These differences could be attributed to variations in foraging years and the extraction methodology employed (maceration at room temperature versus HAE at 46.4 °C). Plant extracts are complex, containing hundreds or even thousands of individual compounds. This complexity arises from the number of bioactive species in the extract and their synergistic, additive, or antagonistic properties [265]. Therefore, the variations in bioactivity results of the present work, when compared with the previous studies, might be accountable to the plant extract particularities mentioned above. Regarding the *Halimium* genus, this work confirms the good antioxidant activity exhibited by *Halimium* ethanolic extracts in previous studies [260,266].

Tyrosinase inhibitory activity. Besides being a target for the development of depigmenting agents, the involvement of tyrosinase in skin-related pathologies, such as hyperpigmentation and melanoma, is currently acknowledged [240,267]. The concentrations (µg/mL) required to inhibit 50% of tyrosinase activity were estimated from the slope of the obtained inhibition percentages (**Table 4.2**). All hydroethanolic extracts inhibited enzyme activity. CH exhibited the most significant result (8 µg/mL), followed by HLAP/PHLR/PHLAP (11, 9, and 9 µg/mL, respectively) and HLR (12 µg/mL). Although using different methods, in the present work, *C. hypocistis* displayed a better IC_{50} than in a previous publication and a similar result to Maisetta and colleagues (Maisetta et al., 2019; Silva et al., 2020).

Cytotoxic activity. Phenolic compounds have shown promising antitumor properties in *in vitro* and *in vivo* studies. Their cytotoxic effect is typically associated with their effect as oxidative stress

modulators, apoptosis inducers, cell proliferation inhibitors, tumour cell cycle blockers, and angiogenesis/metastasis suppressors [268]. The results of the cytotoxic activity against the five tested cell lines are presented in **Table 4.2**. Ellipticine was highly effective against the four tumour cell lines; all values were significantly inferior to the extracts. Regarding the growth inhibition of the human gastric adenocarcinoma (AGS), the best results were obtained with CH (20.9 µg/mL) and HLAP (24 µg/mL) extracts, followed by PHLAP (47.6 µg/mL), and PHLR (53 µg/mL). No cytotoxic activity (up to 400 µg/mL) was observed for the HLR extracts. For the human colorectal adenocarcinoma cell line, the two extracts of the parasited *H. lasianthum* exhibited the best results (PHLAP: 41 µg/mL and PHLR: 44 µg/mL), followed by HLR (55 µg/mL), CH (64.1 µg/mL), and HLAP (70 µg/mL). Concerning breast adenocarcinoma (MCF-7) and non-small cell lung cancer (NCI-H460), the PHLR extract obtained the lowest GI_{50} (23.8 µg/mL and 19.2 µg/mL, respectively) and HLAP the highest (175 µg/mL and 85 µg/mL, respectively). For MCF-7, PHLAP (53 µg/mL) and HLR (50 µg/mL) presented the second best GI_{50} values, followed by CH (90 µg/mL). The second best GI_{50} results for NCI-H460 were exhibited by the CH (50 µg/mL) and HLR (44 µg/mL) extracts, followed by PHLAP (62.4 µg/mL). In absolute terms, the parasited *H. lasianthum* roots extract (PHLR) was the most effective, exhibiting the lowest GI_{50} for three of the four tumour cell lines. NCI-H460 (GI_{50} = 19.2 µg/mL) was the most susceptible cell line to PHLR.

Although using different cell lines and extracts, in the present study (MCF-7: 90 µg/mL) and Magiatis and colleagues' work (MDA-MB-231: 29 to 50 µg/mL), *C. hypocistis* presented similar cytotoxic activity against human breast adenocarcinoma [172].

Table 4.2. Antioxidant, enzyme inhibitory, cytotoxic, and anti-inflammatory activities of *C. hypocistis* and *H. lasianthum* extracts.

	HLR	HLAP	PHLR	PHLAP	CH	Positive control
Antioxidant activity (IC$_{50}$, µg/mL)						Trolox
OxHLIA (*Δt:* 60 min)	14.0 ± 0.1^{ab}	18 ± 1^{ab}	307 ± 12^{d}	18 ± 1^{ab}	7.3 ± 0.3^{a}	21.8 ± 0.2^{b}
TBARS	5.3 ± 0.2^{b}	5.7 ± 0.1^{b}	9.5 ± 0.9^{d}	7.10 ± 0.01^{c}	1.11 ± 0.01^{a}	9.1 ± 0.3^{d}
Enzyme inhibitory activity (IC$_{50}$, µg/mL)						Kojic acid*
Tyrosinase	12 ± 1^{c}	11 ± 1^{bc}	9 ± 1^{bc}	9 ± 2^{bc}	8 ± 1^{b}	1.7 ± 0.2^{a}
Cytotoxic activity (GI$_{50}$, µg/mL)						Ellipticine*
AGS	>400	24 ± 1^{a}	53 ± 4^{c}	47.6 ± 0.8^{b}	20.9 ± 0.9^{a}	1.23 ± 0.03
Caco-2	55 ± 1^{b}	70 ± 2^{d}	44 ± 2^{a}	41 ± 1^{a}	64.1 ± 0.7^{c}	1.21 ± 0.02
MCF-7	50 ± 1.2^{b}	175 ± 8^{d}	23.8 ± 0.8^{a}	53 ± 2^{b}	90 ± 7^{c}	1.02 ± 0.02
NCI-H460	44.0 ± 0.6^{b}	85 ± 4^{d}	19.2 ± 0.4^{a}	62.4 ± 0.5^{c}	50 ± 3^{b}	1.01 ± 0.01
VERO	184 ± 1^{c}	159 ± 7^{b}	61 ± 4^{a}	163 ± 11^{b}	286.2 ± 0.8^{d}	1.41 ± 0.06
Anti-inflammatory activity (IC$_{50}$, µg/mL)						Dexamethasone*
RAW 264.7	76 ± 2^{a}	243 ± 14^{b}	73 ± 4^{a}	223 ± 11^{b}	86 ± 4^{a}	6.3 ± 0.4

HLR: Non-parasited *H. lasianthum* roots extract; **HLAP**: Non-parasited *H. lasianthum* aerial extract; **PHLR**: Parasited *H. lasianthum* roots extract; **PHLAP**: Parasited *H. lasianthum* aerial extract; **CH**: *C. hypocistis* extract; **AGS**: human gastric adenocarcinoma; **Caco-2**: human colorectal adenocarcinoma; **MCF-7**: breast adenocarcinoma; **NCI-H460**: non-small cell lung cancer; **VERO**: kidney epithelial cell line of an African green monkey. The results are presented as IC$_{50}$ or GI$_{50}$ mean $\pm$ SD. In each row, different letters mean significant differences between samples ($p < 0.05$). *The positive controls ellipticine and dexamethasone differ significantly from the plant extracts ($p < 0.05$).

The cytotoxic activity of *C. hypocistis* extracts against MCF-7 and NCI-H460 was also described in previous work [240], where its extracts exhibited higher GI_{50} (117 µg/mL and 102 µg/mL, respectively) compared with the current study (90 µg/mL and 49.8 µg/mL, respectively).

To determine whether the tested extracts have a toxic effect on normal cells, they were tested against the non-tumoral VERO (kidney epithelial cell line of an African green monkey) up to the maximum concentration of 400 µg µg/mL. Except for the extract HLAP against MCF-7 and HLR against AGS, all the other extracts exhibited cytotoxic effects against VERO cells at higher concentrations than the optimal GI_{50} obtained for the tested tumour cell lines. The CH extracts obtained the best result, with a GI_{50} of 286.2 µg/mL.

Anti-inflammatory activity. Inflammation is a non-specific immune response to neutralise external agents and repair tissues. Plants have been successfully employed worldwide in traditional medicine to treat inflammation processes within the body. Therefore, there is a constant pursuit of novel and more efficient naturally occurring molecules or their synthetic derivatives as anti-inflammatory agents [269,270]. The extracts exhibiting the lowest IC_{50} (**Table 4.2**) were CH (86 µg/mL), HLR (76 µg/mL), and PHLR (73 µg/mL), followed by HLAP (243 µg/mL) and PHLAP (223 µg/mL). In the present work, *C. hypocistis* exhibited an anti-inflammatory IC_{50} of 86 µg/mL, lower than the 136 µg/mL previously obtained [240].

Antimicrobial activity. Phenolic compounds are well-known plant-based antimicrobials by increasing their membrane permeability, acidifying the pH, and altering efflux pumping. Scientists have been collecting evidence that plant extracts enhance conventional antimicrobial and preservative activities, serving as adjuvants and replacements. Accordingly, searching for novel compounds derived from plants has become an emergent area of great interest for developing combined treatments [269,271,272]. The five hydroethanolic extracts were assessed for their antibacterial activity (**Table 4.3**) against Gram-positive and Gram-negative bacteria. All the tested extracts exhibited antibacterial

activity. Streptomycin was shown to be the most effective antibiotic; all its MICs and MBCs were inferior to the tested extracts and ampicillin. Both *H. lasianthum* aerial extracts (PHLAP and HLAP, respectively) presented lower MIC (0.50 mg/mL) and MBC (1.00 mg/mL) than the antibiotic ampicillin (MIC: 0.75 mg/mL; MBC: 1.20 mg/mL) against *S.* Typhimurium. Similarly, the parasited *H. lasianthum* aerial extract (MIC: 0.25 mg/mL; MBC: 0.50 mg/mL) produced lower MIC and equal MBC than ampicillin (MIC: 0.40 mg/mL; MBC: 0.50 mg/mL) for *E. coli*. Concerning *B. cereus*, two of the tested extracts (CH and HLR) exhibited equal MICs (0.25 mg/mL) and slightly higher MBC (0.50 mg/mL) than ampicillin (MBC: 0.40 mg/mL). For all the other tested bacteria, ampicillin generated better results. Regarding two tested microorganisms (*E. coli* and *L. monocytogenes*), CH extracts exhibited better MICs and MBCs than in a preliminary study [240].

The antifungal activity of the extracts (**Table 4.3**) was tested against five species capable of synthesising toxic metabolites. All the extracts exhibited antifungal activity against the tested micromycetes. Bifonazole was the most effective fungicide; all its MICs and MFCs were inferior to the tested extracts and ketoconazole. The aerial extracts from the non-parasited *H. lasianthum* exhibited identical MFCs (0.50 mg/mL) than ketoconazole and slightly higher MICs (0.20 mg/mL versus 0.25 mg/mL) against *A. versicolor* and *P. funiculosum*. Similarly, the parasited *H. lasianthum* root extract (PHLR) showed equal MFC (0.50 mg/mL) and slightly higher MIC (0.25 mg/mL) against *P. funiculosum*. *C. hypocistis* (CH) exhibited better MIC (0.25 mg/mL) and MFC (0.25 mg/mL) than the fungicide ketoconazole (MIC and MFC: 1.0 mg/mL) against *T. viride*.

Table 4.3. Antimicrobial activity of *C. hypocistis* and *H. lasianthum* extracts (mg/mL)

	HLR		HLAP		PHLR		PHLAP		CH		Ampicillin		Streptomycin	
	MIC	MBC	MIC	MBC	MIC	MBC	MIC	MBC	MIC	MBC	MIC	MBC	MIC	MBC
Gram-positive bacteria														
Staphylococcus aureus	1.00	2.00	0.50	1.00	0.50	1.00	1.00	2.00	1.00	2.00	0.25	0.45	0.04	0.10
Bacillus cereus	0.25	0.50	0.25	0.50	0.25	0.50	0.50	1.00	0.25	0.50	0.25	0.40	0.10	0.20
Listeria monocytogenes	1.00	2.00	1.00	2.00	0.50	1.00	1.00	2.00	1.00	2.00	0.40	0.50	0.20	0.30
Gram-negative bacteria														
Escherichia coli	1.00	2.00	0.50	1.00	0.50	1.00	0.25	0.50	0.50	1.00	0.40	0.50	0.20	0.30
Salmonella Typhimurium	1.00	2.00	0.50	1.00	1.00	2.00	0.50	1.00	1.00	2.00	0.75	1.20	0.20	0.30
Enterobacter cloacae	1.00	2.00	1.00	2.00	0.50	1.00	1.00	2.00	1.00	2.00	0.25	0.50	0.20	0.30
											Ketoconazole		Bifonazole	
Micromycetes	MIC	MFC	MIC	MFC	MIC	MFC	MIC	MFC	MIC	MFC	MIC	MFC	MIC	MFC
Aspergillus fumigatus	0.50	1.00	0.50	1.00	0.50	1.00	0.50	1.00	0.50	1.00	0.25	0.50	0.15	0.20
Aspergillus niger	0.50	1.00	0.50	1.00	0.50	1.00	0.50	1.00	0.50	1.00	0.20	0.50	0.15	0.20
Aspergillus versicolor	0.50	1.00	0.25	0.50	0.50	1.00	0.50	1.00	0.50	1.00	0.20	0.50	0.15	0.20
Penicillium funiculosum	0.50	1.00	0.25	0.50	0.25	0.50	0.50	1.00	0.50	1.00	0.20	0.50	0.20	0.25
Penicillium verrucosum var. cyclopium	0.50	1.00	0.50	1.00	0.50	1.00	0.50	1.00	0.50	1.00	0.20	0.30	0.10	0.20
Trichoderma viride	0.50	1.00	0.50	1.00	0.50	1.00	0.50	1.00	0.25	0.50	1.00	1.00	0.15	0.20

HLR: Non-parasited *H. lasianthum* roots extract; **HLAP**: Non-parasited *H. lasianthum* aerial extract; **PHLR**: Parasited *H. lasianthum* roots extract; **PHLAP**: Parasited *H. lasianthum* aerial extract; **CH**: *C. hypocistis* extract; **MIC**: Minimum inhibitory concentration in mg/mL; **MBC**: Minimum bactericidal concentration in mg/mL; **MFC**: minimal fungicidal concentration in mg/mL; **Positive controls**: ampicillin, streptomycin, ketoconazole, and bifonazole.

Principal component analysis (PCA)

Principal component analysis (PCA) was applied to analyse the differences between extracts according to their phenolic composition and bioactivities. The model explained 67% of the observed variance with the first two principal components (PCs). Score and loading plots on PC2 vs PC1 are shown in **Figure 4.2**.
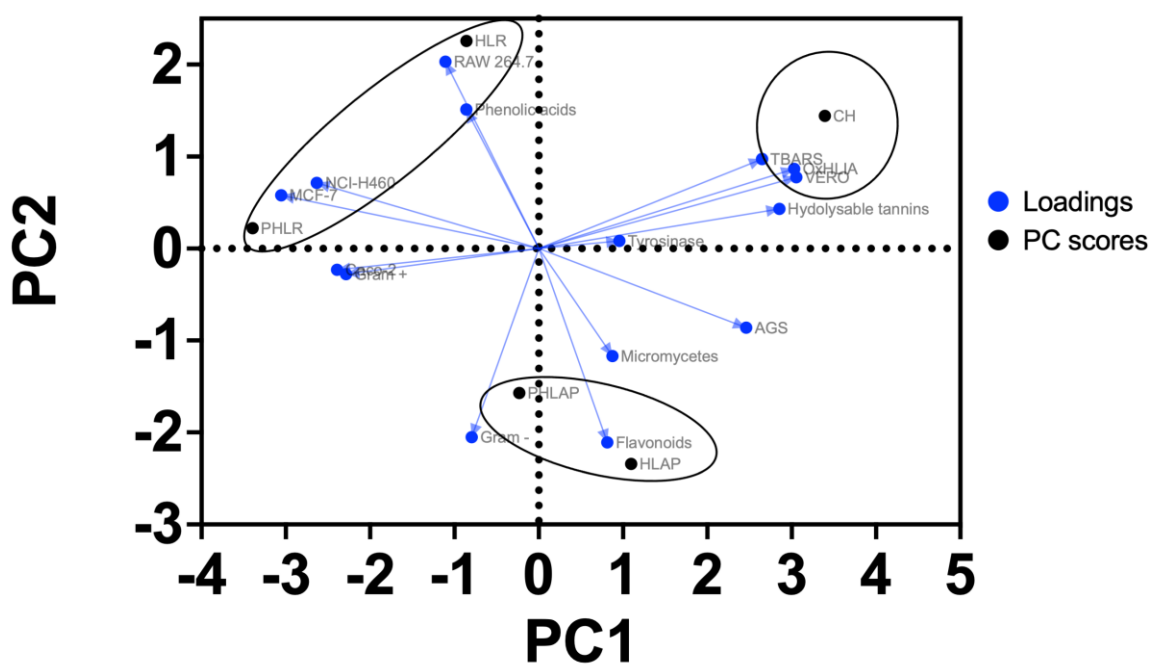
Figure 4.2. Biplot of the five hydroethanolic extracts as PC scores, and phenolic composition and evaluated bioactivities as loadings.

PC1 explained 37.8% of the model total variance, with hydrolysable tannins, OxHLIA, TBARS, AGS, MCF-7, NCI-H460, and VERO the loadings with the biggest impact on this component. Flavonoids, RAW 264.7, and Gram- were the loadings with the highest impact on the PC2, explaining 28.1% of the model's total variance. Analysing **Figure 4.2**, it was possible to distinguish three groups: Group 1, containing the extracts from the host roots (HLR and PHLR); Group 2, comprising the aerial extracts of the host (HLA and PHLA); and Group 3, inclosing *C. hypocistis* extract (CH). Group 1 was characterised by high anti-inflammatory activity, low flavonoid content, high cytotoxic activity against MCF-7 and NCI-H460, and low cytotoxicity against AGS. Group 2 was defined by a high MIC against

Gram-negative bacteria, high flavonoid content, and good cytotoxic activity towards AGS cells. Finally, Group 3 was interpreted as having the best antioxidant activity, high tannin content, and low cytotoxicity against VERO cells. These results highlight the differences between host and parasite phenolic content and bioactivities.

Conclusions

To the authors' best knowledge, this work is the first to compare the phenolic profile and bioactive properties of the parasite *C. hypocistis* and its host, *H. lasianthum.* Except for one compound, trigalloyl-HHDP-glucoside, the phenolic profile of the host (both non-parasited and parasited) was different from that of the parasite, which possibly indicates the existence of a proper pathway of compound biosynthesis in the parasite. Trigalloyl-HHDP-glucoside was identified in the aerial parts of the non-parasitised *H. lasianthum* and *C. hypocistis*. This hypothesis is supported by the PCA analysis, where three defined groups were identified: root extracts from *H. lasianthum* (Group 1), aerial extracts from *H. lasianthum* (Group 2), and *C. hypocistis* extracts (Group 3).

Concerning the bioactivities, this is the first work assessing the antioxidant, anti-tyrosinase, antimicrobial, cytotoxic, and anti-inflammatory activities of *H. lasianthum*. In absolute terms, the *H. lasianthum* extracts exhibited the best growth inhibition for three of the four tumour cell lines, and *C. hypocistis* presented the best antioxidant activity. The present work also highlighted the correlation between *C. hypocistis* hydrolysable tannin content and its antioxidant and anti-tyrosinase activities.

Chapter 5: Optimisation of hydrolysable tannins recovery

The information presented in this chapter was published in the following publication:

Contextualisation and Scope

The first known application of tannin-rich plant material dates to the Mediterranean region, approximately 1500 BC, where they were used to prevent animal skin degradation [273]. Tannins are classified into different categories based on their chemical properties and behaviour when exposed to certain conditions. Hydrolysable tannins, which are further divided into gallotannins and ellagitannins, can be broken down with hot water or tannases. On the other hand, non-hydrolysable tannins are grouped into oligomeric and polymeric proanthocyanidins as condensed tannins [274]. Another classification system, proposed in 2001 by Khanbabaee & van Ree, introduced a new category called 'unclassified tannins', which are partially hydrolysable and combine elements of ellagitannins and condensed tannins. This system categorises tannins into four groups: gallotannins, ellagitannins, complex tannins, and condensed tannins [131,134–136].

Cytinus hypocistis (L.) L. biological properties have been correlated with its high content in hydrolysable tannins. Thus, studying its extraction optimisation will give comprehensive clues for the enhanced recovery of these high-added-value bioactive compounds and their future study as potential skin anti-ageing ingredients [275]. The present work aimed to assess and optimise hydrolysable tannins extraction from *C. hypocistis* using a conventional (Heat-Assisted Extraction – HAE) and a sustainable extraction method (Ultrasound-Assisted Extraction – UAE). During conventional extraction, plant material is homogenised and soaked in a solvent, often under constant stirring and with or without heat treatment [276]. These simple techniques present disadvantages, such as poor efficiency or high solvent consumption. Contrarily, more sustainable non-conventional extraction techniques such as ultrasound, microwave, supercritical fluids, and electrical/mechanical technologies can improve metabolite extraction efficiency and/or selectivity [277–279]. During UAE, different ultrasonic cavitation intensities are used to create micro-bubbles inside the solvent for a certain time; these bubbles expand and collapse, causing vibrations and breaking cell walls, favouring the penetration of solvents and consequent release of compounds [280].

The solubility of tannins is variable; it depends on the target compound, and therefore, solvents with different relative polarities, such as water, ethanol, acetone, and/or methanol, are usually selected. Condensed tannins, for example, have limited solubility in polar organic solvents, whereas ethanol and water are the two generally used solvents for the extraction of hydrolysable tannins [280,281]. Solvents are key factors in determining the class of compounds extracted; in contrast, other independent variables, such as solvent ratio, temperature, pressure, power, and extraction time, affect compound extraction yield and stability [264,282]. These independent variables should be combined in experimental designs with an appropriate optimisation method, such as the Response Surface Methodology (RSM). Contrarily to one-factor-at-a-time approaches, RSM describes the relationship between independent variables and one or more dependent (or response) variables, allowing to determine interaction effects and optimise processes using a low number of experimental runs [283,284]. This study applied two Rotatable Central Composite Designs (RCCDs) to assess the independent variables' linear, quadratic, and interaction effects on the target responses (extract yield and tannin content). A Central Composite Design (CCD) is called rotatable if, at any point, the variance of the predicted response only depends on the distance from the design's centre point. All points at the same radial distance (r) from the centre point have the same magnitude of prediction error; the proper choice of α values is responsible for this uniformity [285].

Graphical abstract

Rotatable Central Composite Design (RCCD)

- 8 Factorial points
- 6 Centre points
- 6 Star points

20 Experimental runs
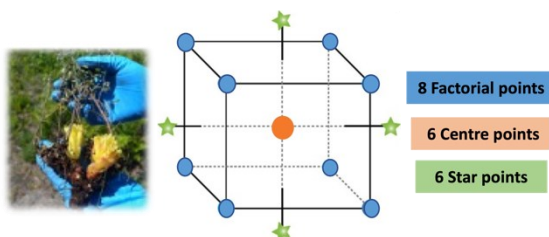
5 levels	Coded values	HAE			UAE		
		t (min)	T (°C)	S (%)	t (min)	P (W)	S (%)
	- 1.68	5	25	0	2	5	0
	-1	28.3	39.2	20.2	10.7	105.5	20.2
	0	62.5	60	50	23.5	252.5	50
	+ 1	96.7	80.8	79.8	36.3	399.5	79.8
	+ 1.68	120	95	100	45	500	100

	Runs	Experimental domain			mg Tannin/g extract	
		t(min)	T(°C) / P(W)	S(%)	Y_{HAE}	Y_{UAE}
8 Factorial points	1	-1	-1	-1	138.08	107.85
	2	+1	-1	-1	134.75	88.58
	3	-1	+1	-1	132.34	92.03
	4	+1	+1	-1	123.20	92.01
	5	-1	-1	+1	242.84	179.63
	6	+1	-1	+1	250.92	173.45
	7	-1	+1	+1	176.83	178.29
	8	+1	+1	+1	184.10	167.73
6 Star points	9	-1.68	0	0	188.14	166.40
	10	+1.68	0	0	200.97	148.88
	11	0	-1.68	0	190.66	157.29
	12	0	+1.68	0	133.88	150.65
	13	0	0	-1.68	105.16	35.57
	14	0	0	+1.68	248.44	165.23
6 Centre points	15	0	0	0	166.79	145.85
	16	0	0	0	169.80	159.04
	17	0	0	0	168.29	155.01
	18	0	0	0	173.91	163.71
	19	0	0	0	170.55	152.96
	20	0	0	0	163.14	163.72

HAE
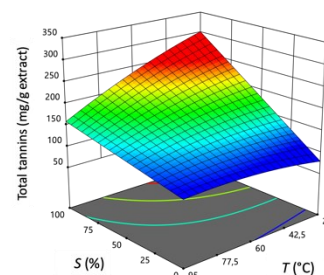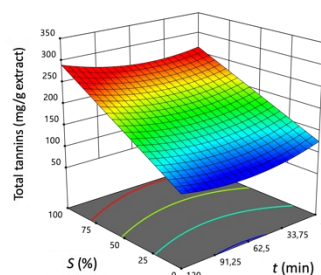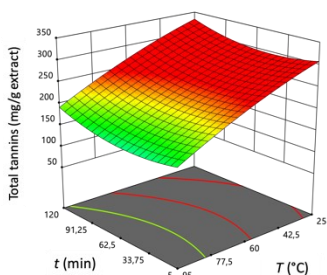
UAE
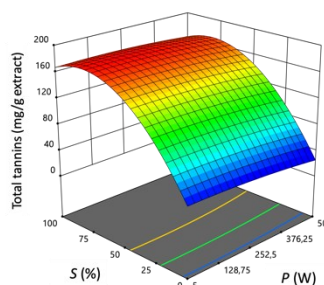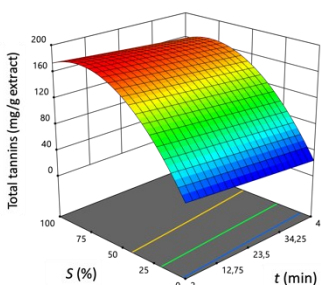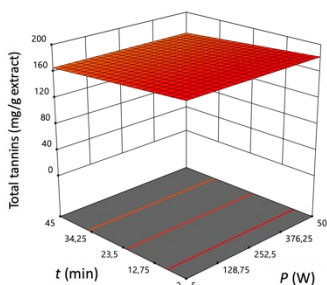
HAE

t (min)	T (°C)	S (%, v/v)	mg Tan/g Ext.
95	46	74	234

UAE

t (min)	P (W)	S (%, v/v)	mg Tan/g Ext.
18	327	69	175

109

Material and methods

Plant collection and extract preparation

Cytinus hypocistis (L.) L. subsp. *macranthus* Wettst plants were collected in July 2019 from the host species *Halimium lasianthum* subsp. *alyssoides* (Lam.) Greuter at three locations in Castro Daire, Portugal. Plant identification, characterisation, and preparation were conducted as previously described [240]. After lyophilisation (Zirbus Technonoly VaCo 10-II, Bad Grund, Germany), plant specimens were milled to a fine powder (~40 mesh) and stored at room temperature for further analysis.

Experimental design

Two three-factor RCCD designs were implemented to optimise the extraction of tannins from *C. hypocistis*. The two designs (for HAE and UAE) investigated the relationship between the independent variables X_1 [t (min): time], X_2 [T (ºC): temperature or P (W): ultrasonic power], and X_3 [S (%): solvent ratio (% of ethanol/water, v/v)], and the dependent variables Y_1 to Y_9. These independent variables and the respective range of values were selected based on previous optimisation studies and research group experience [276,280,286–292]. Considering the chosen design for a three-factor experimentation (X_1, X_2, and X_3), eight ($2^k = 2^3$) factorial points, six axial or star points (2×3), and six centre points were chosen. The software Design-Expert v11 (Stat-Ease, Inc., Minneapolis, MN, USA) was used to generate the 20 experimental runs by entering the factor ranges in terms of alphas ($\alpha = 1.68$), where the α value was $(8)^{1/4} = 1.68$. Each variable to be optimised was coded at five levels: -1.68, -1, 0, +1, and +1.68. The correspondence between coded and natural variables is presented in **Table 5.1**.

Extraction methods

For HAE, 400 mg of plant material was mixed with 20 mL of solvent (hydroethanolic solution at different concentrations, 0–100%). The mixture was then sealed in a vial and positioned in a thermostatic water bath with continuous magnetic stirring. The powdered samples were extracted at different time (t) and temperature (T) intervals, 5 to 120 min and 25 to 95 ºC, respectively. For UAE,

1 g of plant material was mixed with 50 mL of solvent (hydroethanolic solution at different concentrations, 0 – 100%). The beaker containing the mixture was processed with an ultrasonic system (CY-500, Optic Ivymen System, Barcelona, Spain) equipped with a titanium probe. Samples were treated using different ultrasonic power (P: 5–500 W; at 20 kHz frequency) and time (t: 2–45 min) intervals; the temperature was maintained constant (ice was used to prevent samples heating). Both extraction methods, HAE and UAE, were performed with a solid/liquid ratio of 20 g/L. The RSM designs comprised 20 experimental runs (performed in randomised order) planned as mentioned above. After extraction, samples were centrifuged at 3000 g for 10 min and filtered through Whatman paper no 4. Two millilitres of each filtrate were added to ceramic crucibles and used to determine the extraction yield (extract dry weight or extracted solids, %, *w/w*) by removing the solvent in an oven at 100 ºC until constant weight was achieved (~24 h); the remaining filtrate was frozen and lyophilised for total and individual tannin quantification.

Table 5.1. Natural and coded values of the independent variables applied in the RCCD design for optimising tannins extraction from *C. hypocistis*.

| Coded values | Natural values | | | | | |
| | HAE | | | UAE | | |
	t (min)	T (ºC)	S (%)	t (min)	P (W)	S (%)
-1.68	5	25	0	2	5	0
-1	28	39	20	11	106	20
0	62.5	60	50	23.5	253	50
+1	97	81	80	36	400	80
+1.68	120	95	100	45	500	100

t:time in min.; *T*: temperature in ºC; *S*: solvent percentage; *P*: ultrasonic power in watts.

Tannin quantification

Extracts were dissolved in a water/ethanol mixture (80:20, v/v) at a 20 mg/mL final concentration and filtered through a 0.22 μm nylon disposable filter. The seven major tannins present in the sample were analysed by HPLC-DAD-ESI/MS^n (Dionex Ultimate 3000 UPLC, Thermo Scientific, San Jose, CA, USA). Tannins were characterised according to their UV spectra, fragmentation pattern, retention

times, and comparison with available standards [206,293]. For quantification, seven-level calibration curves were obtained from the most similar commercially available standard compounds, namely gallic acid (y = 131538x + 292163; r^2 = 0.9998; LOD = 0.68 µg mL^{-1}; LOQ = 1.61 µg mL^{-1}) and ellagic acid (y = 26719x - 317255; r^2 = 0.9996; LOD = 0.10 µg mL^{-1}; LOQ = 0.48 µg mL^{-1}). The results were expressed in mg tannins/g extract (E).

Extraction modelling and statistical analysis

The responses were expressed in the form of nine dependent variables *(Y)* and used to optimise the recovery of tannins from *C. hypocistis*: Y_1, extraction yield (extract dry weight or extracted solids, %, w/w); Y_2, mg of tetragalloyl-glucoside II per g of extract (E); Y_3, mg of tetragalloyl-glucoside III per g of E; Y_4, mg of pentagalloyl-glucoside per g of E; Y_5, mg of galloyl-bis-HHDP-glucose II per g of E; Y_6, mg of digalloyl-bis-HHDP-glucose II per g of E; Y_7, mg of trigalloyl-bis-HHDP-glucose I per g of E; Y_8, mg of trigalloyl-bis-HHDP-glucose II per g of E; and Y_9, mg of tannins (total) per g of E. As extensively described by Rocha and colleagues [283], fitting procedures, coefficient estimates, and statistical verifications were performed using the software Design-Expert. The ANOVA (analyses of variance) was used to evaluate the significance of the models generated (polynomial equations) and the lack of fit. The test for statistical significance was performed by calculating the *p*-value from the F-value, acknowledging the significance of *p*-value < 0.05. Statistically non-significant terms (*p*-value > 0.05) were omitted to simplify the models (except those required to ensure hierarchy). The adequate precision, the coefficient of determination (R^2), and the adjusted coefficient of determination (R^2_{adj}) were used to assess the adequacy of the polynomial equations to the final responses. For adequate precision, which measures signal-to-noise ratio, the value must be greater than 4, whereas R^2 and R^2_{adj} must exhibit a value close to 1, illustrating an agreement between the theoretical and experimental data [294].

Results and discussion

Experimental data obtained with the two RCCDs

In a previous study [240], a total of seventeen phenolic compounds (sixteen hydrolysable tannins and one catechin) were identified (HPLC-DAD-ESI/MS^n analysis) in this species. The total tannin content, the most abundant seven hydrolysable tannins, and the extraction yield were the selected response variables for the present optimisation work. The HAE and UAE experimental results are presented in **Table 5.2**.

The Y_1 response corresponds to the extraction yield (extract dry weight, %, *w/w*). From the analysis of the experimental results for both methods (**Table 5.2**), it is possible to observe that the % yield and % of the solvent follow an inverse correlation. There is a tendency for the % yield to decrease as the ethanol % increases. For both methodologies, the lowest yield was obtained in run 14 (HAE: 62.5 min; 60 ºC; 100% ethanol *v/v* and UAE: 23.5 min; 253 W; 100% ethanol *v/v*), which combined medium-time and -temperature/-watts potency ($\alpha = 0$) with a high-ethanol percentage ($\alpha = +1.68$). The highest yield was obtained in run 3 for HAE (28 min; 81 ºC; 20% ethanol *v/v*) and run 4 for UAE (36 min; 400 W; 20% ethanol *v/v*). Run 3 combined medium-high-temperature ($\alpha = +1$) with medium-low-time and -solvent percentage ($\alpha = -1$) and run 4 merges medium-low solvent percentage ($\alpha = -1$) with medium-high -time and -watts potency ($\alpha = +1$).

As presented in **Table 5.2**, the seven optimised hydrolysable tannins were: Y_2 and Y_3 - two tetragalloyl-glucoside isomers (II and III); Y_4, a pentagalloyl-glucoside; Y_5, a galloyl-bis-HHDP-glucose II; Y_6, a digalloyl-bis-HHDP-glucose II; Y_7 and Y_8, two trigalloyl-bis-HHDP-glucose isomers (I and II); and Y_9, total tannins. From the analysis of the HAE experimental results for the 7 tannins (**Table 5.2**), it is possible to observe that, in 4 responses (Y_2, Y_6, Y_7, and Y_9), the lowest yield was obtained in run 13 (HAE: 62.5 min; 60 ºC; 0% ethanol *v/v*), which combined medium-time and -temperature ($\alpha = 0$) with a 0 % of ethanol ($\alpha = -1.68$). Whereas the highest yield was obtained in run 6 (HAE: 97 min; 39 ºC; 80% ethanol *v/v*), combining medium-high-time and -solvent percentage ($\alpha = +1$) with medium-low-

temperature (α = -1). For responses Y_4, Y_5, and Y_8, the highest response value was obtained in run 14 (HAE: 62.5 min; 60 ºC; 100% ethanol v/v), in a mixture of medium-time and -temperate (α = 0) with the highest ethanol percentage (α = +1.68). Responses Y_4, Y_5, and Y_8 lowest experimental values were obtained in run 12 for Y_4 and Y_8 (HAE: 62.5 min; 95 ºC; 0% ethanol v/v) and run 13 for Y_5 (HAE: 62.5 min; 60 ºC; 0% ethanol v/v), both using 0 % of ethanol (α = -1.68), and high (α = + 1) to medium-high-temperature (α = + 1.68), respectively. A general overview of the HAE experimental values revealed higher ethanol percentages as the critical factor in increasing the 7 hydrolysable tannins' final responses (response Y_2 to Y_8).

Regarding UAE (**Table 5.2**), the lowest experimental values for all tannins were obtained in run 13 (UAE: 23.5 min; 253 W; 0% ethanol v/v), combining medium-time and -watts (α = 0) with no ethanol (α = -1.68). Equally to HAE, in UAE, low ethanol (0%) was linked to lower experimental response values for tannins (Y_2 to Y_9). For responses Y_2, Y_3, and Y_5, the highest experimental values were obtained within the 6 centre points (UAE: 23.5 min; 253 W; 50% ethanol v/v), which combined medium t, P and S (α = 0). For responses Y_4 and Y_9, it was in run 5 (UAE: 11 min; 106 W; 80% ethanol v/v), with α = -1; -1; +1, respectively. Run 6 (UAE: 36 min; 106 W; 80% ethanol v/v) was the best result for Y_6 response, with α = +1; -1; +1, respectively. Finally, the best result for responses Y_7 and Y_8 was obtained in run 7 (UAE: 11 min; 400 W; 80% ethanol v/v), with α = -1; +1; +1. Similar to HAE, the experimental values for UAE indicated that ethanol percentage is a critical factor in achieving higher yields in responses Y_2 to Y_8.

Models fitting and statistical verification

The conventional one-factor-at-a-time strategy does not account for interactions, while RSM is a statistical tool suitable for modelling and optimising processes involving one or more response variables and determining optimal processing conditions [283,295]. To further analyse the experimental values, the polynomial model (Eq. 1) was applied to assess the impact of the independent

variables on a given response. The parametric values were estimated by fitting the second-order polynomial model to the obtained experimental responses (**Table 5.3**). The coefficients exhibiting confidence interval values ($\alpha = 0.05$) higher than the parameter value were considered non-significant (*ns*) and were not used for model development; the significant values were assessed at a 95% confidence level. The results of ANOVA and regression analyses are also presented in **Table 5.3**, whereas the developed polynomial models are shown in **Table 5.4** (Eq. 2 to Eq. 19). All models exhibited a non-significant (ns) lack of fit (*p*-values > 0.05) and adequate precision greater than 19.2, which shows that the model equations adequately describe the effects of the independent variables on the final responses [296]. As shown in **Table 5.3**, the coefficients R^2 and R^2_{adj} were ≥ 0.92 and 0.88, respectively, indicating that each response variability can be explained by the independent variables involved in the extraction processes. Although the model coefficients are empirical and do not reflect physical or chemical significance, they are valuable tools for predicting untested experimental extraction conditions [297].

Analysis of the theoretical response surface models

The parametric coefficients presented of each term in the mathematical models (**Table 5.4**) provide specific information on the impact of the linear, quadratic, and interaction effects of the independent variables (*t*, *T*/*P*, and *S*) on the extraction of tannins from *C. hypocistis*. The values express the expected change in response per unit change in factor value when all remaining factors are held constant. The higher the parametric value, the more significant is the variable term, regardless of its sign. Additionally, for interaction effects, a positive sign indicates a synergism, while a negative sign indicates an antagonism (since the effect of one independent variable is affected by another variable) [283,298]. The results are also presented as 3D response surface graphs to visually illustrate the independent variables' effect on extraction yield (**Figure 5.1**) and total tannins (**Figure 5.2**) for both HAE and UAE methods. The net surfaces were built with the model equations presented in **Table 5.4**. For each 3D graph, the excluded independent variable was positioned at its optimal value (**Table 5.5**).

Table 5.2. Experimental results for the nine response variables (extraction yield and tannin content).

Run	Experimental domain			Experimental responses																
	X_1: t	X_2: T or P	X_3: S	HAE									UAE								
	(min)	(ºC or W)	(%, v/v)	Y_1	Y_2	Y_3	Y_4	Y_5	Y_6	Y_7	Y_8	Y_9	Y_1	Y_2	Y_3	Y_4	Y_5	Y_6	Y_7	Y_8	Y_9
1	-1	-1	-1	61.21	24.03	17.17	38.90	18.83	17.08	12.99	9.09	138.08	49.19	19.17	21.00	27.62	14.01	13.03	7.41	5.61	107.85
2	+1	-1	-1	63.41	29.97	16.14	37.00	16.98	15.81	10.28	8.56	134.75	60.71	17.25	15.14	24.67	11.30	9.31	6.27	4.63	88.58
3	-1	+1	-1	64.65	27.24	20.20	33.60	17.07	14.94	11.24	8.05	132.34	62.00	17.29	16.12	25.31	11.10	9.82	7.62	4.76	92.03
4	+1	+1	-1	62.56	21.11	28.00	33.60	16.98	12.80	7.27	3.44	123.20	70.03	18.68	16.32	24.16	11.47	9.49	7.24	4.65	92.01
5	-1	-1	+1	52.64	27.13	27.22	79.79	29.12	37.72	27.27	14.59	242.84	40.62	27.50	24.11	51.33	21.04	26.27	17.10	10.81	179.63
6	+1	-1	+1	48.99	38.61	24.00	76.85	28.51	41.32	24.73	16.90	250.92	38.00	28.25	23.66	46.83	20.74	26.57	16.09	11.31	173.45
7	-1	+1	+1	50.35	30.30	29.27	42.66	28.71	20.91	14.74	10.24	176.83	53.32	26.47	26.60	50.23	21.04	24.70	17.66	11.60	178.29
8	+1	+1	+1	50.50	31.25	41.37	39.44	28.71	22.54	10.80	9.99	184.10	48.83	26.24	24.94	46.35	20.94	24.46	15.19	9.61	167.73
9	-1.68	0	0	62.87	29.59	27.00	43.35	25.90	30.05	21.34	10.91	188.14	52.00	25.64	26.93	43.38	20.60	24.47	15.55	9.83	166.40
10	+1.68	0	0	59.71	36.17	31.85	51.30	24.36	29.66	16.25	11.38	200.97	53.00	23.57	23.91	41.47	18.39	20.08	13.07	8.39	148.88
11	0	-1.68	0	54.00	23.56	25.93	52.35	23.22	30.30	22.64	12.66	190.66	40.36	23.76	23.02	42.93	20.00	22.19	15.78	9.62	157.29
12	0	+1.68	0	54.89	25.18	41.47	18.40	19.80	17.73	7.94	3.36	133.88	62.00	23.18	23.22	40.66	18.31	19.44	12.84	8.22	150.65
13	0	0	-1.68	61.91	16.98	11.81	38.22	13.04	11.31	7.20	6.60	105.16	61.00	12.18	8.87	11.99	5.18	3.74	1.65	1.85	35.57
14	0	0	+1.68	46.30	28.14	28.92	81.03	32.09	37.79	23.00	17.47	248.44	35.11	25.36	20.18	47.14	19.74	26.17	15.73	10.90	165.23
15	0	0	0	54.78	26.74	25.54	46.49	25.34	19.80	12.87	10.00	166.79	53.11	25.13	24.24	37.87	16.86	21.09	12.90	7.76	145.85
16	0	0	0	52.34	26.81	26.39	45.32	24.63	22.99	13.62	10.04	169.80	54.15	27.86	26.37	38.30	21.75	21.60	13.57	9.59	159.04
17	0	0	0	53.33	25.32	25.82	45.72	21.50	23.18	15.20	11.54	168.29	54.19	24.59	25.85	40.32	19.33	22.27	14.75	7.90	155.01
18	0	0	0	56.83	27.97	28.65	48.95	21.00	22.82	14.07	10.44	173.91	52.40	27.29	26.44	42.03	20.14	23.22	14.92	9.67	163.71
19	0	0	0	54.39	26.20	30.04	48.74	20.26	22.62	13.02	9.67	170.55	56.00	25.40	23.11	40.78	19.17	21.85	13.34	9.30	152.96
20	0	0	0	55.23	25.36	28.17	48.30	19.84	20.27	13.21	8.00	163.14	53.02	28.28	27.27	42.01	19.71	23.51	13.79	9.15	163.72

Runs 1–8: factorial points; **runs 9–14**: axial or star points; **runs 15–20**: centre points. Response variables: Y_1: extraction yield (extract weight); Y_2: tetragalloyl-glucoside II; Y_3: tetragalloyl-glucoside III; Y_4: pentagalloyl-glucoside; Y_5: galloyl-bis-HHDP-glucose II; Y_6: digalloyl-bis-HHDP-glucose II; Y_7: trigalloyl-bis-HHDP-glucose I; Y_8: trigalloyl-bis-HHDP-glucose II; and Y_9: total tannins; Y_1 units: % (w/w); Y_2 to Y_9 units: mg/g extract (E).

Table 5.3. Parametric coefficients and statistical information of the model fitting procedure for both extraction methods (HAE and UAE). Parametric subscripted 1, 2 and 3 represent the variables t, T/P and S, respectively.

	HAE	Y_1	Y_2	Y_3	Y_4	Y_5	Y_6	Y_7	Y_8	Y_9
Intercept	b_0	54.4±0.4	26.1±0.6	27.7±0.6	47.3±0.7	22.1±0.4	22.2±0.6	14.0±0.3	10.3±0.4	170±2
	b_1	-0.6±0.4*	1.7±0.4	1.8±0.5	ns	-0.4±0.4*	0.1±0.6*	-1.6±0.3	-0.2±0.3*	2±1*
Linear effect	b_2	ns	-0.5±0.4*	4.4±0.5	-10.3±0.6	ns	-4.5±0.6	-4.1±0.3	-2.4±0.3	-18±1
	b_3	-5.5±0.4	3.2±0.4	5.1±0.5	12.3±0.6	5.7±0.4	7.8±0.6	4.6±0.3	2.3±0.3	42±1
	b_{11}	2.4±0.4	2.8±0.4	ns	ns	1.1±0.4	2.0±0.6	1.4±0.3	ns	8±1
Quadratic effect	b_{22}	ns	ns	1.7±05	-4.1±0.5	ns	ns	ns	-0.8±0.3	-4±1
	b_{33}	ns	ns	-3.0±0.5	4.4±0.5	ns	ns	ns	0.6±0.3	ns
	b_{12}	ns	-2.8±0.6	3.0±0.7	ns	ns	ns	ns	-0.8±0.4	ns
Interaction effect	b_{13}	ns	1.6±0.6	ns	ns	ns	ns	ns	0.9±0.4	ns
	b_{23}	ns	ns	ns	-8.2±0.7	ns	-3.8±0.8	-2.7±0.4	ns	-14±2
	Model F-value	82.48	21.86	44.24	222.00	67.67	52.95	116.74	27.55	192.24
	Model p-value	<0.0001	<0.0001	<0.0001	<0.0001	<0.0001	<0.0001	<0.0001	<0.0001	<0.0001
	Lack-of-Fit	0.6565	0.0847	0.4672	0.2349	0.9957	0.1343	0.2933	0.7060	0.1944
Statistics	R^2	0.9393	0.9273	0.9533	0.9875	0.9269	0.9498	0.9766	0.9525	0.9912
	R^2_{adj}	0.9279	0.8849	0.9318	0.9831	0.9132	0.9318	0.9682	0.9179	0.9860
	Ad. Precision	28.99	19.24	27.20	55.58	28.42	25.97	38.57	20.66	50.53
	C.V. (%)	2.56	5.88	6.97	4.30	6.57	9.35	6.97	10.16	2.77
	UAE	Y_1	Y_2	Y_3	Y_4	Y_5	Y_6	Y_7	Y_8	Y_9
Intercept	b_0	53.5±0.5	26.0±0.4	25.5±0.5	41.0±0.5	19.3±0.3	22.1±0.4	14.0±0.2	8.9±0.2	156±2
	b_1	1.0±0.5	ns	-0.9±0.4	-1.2±0.4	ns	-0.8±0.3	-0.7±0.2	-0.4±0.2	-5±1
Linear effect	b_2	6.0±0.5	-0.3±0.3*	0.1±0.3*	ns	ns	-0.8±0.3	ns	ns	ns
	b_3	-7.7±0.5	4.3±0.3	3.6±0.4	11.1±0.4	4.4±0.3	7.2±0.3	4.5±0.2	2.9±0.2	39±1
	b_{11}	ns	ns	ns	ns	ns	ns	ns	ns	ns
Quadratic effect	b_{22}	ns	-0.9±0.3	-0.8±0.4	ns	ns	-0.7±0.3	ns	ns	ns
	b_{33}	-1.5±0.4	-2.5±0.3	-3.9±0.4	-4.0±0.4	-2.6±0.3	-2.8±0.3	-2.0±0.2	-0.9±0.2	-20±1
	b_{12}	ns	ns	ns	ns	ns	ns	ns	ns	ns
Interaction effect	b_{13}	-3.3±0.6	ns	ns	ns	ns	ns	ns	ns	ns
	b_{23}	ns	ns	ns	ns	ns	ns	ns	ns	ns
	Model F-value	97.35	52.78	37.36	251.84	130.72	118.46	165.23	80.26	328.30
	Model p-value	<0.0001	<0.0001	<0.0001	<0.0001	<0.0001	<0.0001	<0.0001	<0.0001	<0.0001
	Lack-of-Fit	0.1941	0.8314	0.7392	0.7002	0.9319	0.2429	0.4954	0.9365	0.9097
Statistics	R^2	0.9720	0.9337	0.9452	0.9793	0.9389	0.9769	0.9687	0.9554	0.9840
	R^2_{adj}	0.9621	0.9160	0.9199	0.9754	0.9318	0.9687	0.9629	0.9435	0.9810
	Ad. Precision	36.21	24.14	22.99	53.41	36.23	38.78	44.14	31.88	62.36
	C.V. (%)	3.27	5.44	6.11	4.20	6.71	6.06	6.52	7.61	3.70

Y_1: extraction yield (extract weight); Y_2: tetragalloyl-glucoside II; Y_3: tetragalloyl-glucoside III; Y_4: pentagalloyl-glucoside; Y_5: galloyl-bis-HHDP-glucose II; Y_6: digalloyl-bis-HHDP-glucose II; Y_7: trigalloyl-bis-HHDP-glucose I; Y_8: trigalloyl-bis-HHDP-glucose II; and Y_9: total tannins. **R^2**: coefficient of determination; **R^2_{ajd}**: adjusted coefficient of determination; **Ad. Precision**: Adequate Precision; **C.V.**: coefficient of variation; **ns**: not significant. *Although statistically non-significant (p-value > 0.05), the terms were added to maintain the hierarchy.

Table 5.4. Quadratic second-order polynomial model (Eq. 1) and the developed polynomial models (Eqs. 2–19) expressed in coded values.

$Y = b_0 + b_1X_1 + b_2X_2 + b_3X_3 + b_{11}X_1^2 + b_{22}X_2^2 + b_{33}X_3^2 + b_{12}X_1X_2 + b_{13}X_1X_3 + b_{23}X_2X_3$			Eq. (1)
HAE		**UAE**	
$Y_1 = 54.4 - 0.6t - 5.5S + 2.4t^2$	Eq. (2)	$Y_1 = 53.5 + 1.0t + 6P - 7.7S - 1.5S^2 - 3.3tP$	Eq. (11)
$Y_2 = 26.1 + 1.7t - 0.5T + 3.2S + 2.8t^2 - 2.8tT + 1.6tS$	Eq. (3)	$Y_2 = 26 - 0.3P + 4.3S - 0.9P^2 - 2.5S^2$	Eq. (12)
$Y_3 = 27.7 + 1.8t + 4.4T + 5.1S + 1.7T^2 - 3S^2 + 3tT$	Eq. (4)	$Y_3 = 25.5 + 0.1P - 0.9t + 3.6S - 0.8P^2 - 3.9S^2$	Eq. (13)
$Y_4 = 47.3 - 10.3T + 12.3S - 4.1T^2 + 4.4S^2 - 8.2TS$	Eq. (5)	$Y_4 = 41 - 1.2t + 11.1S - 4.0S^2$	Eq. (14)
$Y_5 = 22.1 - 0.4t + 5.7S + 1.1t^2$	Eq. (6)	$Y_5 = 19.3 + 4.4S - 2.6S^2$	Eq. (15)
$Y_6 = 22.2 + 0.1t - 4.5T + 7.8S + 2t^2 - 3.8TS$	Eq. (7)	$Y_6 = 22.1 - 0.8t - 0.8P + 7.2S - 0.7P^2 - 2.8S^2$	Eq. (16)
$Y_7 = 14.0 - 16.6t - 4.1T + 4.6S + 1.4t^2 - 2.7TS$	Eq. (8)	$Y_7 = 14 - 0.7t + 4.5S - 2S^2$	Eq. (17)
$Y_8 = 10.3 - 0.2t - 2.4T + 2.3S - 0.8T^2 + 0.6S^2 - 0.8tT + 0.9tS$	Eq. (9)	$Y_8 = 8.9 - 0.4t + 2.9S - 0.9S^2$	Eq. (18)
$Y_9 = 170 + 2t - 18T + 42S + 8t^2 - 4T^2 - 14TS$	Eq. (10)	$Y_9 = 156 - 5t + 39S - 20S^2$	Eq. (19)

Response variables: Y_1: extraction yield (extract weight); Y_2: tetragalloyl-glucoside II; Y_3: tetragalloyl-glucoside III; Y_4: pentagalloyl-glucoside; Y_5: galloyl-bis-HHDP-glucose II; Y_6: digalloyl-bis-HHDP-glucose II; Y_7: trigalloyl-bis-HHDP-glucose I; Y_8: trigalloyl-bis-HHDP-glucose II; and Y_9: total tannins

HAE   **UAE**

(a)   (d)

(b)   (e)

(c)   (f)
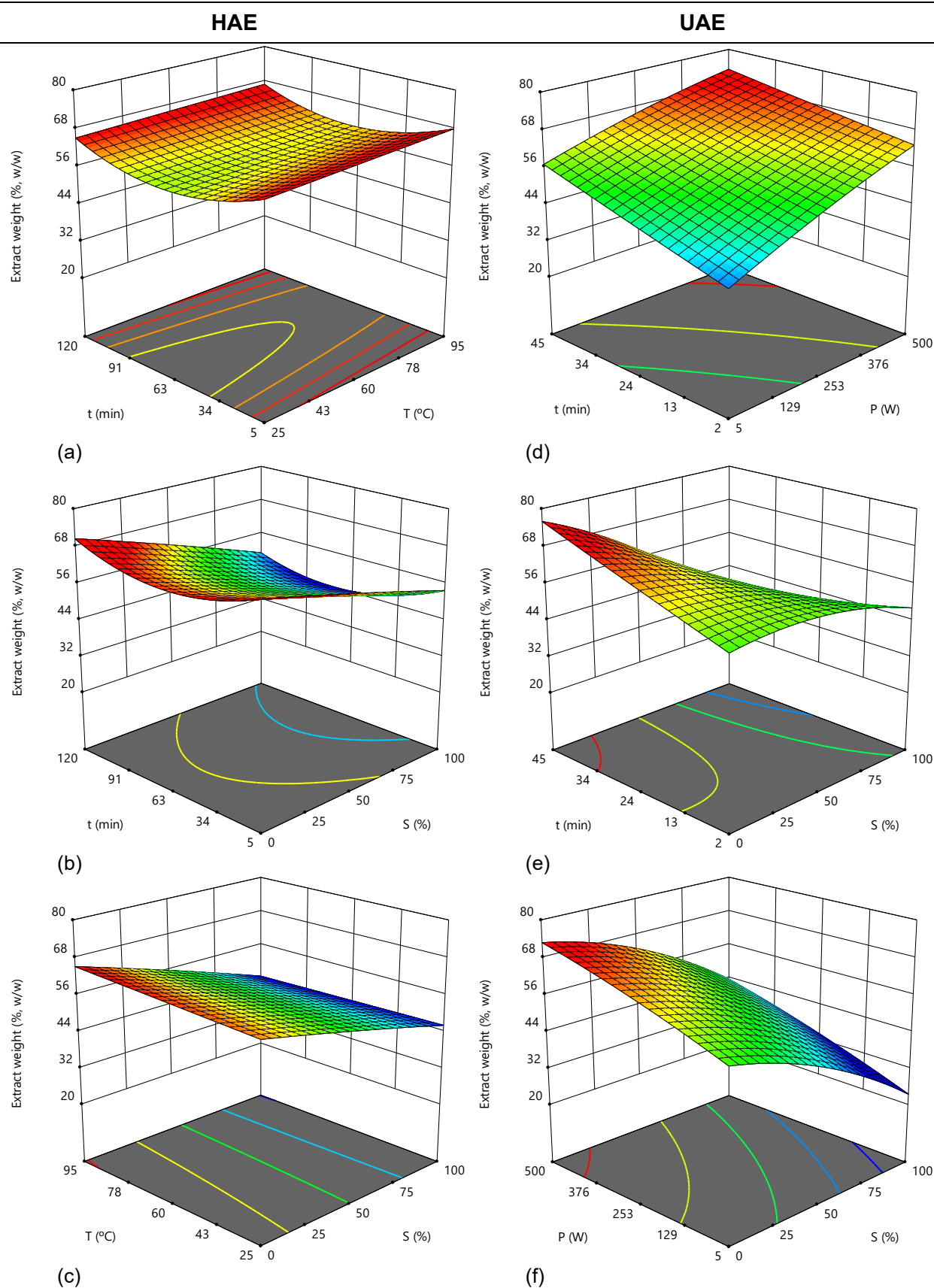
Figure 5.1. Response surface graphs illustrating the independent variables' binary effects on the extraction yield (Y_1: extract weight) obtained with HAE and UAE. In each graph, the excluded variable was fixed at its optimum response value (**Table 5.5**).

HAE

UAE

(a)

(b)

(c)

(d)

(e)

(f)
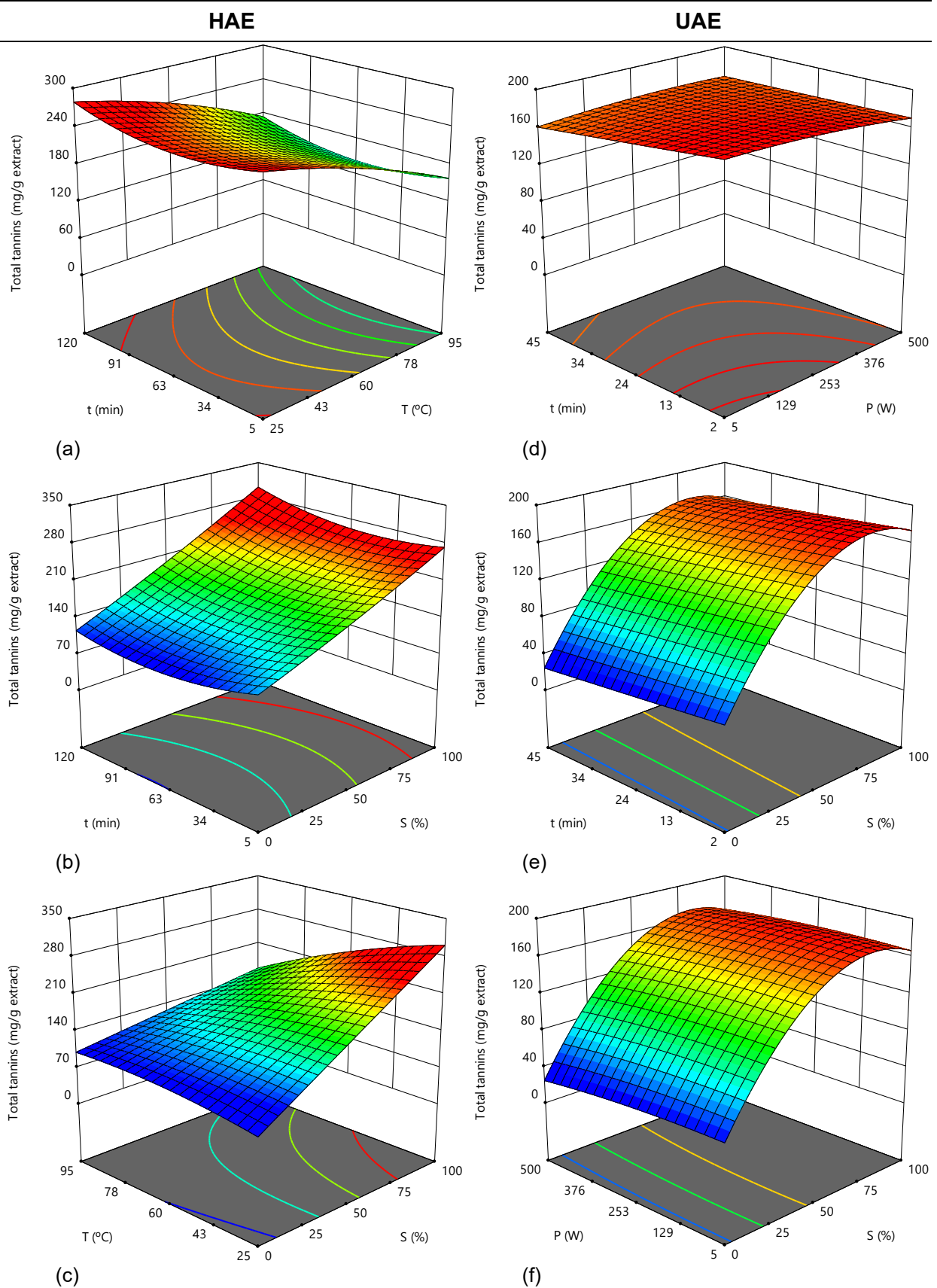
Figure 5.2. Response surface graphs illustrating the independent variables' binary effects on the total tannin content (Y_9) obtained with HAE and UAE. In each graph, the excluded variable was fixed at its optimum response value (**Table 5.5**).

Table 5.5. Optimal HAE and UAE conditions expressed as natural values that lead to optimal response values.

	Optimal HAE conditions			Optimum response
	t (min)	T (°C)	S (ethanol %, v/v)	
For each response variable				
Y_1	27.3	45.5	0.0	67±1% (w/w)
Y_2	104.0	51.3	65.9	36.4±0.9 mg/g E
Y_3	79.0	83.0	69.9	39.5±0.9 mg/g E
Y_4	62.5	48.7	83.7	76±1 mg/g E
Y_5	57.8	60.0	95.9	30.9±0.8 mg/g E
Y_6	89.9	50.7	96.1	40±1 mg/g E
Y_7	29.3	44.1	82.5	27.3±0.6 mg/g E
Y_8	70.8	48.0	85.4	16.6±0.6 mg/g E
Y_9	65.7	52.1	98.8	245±3 mg/g E
Considering all response variables				
Y_1	95.1	46.4	74.3	53±1% (w/w)
Y_9				203±3 mg/g E

	Optimal UAE conditions			Optimum response
	t (min)	P (W)	S (ethanol %, v/v)	
For each response variable				
Y_1	28.4	456.0	22.7	69±1% (w/w)
Y_2	9.3	217.8	71.1	27.8±0.4 mg/g E
Y_3	17.4	289.1	64.4	26.9±0.5 mg/g E
Y_4	19.8	274.9	76.2	48.0±0.5 mg/g E
Y_5	15.7	240.2	70.9	21.1±0.4 mg/g E
Y_6	19.1	184.8	76.0	26.7±0.5 mg/g E
Y_7	18.3	231.4	74.2	16.6±0.3 mg/g E
Y_8	18.8	208.6	77.0	10.9±0.2 mg/g E
Y_9	19.5	405.1	72.4	176±2 mg/g E
Considering all response variables				
Y_1	18.7	327.4	69.3	53±1% (w/w)
Y_9				173±2 mg/g E

Y_1: extraction yield (extract weight); Y_2: tetragalloyl-glucoside II; Y_3: tetragalloyl-glucoside III; Y_4: pentagalloyl-glucoside; Y_5: galloyl-bis-HHDP-glucose II; Y_6: digalloyl-bis-HHDP-glucose II; Y_7: trigalloyl-bis-HHDP-glucose I; Y_8: trigalloyl-bis-HHDP-glucose II; and Y_9: total tannins.

The intercept is the expected mean value of Y (response) when all independent variables are equal to zero ($X = 0$). As shown in **Table 5.3**, although the two designs (HAE and UAE) present similar intercept values for all nine responses, for Y_3, Y_4, Y_5, Y_8, and Y_9, the HAE values were slightly superior. Regarding the HAE-Y_1 response, the variables S and t significantly affected the extraction yield. The negative linear effect of solvent (-5.5S) is perfectly illustrated by the surface curvature of the graphs, where this variable is represented (**Figures 5.1b** and **c**). The positive quadratic effect of time ($2.4t^2$) is visible in **Figures 5.1a** and **b**. Apart from the variables S and t, P also influenced the UAE-Y_1 response. The variables t and P had a positive linear effect ($1t$ and $6P$, respectively), which is visible in **Figure 1d**; whereas S and its quadratic effect had a negative impact on Y_1 (-7.7S and -1.5S^2, respectively), evidenced by the curvature in graphs (**d**) and (**e**) of **Figure 5.1**. For both methods, it was possible to observe the importance of the solvent (S) variable; an increase in ethanol percentage presented the most significant impact (negative) on the two Y_1 responses (**Figure 5.1**).

Concerning total tannins, the response surfaces obtained for HAE were more complex than those of UAE (**Figures 5.1** and 5.**2**), as predicted by the theoretical models (Eqs. 10 and 19 in **Table 5.4)**. Considering tannins' final responses for HAE, the linear impact of ethanol (S) was positive for all responses, whereas the other variables presented both positive and negative effects on the final responses. The linear effect of t was positive for responses Y_2 ($1.7t$) and Y_3 ($1.8t$), negative for Y_5 (-0.4t) and Y_7 (-1.6t), and non-significant for Y_4, Y_6, Y_8, and Y_9. The linear effect of T was positive for Y_3 ($4.4T$), negative for Y_4 (-10.3T), Y_7 (-4.5T), Y_8 (-4.1T), and Y_9 (-2.4T), and non-significant for the remaining two responses (Y_2 and Y_6). Concerning the quadratic effect of the independent variables t^2, T^2, and S^2: t^2 positively affected Y_2 ($2.8t^2$), Y_5 ($1.1t^2$), Y_6 ($2.0t^2$), Y_7 ($1.4t^2$), and Y_9 ($8.0t^2$) final responses; T^2 affected positively the response Y_3 ($1.7T^2$) and negatively Y_4 (-4.1T^2), Y_8 (-0.8T^2), and Y_9 (-4.0T^2); while S^2 positively impacted Y_4 ($4.4S^2$) and Y_8 ($0.6S^2$) and had a negative effect on Y_3 (-3.0S^2). For all the other responses, the quadratic effects of the independent variables were non-significant. Finally, for the interaction effects of the independent variables during HAE, it was possible to observe that the

interaction effect of T and S was either non-significant or had a negative effect on the tannin final responses (Y_4: -8.2TS, Y_6: -3.8TS, Y_7: -2.7TS, and Y_9: -14TS). The interaction effect of t and T negatively affected Y_2: -2.8tT and Y_8: -0.8tT responses; contrarily, it positively affected Y_3 (3.0tT) response. The interaction effect between t and S also positively impacted Y_2: 1.6tS and Y_8: 0.9tS. For all the other responses, the interaction effect was non-significant. Similarly, to the values obtained for the 20 experimental runs (**Table 5.3**), it was possible to infer the importance of the solvent (S) variable on tannins' final responses from the mathematical models presented in **Table 5.4**; S had the most significant impact (positive) on responses Y_2 to Y_9. Concerning total tannins (Y_9), **Figure 5.2** pictures the positive impact of both low T, perfectly noticeable in graphs (**a**) and (**c**), and high S, visible in graphs (**b**) and (**c**) and graphs (**e**) and (**f**) for HAE and UAE, respectively.

During the UAE method, the linear effect of the variable S was responsible for the only positive effect in all tannin responses (Y_2 to Y_9). UAE of total tannins (Y_9) was mainly affected by the independent variable S. The highest quantity of total tannins was obtained when *C. hypocistis* powder was sonicated with high ethanol percentages; this effect is noticeable on the surface graphs where this variable is represented (**Figures 5.2e** and **f**). The ultrasonic power (P) and time (t) variables had a non-significant or slightly negative effect (respectively) on this response (**Figure 5.2d**). Despite the positive linear effect of S, its quadratic effect (S^2) was negative for all responses. When present, the linear effect of P (Y_6: -0.8P) and the quadratic effect of P^2 (Y_2: -0.9P^2; Y_3: -0.8P^2; and Y_6: -0.7P^2) had a minor negative or non-significant impact on all the final responses. The quadratic effect of S^2 had a negative effect on all the responses, from -20.0S^2 to -0.9S^2. Differently, no interaction effects were observed in the UAE process.

Although the linear effect of the solvent (S) had the most significant impact on the responses for both extraction methods, the use of RSM was important because it allowed for the assessment of the quadratic and interaction effects of the variables. The parametric values of the different variables facilitate the determination of the optimum conditions for each response.

HAE and UAE: Individual, global, and comparison of the two methods optimal conditions

From the response surface graphs (**Figures 5.1** and 5.**2**), it can be inferred that an optimal extraction value can be obtained as a single point in almost all combinations. Accordingly, the extraction conditions that lead to an absolute maximum were computed for both methods and are presented in **Table 5.5**. The optimal HAE conditions for tannin recovery were mainly characterised by longer extraction times (27.3 to 104 min) and medium to high temperatures (44.1 to 83 ºC). Regarding the solvent, the recovery of tannins from *C. hypocistis* was favoured by higher solvent percentages (65.9 to 98.8%, *v/v*), which is easily perceived on the response surface graphs of **Figure 5.2**. The optimal UAE conditions for tannin recovery were characterised by short extraction times (9.3 to 28.4 min), medium to high ultrasound power (184.8 to 456 W), and increased ethanol percentages (64.4 to 77%, *v/v*). Since the industrial sector is interested in natural extracts, optimising processes to obtain higher amounts of extract weight and tannins using sustainable extraction methods is important. The global conditions that simultaneously maximise the extraction yield and the total tannins content were also determined by selecting "maximise" for these response variables and giving them equal "importance" in the Design-Expert analysis (**Table 5.5**). Based on this second optimisation step, 95.1 min processing at 46.4 ºC with 74.3% ethanol (*v/v*) and 18.7 min of sonication at 69.3 W using 69.3% ethanol (*v/v*) were the optimal HAE and UAE conditions, respectively, that maximised the target response variables. The HAE and UAE were compared to determine the most suitable method to facilitate tannin recovery. UAE has shown some advantages over HAE [299] for intracellular extraction, herein demonstrated by significantly shorter processing times. According to previous reports, acoustic cavitation promotes solvent penetration into the plant material and the consequent release of compounds, enhancing mass transfer faster than when using temperature as an intensification factor [299]. Interestingly, although the lower ethanol percentages gave rise to higher extraction yields (possibly due to greater recovery of water-soluble carbohydrates), the highest levels of tannins were achieved using higher ethanol percentages (**Figure 5.3**).

Therefore, the variable solvent effectively contributed to the selectivity of the extraction processes. These results are supported by those previously reported by Liang and colleagues [300], who optimised heat reflux and UAE methods to recover hydrolysable tannins from water caltrop (*Trapa quadrispinosa*) pericarps and found UAE as a time and energy-saving method when compared to heat reflux. The high temperature in heat reflux led to compound degradation, verified in the present study for HAE (**Figure 5.3**). The authors also reported ethanol/water mixtures (60:40, *v/v*) as preferable to other organic solvents.

Experimental validation of the predictive models

The global HAE and UAE conditions that maximise both the extraction yield and the recovery of tannins from *C. hypocistis* were experimentally tested to evaluate the predictive accuracy of the theoretical models.

The experimental data for extraction yield and total tannins agrees with the model-predicted values, as confirmed by the post-analysis verification performed using the Design-Expert software ($\alpha = 0.05$). The HAE and UAE processes yielded 54±1% and 52±2% of extract weight, values that did not differ significantly from the predicted 53±1% and 53±1%, respectively (**Table 5.5**).

Furthermore, while each gram of extract obtained by HAE contained 200±4 mg of total tannins, the UAE resulted in 178±8 mg of target total tannins. The predictive capacity of the mathematical models was thus experimentally validated for these dependent variables. However, despite the good agreement for the extraction yields and total tannin contents obtained with the two extraction methods, the contents of some of the individual compounds were not within the model-predicted values, as shown in **Table S5.1** provided in the **supplementary material**.
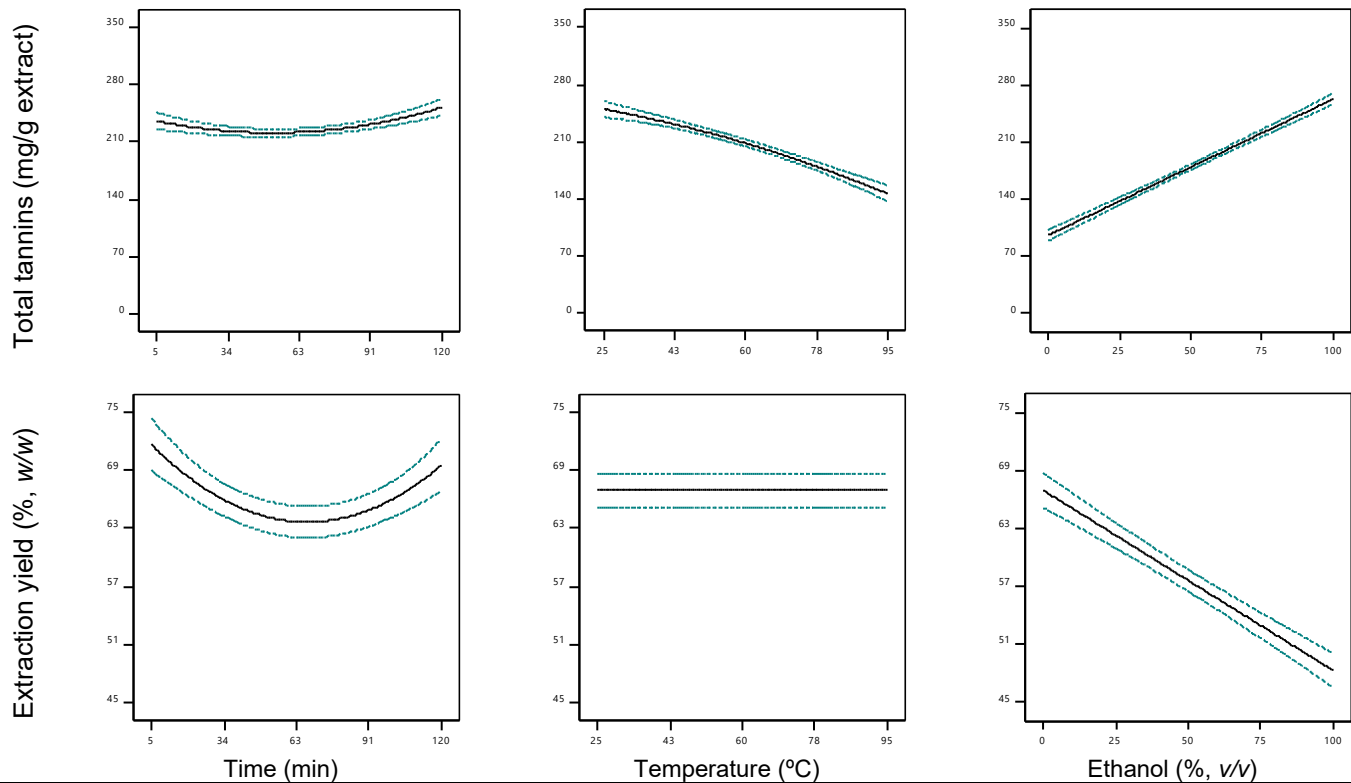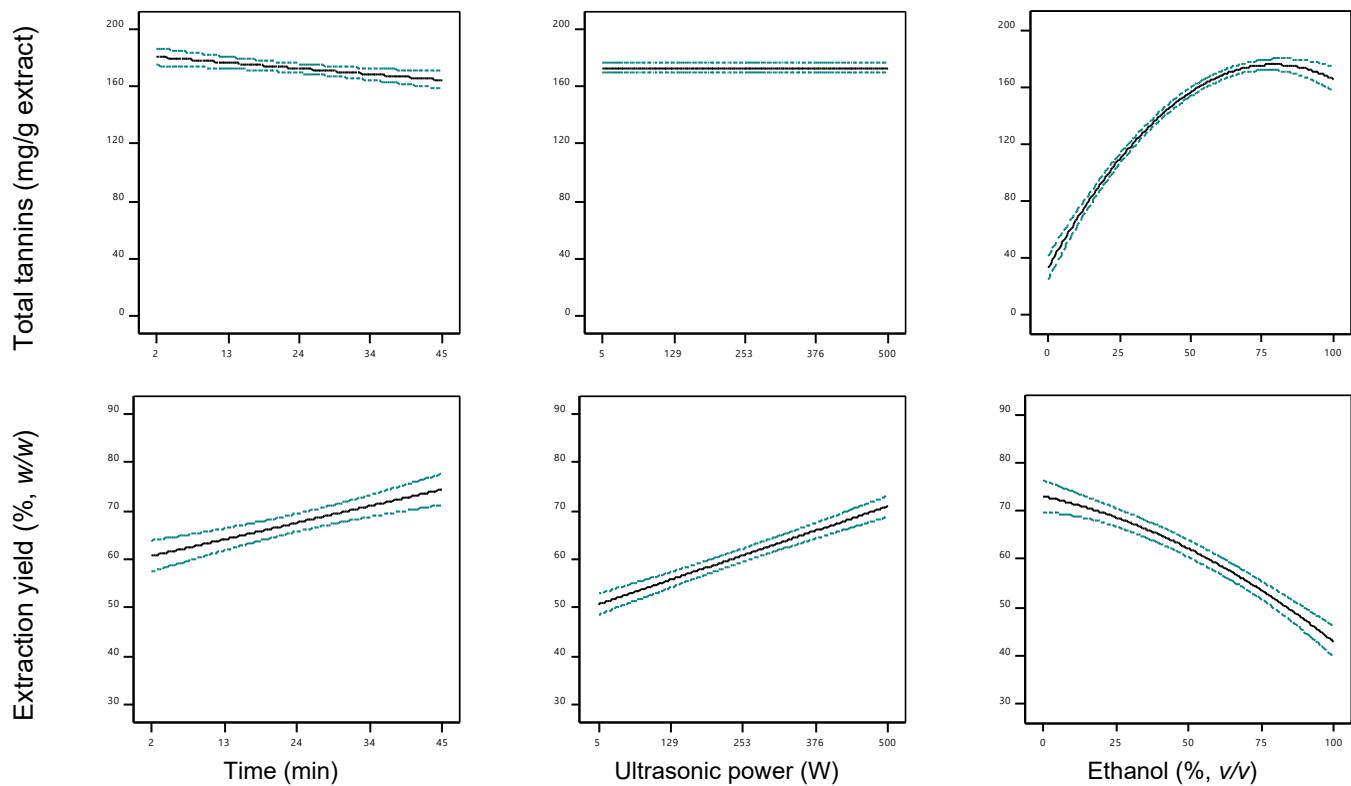
Figure 5.3. 2D response graphs for the effects of the independent variables on the extraction yield (Y_1: extract weight) and total tannin content (Y_9) obtained with HAE and UAE. The excluded variables were fixed in each graph at their optimal value (**Table 5.5**).

Conclusions

The present study demonstrated the capacity of the tested methods to extract tannins from *C. hypocistis* successfully. HAE offered slightly higher response values but required a longer processing time than UAE (95.1 versus 18.7 min, respectively). As an intensification factor, HAE needed 46.4 ºC and UAE, 327.4 W. Both methods required high ethanol percentages, 74.3% and 69.3%, respectively, to maximise the extract weight and tannin content simultaneously. Although the solvent percentage was the most relevant variable in both extraction processes, all three tested independent variables (t, T/P, and S) significantly affected the analysed responses, justifying the use of RSM. Summarising, the optimum UAE conditions to obtain the maximum extraction yield (Y_1) and the highest total tannin content (Y_2) were: (Y_1) 28.4 min, 456 W, and 22.7% ethanol; 19.5 min, 405.1 W, and 72.4% ethanol. Finally, 18.7 min, 327 W, and 69.3% ethanol were required to simultaneously maximise both conditions.

Chapter 6: Investigate *Cytinus hypocistis* skin anti-ageing properties

The information presented in this chapter is currently being prepared for publication.

EN ESTA VERSIÓN DE LA TESIS NO SE MUESTRA
EL CAPITULO 6 POR CONFLICTO CON UNA
POSIBLE PUBLICACIÓN FUTURA

PART III

Final remarks

Chapter 7: Integrative discussion

The thesis's primary objective was to valorise the parasitic species *Cytinus hypocistis* (L.) L. subsp. *macranthus* Wettst. This encompassed its thorough chemical and bioactive characterisation, the exploitation of its most bioactive compounds, and the investigation of their skin anti-ageing properties. The chemical and bioactive characterisations of *C. hypocistis* are unveiled in **Chapters 3 and 4**. The comprehensive nutritional analysis (**Chapter 3**) of the whole plant and its nectar unveiled a well-balanced nutritional profile, shedding light on its historical significance as a source of sustenance during periods of scarcity [159,172]. Its nectar proved to be a good source of protein and unsaturated fatty acids, approximately 2-fold higher than the whole plant. Polyunsaturated fatty acids were significant, comprising approximately 47% of the total fatty acids in the entire plant and 49% in its nectar. This can be attributed to the high linoleic acid content in both samples, which accounted for 40.08% and 39.90%, respectively. Interestingly, linoleic acid is an essential fatty acid that humans cannot synthesise [192]. High percentages of linoleic and α-linolenic acids have also been described in other edible flowers, including *Calendula officinalis* L. and *Trifolium angustifolium* L. [193].

The phytochemical profiles of the whole plant, its petals, stalks, and nectar were also evaluated. Seventeen phenolic compounds were identified in all samples, with the highest concentration observed in the petals and the lowest in the nectar. Galloyl-bis-HHDP-glucose was the most abundant compound in all samples, exhibiting its highest concentration in the petals and the whole plant. All extracts exhibited antidiabetic, anti-tyrosinase, antibacterial, and cytotoxicity against the tested tumour cell lines, with no toxicity observed on a non-tumour cell line. Among the assessed activities, the antioxidant capacity presented notable results, with no significant differences observed between the petals and the whole plant. Phenolic compounds represent a ubiquitous group of secondary metabolites in plants, known for their multifaceted biological effects [202]. Of particular significance, the presence of galloyl moieties has been recognised as a critical factor in the remarkable bioactivity of tannin-rich plants, playing multiple functional roles such as antimicrobial, anti-inflammatory, antidiabetic, and antioxidant activities [158].

Chapter 4 delves into a comparative chemical and bioactive study between *C. hypocistis* and its host to decipher whether the bioactive properties of the parasite are linked to its high hydrolysable tannin content or a potential exchange of phenolic compounds with its host. A total of five hydroethanolic extracts were analysed: *C. hypocistis* (CH); parasited *H. lasianthum* aerial parts (PHLAP); parasited *H. lasianthum* roots (PHLR); non-parasited *H. lasianthum* aerial parts (HLAP); and the non-parasited *H. lasianthum* aerial roots (HLR). Flavonoids were the principal group of phenolic compounds identified in the host extracts, while hydrolysable tannins were the major group in the parasite. These results align with the data presented in **Chapter 3** and the only published study regarding the *Halimium* genus phytochemical profile [260]. Except for one compound, trigalloyl-HHDP-glucoside, the phenolic profile of the host (both non-parasited and parasited) was different from that of the parasite, which possibly indicates the existence of a proper pathway of compound biosynthesis in the parasite. This hypothesis was supported by the PCA analysis, where three defined groups were identified based on phenolic composition and bioactivities: root extracts from *H. lasianthum*, aerial extracts from *H. lasianthum*, and *C. hypocistis* extracts.

Interestingly, the phytochemical analysis conducted in **Chapter 4** reveals variations in the concentration of specific phenolic compounds in the *Cytinus hypocistis* whole plant extract compared to **Chapter 3**. Galloyl-bis-HHDP-glucose, while still the predominant compound in the extract, displayed a notable decrease in concentration, nearly halving from the sample harvested in 2019 (**Chapter 3**) to 2020 (**Chapter 4**). This discrepancy extended to the bioactivities, such as the antioxidant capacity, with a less favourable IC_{50} value. The variances observed may be attributed to the differences in foraging time and extraction methods (maceration at room temperature versus HAE), which have been recognised as factors influencing plant phenolic composition and concentration [262–264]. It's important to note that plant extracts are complex, containing hundreds or even thousands of individual compounds. This complexity arises from the number of bioactive species in the extract and their synergistic, additive, or antagonistic properties [265].

Given the valuable insights gained within these **Chapters (3 and 4)**, it is likely that hydrolysable tannins play a crucial role in the studied bioactivities. As such, increasing their concentration could be highly beneficial in enhancing the desired properties of the extract. However, it was also observed that the harvest year significantly impacts the final chemical composition, and it would be worthwhile to gain a deeper understanding of this effect. Hence, the forthcoming chapters of this thesis were committed to optimising the extraction of hydrolysable tannins (**Chapter 5**) and delving into the impact of the foraging year on extract composition, along with the potential implications of these compounds on *C. hypocistis* skin anti-ageing properties (**Chapter 6**).

In the work described in **Chapter 5**, Response Surface Methodology (RSM) was applied to optimise tannin extraction using Heat-Assisted (HAE) and Ultrasound-Assisted (UAE) methods. The two experimental designs (for HAE and UAE) investigated the relationship between the independent variables X_1 [t (min): time], X_2 [T (ºC): temperature or P (W): ultrasonic power], and X_3 [S (%): solvent ratio (% of ethanol/water, v/v)], and the dependent variables (Y). The Y was expressed in the form of nine responses: seven responses (Y_2-Y_7) corresponding to the tannins at the highest concentration in the extract, and two responses corresponding to the extraction yield (Y_1) and the mg of tannins per g of extract (Y_9). The results from both extraction systems revealed the variable solvent effectively contributed to the selectivity of the extraction processes. Interestingly, although the lower ethanol percentages gave rise to higher extraction yields (possibly due to greater recovery of water-soluble carbohydrates), the highest concentrations of tannins were achieved using higher ethanol percentages. Despite the solvent percentage being the most relevant variable in both extraction processes, all three tested independent variables (t, T/P, and S) significantly affected the analysed responses, justifying the use of RSM. UAE is known to have some advantages over HAE, demonstrated by significantly shorter processing times [299]. According to previous works, acoustic cavitation promotes the release of compounds faster than when using temperature as an intensification factor [299]. These results (**Chapter 5**) were supported by those previously reported by Liang and colleagues [300], who

optimised heat reflux and UAE methods to recover hydrolysable tannins from water caltrop (*Trapa quadrispinosa*) pericarps and found UAE as a time and energy-saving method when compared to heat reflux. Similarly to heat reflux, the high temperatures of HAE led to compound degradation. These authors also reported ethanol/water mixtures (60:40, *v/v*) preferable to other organic solvents, supporting the solvent selection of the present work [300].

The impact of the foraging year on extract composition and the potential correlation of these compounds on *C. hypocistis* skin anti-ageing properties was assessed in **Chapter 6**. Nine extracts (3 extraction conditions x 3 different years) were prepared using UAE following the optimum variables determined in Chapter. 5 These samples were bio-assayed for their cytotoxic, phototoxic, antioxidant, and enzyme-inhibitory properties (tyrosinase, collagenase, and elastase). Interestingly, among the studied bioactivities, the anti-elastase results exhibited a significant variation among the samples from the different years. A bioassay-guided fractionation was performed to identify the discriminant features responsible for this variation, followed by its purification and structural elucidation. Remarkably, one of the purified subfractions exhibited a tenfold improvement in neutrophil elastase inhibition efficacy compared to the crude extract; its effectiveness fell within the same range as SPCK, a potent irreversible elastase inhibitor. Overall, this subfraction also presented better antioxidant and enzyme inhibitory properties than the crude extract and positive controls, with no phototoxicity and cytotoxicity against different skin cell lines. Following dereplication, compounds exhibiting the molecular formula $C_{34}H_{24}O_{22}$ emerged as the most discriminant features, a finding subsequently validated within the most bioactive subfraction (P19.9) through 2D NMR analysis and annotated as 2,3:4,6-bis(hexahydroxydiphenoyl)glucose. The strong intensities of the HMBC cross peaks ($\delta_H \rightarrow \delta_C$) indicated a major compound with a *S,S* axial configuration as found in pedunculagin. Interestingly, pedunculagin was tentatively identified in Chapter 3 through HPLC-DAD-ESI/MS^n in extracts from the first year (the same year that originated P19.9) but not in the second and third years [240,314,328]. However, the purified P19.9 seems to remain a mixture of configurational isomers that

could include differences in sugar found in different ellagitannins, such as $(S,S)_{axial}$-α-D-pyranose in potentillin [333], $(S,S)_{axial}$-β-D-pyranose in casuarictin, or indicate that the subfraction was not to fully purified [334]. Therefore, this might indicate that the anti-ageing compound found in *Cytinus hypocistis* could be a mixture of configurational isomers of pedunculagin.

Pedunculagin has already been described as a potent neutrophil elastase inhibitor [339]. In fact, ellagitannins such as pedunculagin or the putative novel identified compound isolated in this study, present an ideal framework as innovative inhibitors of human neutrophil elastase. This is attributed to their glucosyl core linked to HHDP moieties, which play a crucial role in establishing π-π interactions with the aromatic side chains of the enzyme [340].

Chapter 8: Conclusion

Prior to the conduct of the research presented in this thesis, a comprehensive characterisation of the chemical composition of *Cytinus hypocistis* had not been undertaken, and its active constituents had yet to be disclosed. Nonetheless, other authors pointed out hydrolysable tannins as the compounds responsible for the plant's bioactive properties. Interestingly, this class of tannins are renowned for their potent antioxidant effects and capacity to inhibit the precursors of elastolytic enzymes, making them attractive targets for delaying skin ageing. Therefore, the main objective of the work presented in this thesis was to valorise the underexplored parasitic species *Cytinus hypocistis* (L.) L. subsp. *macranthus* Wettst by conducting its comprehensive characterisation, followed by a more detailed investigation of its skin anti-ageing properties. According to this, each Chapter describes the work performed to achieve the proposed specific objectives described in Chapter 2.

Thus, in Chapter 3, the underexplored species' chemical and bioactive characterisation shed light on its historical significance as famine food and its potential as a source of bioactive compounds with a broad spectrum of biological activities. Furthermore, it was possible to tentatively confirm the identity of the hydrolysable tannins behind its bioactive properties.

Chapter 4 investigated the potential phytochemical exchange between the host and the parasite and provided insights into the intricate ecological relationship between these two plant species. Flavonoids were the principal group of phenolic compounds identified in the host extracts, while hydrolysable tannins were the major group in the parasite. Except for one compound, the phenolic profile of the host was different from that of the parasite, which possibly indicates the existence of a proper pathway of compound biosynthesis in the parasite.

Chapter 5 involved optimising two methodologies to obtain extracts rich in hydrolysable tannins. Response surface methodology was used to maximise the extraction yield, total tannin content, and the average between both responses. The results revealed that the variable solvent effectively contributed to the selectivity of the extraction processes, with ultrasound-assisted extraction being selected as the better extraction methodology for further studies.

Finally, Chapter 6 sheds light on *C. hypocistis*'s phytochemical profile variation and its correlation with the species' skin anti-ageing properties. The biochemometric analysis identified the compound 2,3:4,6-bis(hexahydroxydiphenoyl)glucose, with a molecular mass of 784.075 Da, as the discriminant feature responsible for the outstanding human neutrophil elastase inhibition. Upon structural elucidation, all indications suggest that the compound might be a mixture of configurational isomers of pedunculagin. The subfraction containing this compound exhibited excellent inhibitory activity compared to the crude extract. However, chemical synthesis efforts followed by biological activity confirmation would be necessary to confirm the compound's stereochemistry specific to its anti-ageing properties.

This thesis has significantly enhanced the understanding of this unexplored species, creating new opportunities for exploration across various scientific domains. The host-parasite relationship can be more thoroughly investigated through metabolomic methodologies to confirm the presence of any shared secondary metabolites and explore the specific metabolic pathways of the parasite. Moreover, the thesis underscores the pivotal role of ellagitannins as anti-ageing compounds, particularly as neutrophil elastase inhibitors. This enzyme extends its impact to intricate conditions such as psoriasis, chronic lung diseases, cancer, and cystic fibrosis. Consequently, the chemical synthesis of ellagitannins-based compounds holds promise for developing novel and potent inhibitors in skin ageing and other health-related domains.

REFERENCES

1. Gilaberte, Y.; Prieto-Torres, L.; Pastushenko, I.; Juarranz, Á. Anatomy and Function of the Skin. In *Nanoscience in Dermatology*; Academic Press, 2016; pp. 1–14 ISBN 9780128029459.

2. Gu, Y.; Han, J.; Jiang, C.; Zhang, Y. Biomarkers, Oxidative Stress and Autophagy in Skin Aging. *Ageing Res Rev* **2020**, *59*, 101036, doi:10.1016/J.ARR.2020.101036.

3. Proksch, E.; Brandner, J.M.; Jensen, J.M. The Skin: An Indispensable Barrier. *Exp Dermatol* **2008**, *17*, 1063–1072, doi:10.1111/J.1600-0625.2008.00786.X.

4. Kahremany, S.; Hofmann, L.; Gruzman, A.; Dinkova-Kostova, A.T.; Cohen, G. NRF2 in Dermatological Disorders: Pharmacological Activation for Protection against Cutaneous Photodamage and Photodermatosis. *Free Radic Biol Med* **2022**, *188*, 262, doi:10.1016/J.FREERADBIOMED.2022.06.238.

5. Zorina, A.; Zorin, V.; Isaev, A.; Kudlay, D.; Vasileva, M.; Kopnin, P. Dermal Fibroblasts as the Main Target for Skin Anti-Age Correction Using a Combination of Regenerative Medicine Methods. *Curr Issues Mol Biol* **2023**, *45*, 3829, doi:10.3390/CIMB45050247.

6. Layers of Epidermis - Labster Available online: https://theory.labster.com/epidermis_layers/ (accessed on 7 November 2023).

7. Segre, J.A. Epidermal Barrier Formation and Recovery in Skin Disorders. *Journal of Clinical Investigation* **2006**, *116*, 1150, doi:10.1172/JCI28521.

8. Denat, L.; Kadekaro, A.L.; Marrot, L.; Leachman, S.A.; Abdel-Malek, Z.A. Melanocytes as Instigators and Victims of Oxidative Stress. *Journal of Investigative Dermatology* **2014**, *134*, 1512–1518, doi:10.1038/JID.2014.65.

9. Shain, A.H.; Bastian, B.C. From Melanocytes to Melanomas. *Nature Reviews Cancer 2016 16:6* **2016**, *16*, 345–358, doi:10.1038/nrc.2016.37.

10. Johnson, K.O. The Roles and Functions of Cutaneous Mechanoreceptors. *Curr Opin Neurobiol* **2001**, *11*, 455–461, doi:10.1016/S0959-4388(00)00234-8.

11. Romani, N.; Clausen, B.E.; Stoitzner, P. Langerhans Cells and More: Langerin-Expressing Dendritic Cell Subsets in the Skin. *Immunol Rev* **2010**, *234*, 120–141, doi:10.1111/J.0105-2896.2009.00886.X.

12. Simões, M.C.F.; Sousa, J.J.S.; Pais, A.A.C.C. Skin Cancer and New Treatment Perspectives: A Review. *Cancer Lett* **2015**, *357*, 8–42, doi:10.1016/J.CANLET.2014.11.001.

13. Lai-Cheong, J.E.; McGrath, J.A. Structure and Function of Skin, Hair and Nails. *Medicine* **2017**, *45*, 347–351, doi:10.1016/J.MPMED.2017.03.004.

14. Sorrell, J.M.; Caplan, A.I. Fibroblast Heterogeneity: More than Skin Deep. *J Cell Sci* **2004**, *117*, 667–675, doi:10.1242/JCS.01005.

15. Reilly, D.M.; Lozano, J. Skin Collagen through the Lifestages: Importance for Skin Health and Beauty. *Plast Aesthet Res* **2021**, *8*, null-null, doi:10.20517/2347-9264.2020.153.

16. Rinnerthaler, M.; Bischof, J.; Streubel, M.K.; Trost, A.; Richter, K. Oxidative Stress in Aging Human Skin. *Biomolecules 2015, Vol. 5, Pages 545-589* **2015**, *5*, 545–589, doi:10.3390/BIOM5020545.

17. Liu, N.; Matsumura, H.; Kato, T.; Ichinose, S.; Takada, A.; Namiki, T.; Asakawa, K.; Morinaga, H.; Mohri, Y.; De Arcangelis, A.; et al. Stem Cell Competition Orchestrates Skin Homeostasis and Ageing. *Nature 2019 568:7752* **2019**, *568*, 344–350, doi:10.1038/s41586-019-1085-7.

18. Naylor, E.C.; Watson, R.E.B.; Sherratt, M.J. Molecular Aspects of Skin Ageing. *Maturitas* **2011**, *69*, 249–256, doi:10.1016/J.MATURITAS.2011.04.011.

19. Waller, J.M.; Maibach, H.I. Age and Skin Structure and Function, a Quantitative Approach (II): Protein, Glycosaminoglycan, Water, and Lipid Content and Structure. *Skin Research and Technology* **2006**, *12*, 145–154, doi:10.1111/J.0909-752X.2006.00146.X.

20. Quan, T.; Qin, Z.; Xia, W.; Shao, Y.; Voorhees, J.J.; Fisher, G.J. Matrix-Degrading Metalloproteinases in Photoaging. *Journal of Investigative Dermatology Symposium Proceedings* **2009**, *14*, 20–24, doi:10.1038/JIDSYMP.2009.8.

21. Pittayapruek, P.; Meephansan, J.; Prapapan, O.; Komine, M.; Ohtsuki, M. Role of Matrix Metalloproteinases in Photoaging and Photocarcinogenesis. *Int J Mol Sci* **2016**, *17*, doi:10.3390/IJMS17060868.

22. Philips, N.; Auler, S.; Hugo, R.; Gonzalez, S. Beneficial Regulation of Matrix Metalloproteinases for Skin Health. *Enzyme Res* **2011**, *2011*, doi:10.4061/2011/427285.

23. Costello, L.; Dicolandrea, T.; Tasseff, R.; Isfort, R.; Bascom, C.; von Zglinicki, T.; Przyborski, S. Tissue Engineering Strategies to Bioengineer the Ageing Skin Phenotype in Vitro. *Aging Cell* **2022**, *21*, e13550, doi:10.1111/ACEL.13550.

24. Viña, J.; Borrás, C.; Miquel, J. Theories of Ageing. *IUBMB Life* **2007**, *59*, 249–254, doi:10.1080/15216540601178067.

25. Pomatto, L.C.D.; Davies, K.J.A. Adaptive Homeostasis and the Free Radical Theory of Ageing. *Free Radic Biol Med* **2018**, *124*, 420–430, doi:10.1016/J.FREERADBIOMED.2018.06.016.

26. Beckman, K.B.; Ames, B.N. The Free Radical Theory of Aging Matures. *Physiol Rev* **1998**, *78*, 547–581, doi:10.1152/PHYSREV.1998.78.2.547.

27. HARMAN, D. Aging: A Theory Based on Free Radical and Radiation Chemistry. *J Gerontol* **1956**, *11*, 298–300, doi:10.1093/GERONJ/11.3.298.

28. Harman, D. Free Radical Theory of Aging. *Mutation Research/DNAging* **1992**, *275*, 257–266, doi:10.1016/0921-8734(92)90030-S.

29. Gladyshev, V.N. The Free Radical Theory of Aging Is Dead. Long Live the Damage Theory! *Antioxid Redox Signal* **2014**, *20*, 727, doi:10.1089/ARS.2013.5228.

30. Zhang, Y.; Ikeno, Y.; Qi, W.; Chaudhuri, A.; Li, Y.; Bokov, A.; Thorpe, S.R.; Baynes, J.W.; Epstein, C.; Richardson, A.; et al. Mice Deficient in Both Mn Superoxide Dismutase and Glutathione Peroxidase-1 Have Increased Oxidative Damage and a Greater Incidence of Pathology but No Reduction in Longevity. *The Journals of Gerontology: Series A* **2009**, *64A*, 1212–1220, doi:10.1093/GERONA/GLP132.

31. Mele, J.; Van Remmen, H.; Vijg, J.; Richardson, A. Characterization of Transgenic Mice That Overexpress Both Copper Zinc Superoxide Dismutase and Catalase. *https://home.liebertpub.com/ars* **2006**, *8*, 628–638, doi:10.1089/ARS.2006.8.628.

32. Pérez, V.I.; Van Remmen, H.; Bokov, A.; Epstein, C.J.; Vijg, J.; Richardson, A. The Overexpression of Major Antioxidant Enzymes Does Not Extend the Lifespan of Mice. *Aging Cell* **2009**, *8*, 73–75, doi:10.1111/J.1474-9726.2008.00449.X.

33. Yang, W.; Hekimi, S. A Mitochondrial Superoxide Signal Triggers Increased Longevity in Caenorhabditis Elegans. *PLoS Biol* **2010**, *8*, e1000556, doi:10.1371/JOURNAL.PBIO.1000556.

34. Sohal, R.S.; Orr, W.C. The Redox Stress Hypothesis of Aging. *Free Radic Biol Med* **2012**, *52*, 539, doi:10.1016/J.FREERADBIOMED.2011.10.445.

35. Gladyshev, V.N.; Kritchevsky, S.B.; Clarke, S.G.; Cuervo, A.M.; Fiehn, O.; de Magalhães, J.P.; Mau, T.; Maes, M.; Moritz, R.L.; Niedernhofer, L.J.; et al. Molecular Damage in Aging. *Nature Aging 2021 1:12* **2021**, *1*, 1096–1106, doi:10.1038/s43587-021-00150-3.

36. Rinnerthaler, M.; Bischof, J.; Streubel, M.K.; Trost, A.; Richter, K. Oxidative Stress in Aging Human Skin. *Biomolecules* **2015**, *5*, 545, doi:10.3390/BIOM5020545.

37. Warraich, U. e. A.; Hussain, F.; Kayani, H.U.R. Aging - Oxidative Stress, Antioxidants and Computational Modeling. *Heliyon* **2020**, *6*, doi:10.1016/J.HELIYON.2020.E04107.

38. Russell-Goldman, E.; Murphy, G.F. The Pathobiology of Skin Aging: New Insights into an Old Dilemma. *Am J Pathol* **2020**, *190*, 1356–1369, doi:10.1016/J.AJPATH.2020.03.007.

39. Farage, M.A.; Miller, K.W.; Elsner, P.; Maibach, H.I. Intrinsic and Extrinsic Factors in Skin Ageing: A Review. *Int J Cosmet Sci* **2008**, *30*, 87–95, doi:10.1111/J.1468-2494.2007.00415.X.

40. Chaiprasongsuk, A.; Panich, U. Role of Phytochemicals in Skin Photoprotection via Regulation of Nrf2. *Front Pharmacol* **2022**, *13*, 823881, doi:10.3389/FPHAR.2022.823881/BIBTEX.

41. Amaro-Ortiz, A.; Yan, B.; D'Orazio, J.A. Ultraviolet Radiation, Aging and the Skin: Prevention of Damage by Topical CAMP Manipulation. *Molecules* **2014**, *19*, 6202, doi:10.3390/MOLECULES19056202.

42. Kammeyer, A.; Luiten, R.M. Oxidation Events and Skin Aging. *Ageing Res Rev* **2015**, *21*, 16–29, doi:10.1016/J.ARR.2015.01.001.

43. Kohl, E.; Steinbauer, J.; Landthaler, M.; Szeimies, R.M. Skin Ageing. *Journal of the European Academy of Dermatology and Venereology* **2011**, *25*, 873–884, doi:10.1111/J.1468-3083.2010.03963.X.

44. Flament, F.; Bazin, R.; Laquieze, S.; Rubert, V.; Simonpietri, E.; Piot, B. Effect of the Sun on Visible Clinical Signs of Aging in Caucasian Skin. *Clin Cosmet Investig Dermatol* **2013**, *6*, 221–232, doi:10.2147/CCID.S44686.

45. Saewan, N.; Jimtaisong, A. Natural Products as Photoprotection. *J Cosmet Dermatol* **2015**, *14*, 47–63, doi:10.1111/JOCD.12123.

46. Bagde, A.; Mondal, A.; Singh, M. Drug Delivery Strategies for Chemoprevention of UVB-Induced Skin Cancer: A Review. *Photodermatol Photoimmunol Photomed* **2018**, *34*, 60–68, doi:10.1111/PHPP.12368.

47. Hoisington, R.D.; Whiteside, M.; Herndon, J.M. Unequivocal Detection of Solar Ultraviolet Radiation 250-300 Nm (UV-C) at Earth's Surface. *European Journal of Applied Sciences* **2023**, *11*, 455-472., doi:10.14738/AIVP.112.14429.

48. Matsumura, Y.; Ananthaswamy, H.N. Toxic Effects of Ultraviolet Radiation on the Skin. *Toxicol Appl Pharmacol* **2004**, *195*, 298–308, doi:10.1016/j.taap.2003.08.019.

49. Finlayson, L.; Barnard, I.R.M.; McMillan, L.; Ibbotson, S.H.; Brown, C.T.A.; Eadie, E.; Wood, K. Depth Penetration of Light into Skin as a Function of Wavelength from 200 to 1000 Nm. *Photochem Photobiol* **2022**, *98*, 974–981, doi:10.1111/PHP.13550.

50. MacDonald-Wicks, L.K.; Wood, L.G.; Garg, M.L. Methodology for the Determination of Biological Antioxidant Capacity in Vitro: A Review. *J Sci Food Agric* **2006**, *86*, 2046–2056, doi:10.1002/jsfa.2603.

51. Patra, V.K.; Byrne, S.N.; Wolf, P. The Skin Microbiome: Is It Affected by UV-Induced Immune Suppression? *Front Microbiol* **2016**, *7*, 195932, doi:10.3389/FMICB.2016.01235/BIBTEX.

52. Van Avondt, K.; Strecker, J.K.; Tulotta, C.; Minnerup, J.; Schulz, C.; Soehnlein, O. Neutrophils in Aging and Aging-Related Pathologies. *Immunol Rev* **2023**, *314*, 357–375, doi:10.1111/IMR.13153.

53. Rijken, F.; Kiekens, R.C.M.; Bruijnzeel, P.L.B. Skin-Infiltrating Neutrophils Following Exposure to Solar-Simulated Radiation Could Play an Important Role in Photoageing of Human Skin. *Br J Dermatol* **2005**, *152*, 321–328, doi:10.1111/J.1365-2133.2004.06335.X.

54. Zhang, S.; Duan, E. Fighting against Skin Aging: The Way from Bench to Bedside. *Cell Transplant* **2018**, *27*, 729–738, doi:10.1177/0963689717725755.

55. Gromkowska-Kępka, K.J.; Puścion-Jakubik, A.; Markiewicz-Żukowska, R.; Socha, K. The Impact of Ultraviolet Radiation on Skin Photoaging — Review of in Vitro Studies. *J Cosmet Dermatol* **2021**, *20*, 3427–3431, doi:10.1111/jocd.14033.

56. Kosmadaki, M.G.; Gilchrest, B.A. The Role of Telomeres in Skin Aging/Photoaging. *Micron* **2004**, *35*, 155–159, doi:10.1016/J.MICRON.2003.11.002.

57.	Fitsiou, E.; Pulido, T.; Campisi, J.; Alimirah, F.; Demaria, M. Cellular Senescence and the Senescence-Associated Secretory Phenotype as Drivers of Skin Photoaging. *Journal of Investigative Dermatology* **2021**, *141*, 1119–1126, doi:10.1016/J.JID.2020.09.031.

58.	Takasugi, M. Emerging Roles of Extracellular Vesicles in Cellular Senescence and Aging. *Aging Cell* **2018**, *17*, e12734, doi:10.1111/ACEL.12734.

59.	Wlaschek, M.; Maity, P.; Makrantonaki, E.; Scharffetter-Kochanek, K. Connective Tissue and Fibroblast Senescence in Skin Aging. *Journal of Investigative Dermatology* **2021**, *141*, 985–992, doi:10.1016/J.JID.2020.11.010.

60.	Nelson, G.; Wordsworth, J.; Wang, C.; Jurk, D.; Lawless, C.; Martin-Ruiz, C.; von Zglinicki, T. A Senescent Cell Bystander Effect: Senescence-Induced Senescence. *Aging Cell* **2012**, *11*, 345–349, doi:10.1111/J.1474-9726.2012.00795.X.

61.	Passos, J.F.; Nelson, G.; Wang, C.; Richter, T.; Simillion, C.; Proctor, C.J.; Miwa, S.; Olijslagers, S.; Hallinan, J.; Wipat, A.; et al. Feedback between P21 and Reactive Oxygen Production Is Necessary for Cell Senescence. *Mol Syst Biol* **2010**, *6*, 347, doi:10.1038/MSB.2010.5.

62.	Shin, S.H.; Lee, Y.H.; Rho, N.K.; Park, K.Y. Skin Aging from Mechanisms to Interventions: Focusing on Dermal Aging. *Front Physiol* **2023**, *14*, 1195272, doi:10.3389/FPHYS.2023.1195272/BIBTEX.

63.	Rittié, L.; Fisher, G.J. UV-Light-Induced Signal Cascades and Skin Aging. *Ageing Res Rev* **2002**, *1*, 705–720, doi:10.1016/S1568-1637(02)00024-7.

64.	Heyworth, P.G.; Knaus, U.G.; Settleman, J.; Curnutte, J.T.; Bokoch, G.M. Regulation of NADPH Oxidase Activity by Rac GTPase Activating Protein(s). *https://doi.org/10.1091/mbc.4.11.1217* **2017**, *4*, 1217–1223, doi:10.1091/MBC.4.11.1217.

65.	Kammeyer, A.; Luiten, R.M. Oxidation Events and Skin Aging. *Ageing Res Rev* **2015**, *21*, 16–29, doi:10.1016/J.ARR.2015.01.001.

66.	Cole, M.A.; Quan, T.; Voorhees, J.J.; Fisher, G.J. Extracellular Matrix Regulation of Fibroblast Function: Redefining Our Perspective on Skin Aging. *J Cell Commun Signal* **2018**, *12*, 35–43, doi:10.1007/S12079-018-0459-1/FIGURES/5.

67.	Xu, Y.; Shao, Y.; Voorhees, J.J.; Fisher, G.J. Oxidative Inhibition of Receptor-Type Protein-Tyrosine Phosphatase Kappa by Ultraviolet Irradiation Activates Epidermal Growth Factor Receptor in Human Keratinocytes. *J Biol Chem* **2006**, *281*, 27389–27397, doi:10.1074/JBC.M602355200.

68.	Rehman, S.; Rahimi, N.; Dimri, M. Biochemistry, G Protein Coupled Receptors. *StatPearls* **2023**.

69.	Coso, O.A.; Chiariello, M.; Yu, J.C.; Teramoto, H.; Crespo, P.; Xu, N.; Miki, T.; Silvio Gutkind, J. The Small GTP-Binding Proteins Rac1 and Cdc42 Regulate the Activity of the JNK/SAPK Signaling Pathway. *Cell* **1995**, *81*, 1137–1146, doi:10.1016/S0092-8674(05)80018-2.

70.	Zorina, A.; Zorin, V.; Kudlay, D.; Kopnin, P. Molecular Mechanisms of Changes in Homeostasis of the Dermal Extracellular Matrix: Both Involutional and Mediated by Ultraviolet Radiation. *International Journal of Molecular Sciences 2022, Vol. 23, Page 6655* **2022**, *23*, 6655, doi:10.3390/IJMS23126655.

71.	Miekus, N.; Luise, C.; Sippl, W.; Baczek, T.; Schmelzer, C.E.H.; Heinz, A. MMP-14 Degrades Tropoelastin and Elastin. *Biochimie* **2019**, *165*, 32–39, doi:10.1016/J.BIOCHI.2019.07.001.

72.	Lee, H.; Hong, Y.; Kim, M. Structural and Functional Changes and Possible Molecular Mechanisms in Aged Skin. *International Journal of Molecular Sciences 2021, Vol. 22, Page 12489* **2021**, *22*, 12489, doi:10.3390/IJMS222212489.

73. Daseke, M.J.; Chalise, U.; Becirovic-Agic, M.; Salomon, J.D.; Cook, L.M.; Case, A.J.; Lindsey, M.L. Neutrophil Signaling during Myocardial Infarction Wound Repair. *Cell Signal* **2021**, *77*, 109816, doi:10.1016/J.CELLSIG.2020.109816.

74. Landén, N.X.; Li, D.; Ståhle, M. Transition from Inflammation to Proliferation: A Critical Step during Wound Healing. *Cellular and Molecular Life Sciences* **2016**, *73*, 3861, doi:10.1007/S00018-016-2268-0.

75. Sharma, M.R.; Mitrani, R.; Werth, V.P. Effect of TNFα Blockade on UVB-Induced Inflammatory Cell Migration and Collagen Loss in Mice. *J Photochem Photobiol B* **2020**, *213*, 112072, doi:10.1016/J.JPHOTOBIOL.2020.112072.

76. Takeuchi, H.; Gomi, T.; Shishido, M.; Watanabe, H.; Suenobu, N. Neutrophil Elastase Contributes to Extracellular Matrix Damage Induced by Chronic Low-Dose UV Irradiation in a Hairless Mouse Photoaging Model. *J Dermatol Sci* **2010**, *60*, 151–158, doi:10.1016/J.JDERMSCI.2010.09.001.

77. Lin, L.; Betsuyaku, T.; Heimbach, L.; Li, N.; Rubenstein, D.; Shapiro, S.D.; An, L.; Giudice, G.J.; Diaz, L.A.; Senior, R.M.; et al. Neutrophil Elastase Cleaves the Murine Hemidesmosomal Protein BP180/Type XVII Collagen and Generates Degradation Products That Modulate Experimental Bullous Pemphigoid. *Matrix Biology* **2012**, *31*, 38–44, doi:10.1016/J.MATBIO.2011.09.003.

78. Lerman, I.; Hammes, S.R. Neutrophil Elastase in the Tumor Microenvironment. *Steroids* **2018**, *133*, 96–101, doi:10.1016/J.STEROIDS.2017.11.006.

79. Wilkinson, D.J.; Falconer, A.M.D.; Wright, H.L.; Lin, H.; Yamamoto, K.; Cheung, K.; Charlton, S.H.; Arques, M. del C.; Janciauskiene, S.; Refaie, R.; et al. Matrix Metalloproteinase-13 Is Fully Activated by Neutrophil Elastase and Inactivates Its Serpin Inhibitor, Alpha-1 Antitrypsin: Implications for Osteoarthritis. *FEBS J* **2022**, *289*, 121–139, doi:10.1111/FEBS.16127.

80. Wagner, C.J.; Schultz, C.; Mall, M.A. Neutrophil Elastase and Matrix Metalloproteinase 12 in Cystic Fibrosis Lung Disease. *Molecular and Cellular Pediatrics 2016 3:1* **2016**, *3*, 1–7, doi:10.1186/S40348-016-0053-7.

81. Garratt, L.W.; Sutanto, E.N.; Ling, K.M.; Looi, K.; Iosifidis, T.; Martinovich, K.M.; Shaw, N.C.; Kicic-Starcevich, E.; Knight, D.A.; Ranganathan, S.; et al. Matrix Metalloproteinase Activation by Free Neutrophil Elastase Contributes to Bronchiectasis Progression in Early Cystic Fibrosis. *European Respiratory Journal* **2015**, *46*, 384–394, doi:10.1183/09031936.00212114.

82. Shapiro, S.D.; Goldstein, N.M.; Houghton, A.M.G.; Kobayashi, D.K.; Kelley, D.; Belaaouaj, A. Neutrophil Elastase Contributes to Cigarette Smoke-Induced Emphysema in Mice. *Am J Pathol* **2003**, *163*, 2329–2335, doi:10.1016/S0002-9440(10)63589-4.

83. Itoh, Y.; Nagase, H. Preferential Inactivation of Tissue Inhibitor of Metalloproteinase-1 That Is Bound to the Precursor of Matrix Metalloproteinase 9 (Progelatinase B) by Human Neutrophil Elastase. *Journal of Biological Chemistry* **1995**, *270*, 16518–16521, doi:10.1074/jbc.270.28.16518.

84. Arafat, S.N.; Robert, M.C.; Abud, T.; Spurr-Michaud, S.; Amparo, F.; Dohlman, C.H.; Dana, R.; Gipson, I.K. Elevated Neutrophil Elastase in Tears of Ocular Graft-Versus-Host Disease Patients. *Am J Ophthalmol* **2017**, *176*, 46–52, doi:10.1016/J.AJO.2016.12.026.

85. Imokawa, G. Epithelial–Mesenchymal Interaction Mechanisms Leading to the over-Expression of Neprilysin Are Involved in the UVB-Induced Formation of Wrinkles in the Skin. *Exp Dermatol* **2016**, *25*, 2–13, doi:10.1111/EXD.13083.

86. Morisaki, N.; Moriwaki, S.; Sugiyama-Nakagiri, Y.; Haketa, K.; Takema, Y.; Imokawa, G. Neprilysin Is Identical to Skin Fibroblast Elastase: Its Role in Skin Aging and UV Responses. *J Biol Chem* **2010**, *285*, 39819–39827, doi:10.1074/JBC.M110.161547.

87. Morisaki, N.; Ohuchi, A.; Moriwaki, S. The Role of Neprilysin in Regulating the Hair Cycle. *PLoS One* **2013**, *8*, e55947, doi:10.1371/JOURNAL.PONE.0055947.

88. Bou-Gharios, G.; Osman, J.; Atherton, A.; Monoghan, P.; Vancheeswaran, R.; Black, C.; Olsen, I. Expression of Ectopeptidases in Scleroderma. *Ann Rheum Dis* **1995**, *54*, 111–116, doi:10.1136/ARD.54.2.111.

89. Mora Huertas, A.C.; Schmelzer, C.E.H.; Luise, C.; Sippl, W.; Pietzsch, M.; Hoehenwarter, W.; Heinz, A. Degradation of Tropoelastin and Skin Elastin by Neprilysin. *Biochimie* **2018**, *146*, 73–78, doi:10.1016/J.BIOCHI.2017.11.018.

90. Chen, C.Y.; Zhang, J.Q.; Li, L.; Guo, M.M.; He, Y.F.; Dong, Y.M.; Meng, H.; Yi, F. Advanced Glycation End Products in the Skin: Molecular Mechanisms, Methods of Measurement, and Inhibitory Pathways. *Front Med (Lausanne)* **2022**, *9*, doi:10.3389/FMED.2022.837222.

91. Yoshinaga, E.; Kawada, A.; Ono, K.; Fujimoto, E.; Wachi, H.; Harumiya, S.; Nagai, R.; Tajima, S. N(ε)-(Carboxymethyl)Lysine Modification of Elastin Alters Its Biological Properties: Implications for the Accumulation of Abnormal Elastic Fibers in Actinic Elastosis. *J Invest Dermatol* **2012**, *132*, 315–323, doi:10.1038/JID.2011.298.

92. Dunn, J.A.; Thorpe, S.R.; Baynes, J.W.; McCance, D.R.; Lyons, T.J.; Baynes, J.W. Age-Dependent Accumulation of N Epsilon-(Carboxymethyl)Lysine and N Epsilon-(Carboxymethyl)Hydroxylysine in Human Skin Collagen. *Biochemistry* **1991**, *30*, 1205–1210, doi:10.1021/BI00219A007.

93. Asadipooya, K.; Uy, E.M. Advanced Glycation End Products (AGEs), Receptor for AGEs, Diabetes, and Bone: Review of the Literature. *J Endocr Soc* **2019**, *3*, 1799–1818, doi:10.1210/JS.2019-00160.

94. Ott, C.; Jacobs, K.; Haucke, E.; Navarrete Santos, A.; Grune, T.; Simm, A. Role of Advanced Glycation End Products in Cellular Signaling. *Redox Biol* **2014**, *2*, 411–429, doi:10.1016/J.REDOX.2013.12.016.

95. Sies, H. Oxidative Stress: A Concept in Redox Biology and Medicine. *Redox Biol* **2015**, *4*, 180–183, doi:10.1016/j.redox.2015.01.002.

96. Sies, H.; Berndt, C.; Jones, D.P. Oxidative Stress. *Annu Rev Biochem* **2017**, *86*, 715–748, doi:10.1146/annurev-biochem-061516-045037.

97. Poole, L.B. The Basics of Thiols and Cysteines in Redox Biology and Chemistry. *Free Radic Biol Med* **2015**, *80*, 148–157, doi:10.1016/j.freeradbiomed.2014.11.013.

98. Berndt, C.; Lillig, C.H.; Flohé, L. Redox Regulation by Glutathione Needs Enzymes. *Front Pharmacol* **2014**, *5 JUL*, doi:10.3389/fphar.2014.00168.

99. Mirończuk-Chodakowska, I.; Witkowska, A.M.; Zujko, M.E. Endogenous Non-Enzymatic Antioxidants in the Human Body. *Adv Med Sci* **2018**, *63*, 68–78, doi:10.1016/j.advms.2017.05.005.

100. Valko, M.; Leibfritz, D.; Moncol, J.; Cronin, M.T.D.; Mazur, M.; Telser, J. Free Radicals and Antioxidants in Normal Physiological Functions and Human Disease. *International Journal of Biochemistry and Cell Biology* **2007**, *39*, 44–84, doi:10.1016/j.biocel.2006.07.001.

101. Bouayed, J.; Bohn, T. Exogenous Antioxidants—Double-Edged Swords in Cellular Redox State: Health Beneficial Effects at Physiologic Doses versus Deleterious Effects at High Doses. *Oxid Med Cell Longev* **2010**, *3*, 237, doi:10.4161/OXIM.3.4.12858.

102. Sies, H.; Berndt, C.; Jones, D.P. Oxidative Stress. *Annu Rev Biochem* **2017**, *86*, 715–748, doi:10.1146/annurev-biochem-061516-045037.

103. Kurutas, E.B. The Importance of Antioxidants Which Play the Role in Cellular Response against Oxidative/Nitrosative Stress: Current State. *Nutr J* **2016**, *15*, doi:10.1186/s12937-016-0186-5.

104. Moussa, Z.; M.A. Judeh, Z.; A. Ahmed, S. Nonenzymatic Exogenous and Endogenous Antioxidants. In *Free Radical Medicine and Biology*; IntechOpen, 2019.

105. Addor, F.A.S. Antioxidants in Dermatology. *An Bras Dermatol* **2017**, *92*, 356, doi:10.1590/ABD1806-4841.20175697.

106. Langton, A.K.; Graham, H.K.; Griffiths, C.E.M.; Watson, R.E.B. Ageing Significantly Impacts the Biomechanical Function and Structural Composition of Skin. *Exp Dermatol* **2019**, *28*, 981–984, doi:10.1111/EXD.13980.

107. Zargaran, D.; Zoller, F.; Zargaran, A.; Weyrich, T.; Mosahebi, A. Facial Skin Ageing: Key Concepts and Overview of Processes. *Int J Cosmet Sci* **2022**, *44*, 414–420, doi:10.1111/ICS.12779.

108. Katoh, N.; Tennstedt, D.; Abellan van Kan, G.; Saint Aroman, M.; Loir, A.; Bacqueville, D.; Duprat, L.; Guiraud, B.; Bessou-Touya, S.; Duplan, H. Gerontodermatology: The Fragility of the Epidermis in Older Adults. *Journal of the European Academy of Dermatology and Venereology* **2018**, *32*, 1–20, doi:10.1111/JDV.15253.

109. Bosset, S.; Bonnet-Duquennoy, M.; Barré, P.; Chalon, A.; Lazou, K.; Kurfurst, R.; Bonté, F.; Schnébert, S.; Disant, F.; Le Varlet, B.; et al. Decreased Expression of Keratinocyte Beta1 Integrins in Chronically Sun-Exposed Skin in Vivo. *Br J Dermatol* **2003**, *148*, 770–778, doi:10.1046/J.1365-2133.2003.05159.X.

110. Peng, H.Y.; Lin, C.C.; Wang, H.Y.; Shih, Y.; Chou, S.T. The Melanogenesis Alteration Effects of Achillea Millefolium L. Essential Oil and Linalyl Acetate: Involvement of Oxidative Stress and the JNK and ERK Signaling Pathways in Melanoma Cells. *PLoS One* **2014**, *9*, e95186, doi:10.1371/JOURNAL.PONE.0095186.

111. Chitsazan, A.; Mukhopadhyay, P.; Ferguson, B.; Handoko, H.Y.; Walker, G.J. Keratinocyte Cytokine Networks Associated with Human Melanocytic Nevus Development. *Journal of Investigative Dermatology* **2019**, *139*, 177–185, doi:10.1016/J.JID.2018.06.180.

112. Vachtenheim, J.; Borovanský, J. "Transcription Physiology" of Pigment Formation in Melanocytes: Central Role of MITF. *Exp Dermatol* **2010**, *19*, 617–627, doi:10.1111/J.1600-0625.2009.01053.X.

113. Zouboulis, C.C.; Ganceviciene, R.; Liakou, A.I.; Theodoridis, A.; Elewa, R.; Makrantonaki, E. Aesthetic Aspects of Skin Aging, Prevention, and Local Treatment. *Clin Dermatol* **2019**, *37*, 365–372, doi:10.1016/J.CLINDERMATOL.2019.04.002.

114. Choe, C.S.; Schleusener, J.; Lademann, J.; Darvin, M.E. Age Related Depth Profiles of Human Stratum Corneum Barrier-Related Molecular Parameters by Confocal Raman Microscopy in Vivo. *Mech Ageing Dev* **2018**, *172*, 6–12, doi:10.1016/J.MAD.2017.08.011.

115. Biniek, K.; Kaczvinsky, J.; Matts, P.; Dauskardt, R.H. Understanding Age-Induced Alterations to the Biomechanical Barrier Function of Human Stratum Corneum. *J Dermatol Sci* **2015**, *80*, 94–101, doi:10.1016/J.JDERMSCI.2015.07.016.

116. Langton, A.K.; Halai, P.; Griffiths, C.E.M.; Sherratt, M.J.; Watson, R.E.B. The Impact of Intrinsic Ageing on the Protein Composition of the Dermal-Epidermal Junction. *Mech Ageing Dev* **2016**, *156*, 14–16, doi:10.1016/J.MAD.2016.03.006.

117. Shin, J.W.; Kwon, S.H.; Choi, J.Y.; Na, J.I.; Huh, C.H.; Choi, H.R.; Park, K.C. Molecular Mechanisms of Dermal Aging and Antiaging Approaches. *International Journal of Molecular Sciences 2019, Vol. 20, Page 2126* **2019**, *20*, 2126, doi:10.3390/IJMS20092126.

118. Ghosh, K.; Capell, B.C. The Senescence-Associated Secretory Phenotype: Critical Effector in Skin Cancer and Aging. *Journal of Investigative Dermatology* **2016**, *136*, 2133–2139, doi:10.1016/J.JID.2016.06.621.

119. Langton, A.K.; Sherratt, M.J.; Griffiths, C.E.M.; Watson, R.E.B. Differential Expression of Elastic Fibre Components in Intrinsically Aged Skin. *Biogerontology* **2012**, *13*, 37–48, doi:10.1007/S10522-011-9332-9/FIGURES/5.

120. Varani, J.; Spearman, D.; Perone, P.; Fligiel, S.E.G.; Datta, S.C.; Wang, Z.Q.; Shao, Y.; Kang, S.; Fisher, G.J.; Voorhees, J.J. Inhibition of Type I Procollagen Synthesis by Damaged Collagen in Photoaged Skin and by Collagenase-Degraded Collagen in Vitro. *Am J Pathol* **2001**, *158*, 931–942, doi:10.1016/S0002-9440(10)64040-0.

121. Varani, J.; Dame, M.K.; Rittie, L.; Fligiel, S.E.G.; Kang, S.; Fisher, G.J.; Voorhees, J.J. Decreased Collagen Production in Chronologically Aged Skin: Roles of Age-Dependent Alteration in Fibroblast Function and Defective Mechanical Stimulation. *Am J Pathol* **2006**, *168*, 1861–1868, doi:10.2353/AJPATH.2006.051302.

122. Fisher, G.J.; Quan, T.; Purohit, T.; Shao, Y.; Moon, K.C.; He, T.; Varani, J.; Kang, S.; Voorhees, J.J. Collagen Fragmentation Promotes Oxidative Stress and Elevates Matrix Metalloproteinase-1 in Fibroblasts in Aged Human Skin. *Am J Pathol* **2009**, *174*, 101–114, doi:10.2353/AJPATH.2009.080599.

123. Chung, J.H.; Eun, H.C. Angiogenesis in Skin Aging and Photoaging. *J Dermatol* **2007**, *34*, 593–600, doi:10.1111/J.1346-8138.2007.00341.X.

124. Sellheyer, K. Pathogenesis of Solar Elastosis: Synthesis or Degradation? *J Cutan Pathol* **2003**, *30*, 123–127, doi:10.1034/J.1600-0560.2003.00018.X.

125. Gordon, J.R.S.; Brieva, J.C. Unilateral Dermatoheliosis. *https://doi.org/10.1056/NEJMicm1104059* **2012**, *366*, e25, doi:10.1056/NEJMICM1104059.

126. Gioxari, A.; Kogiannou, D.A.A.; Kalogeropoulos, N.; Kaliora, A.C. Phenolic Compounds: Bioavailability and Health Effects. In *Encyclopedia of Food and Health*; Elsevier Inc., 2016; pp. 339–345 ISBN 9780123849533.

127. Lattanzio, V.; Kroon, P.A.; Quideau, S.; Treutter, D. Plant Phenolics– Secondary Metabolites with Diverse Functions. In *Recent Advances in Polyphenol Research*; Wiley-Blackwell: Oxford, UK, 2008; Vol. 1, pp. 1–35.

128. Shirmohammadli, Y.; Efhamisisi, D.; Pizzi, A. Tannins as a Sustainable Raw Material for Green Chemistry: A Review. *Ind Crops Prod* **2018**, *126*, 316–332, doi:10.1016/j.indcrop.2018.10.034.

129. Sharma, K.P. Tannin Degradation by Phytopathogen's Tannase: A Plant's Defense Perspective. *Biocatal Agric Biotechnol* **2019**, *21*, 101342, doi:10.1016/j.bcab.2019.101342.

130. Sharma, K.P. Tannin Degradation by Phytopathogen's Tannase: A Plant's Defense Perspective. *Biocatal Agric Biotechnol* **2019**, *21*, 101342, doi:10.1016/j.bcab.2019.101342.

131. Khanbabaee, K.; van Ree, T. Tannins: Classification and Definition. *Nat Prod Rep* **2001**, *18*, 641–649, doi:10.1039/b101061l.

132. Morimoto, S.; Nonaka, G.; Nishioka, I. Tannins and Related Compounds. XXXVIII.1) Isolation and Characterization of Flavan-3-Ol Glucosides and Procyanidin Oligomers from Cassia Bark (Cinnamomum Cassia Blume). *Chem Pharm Bull (Tokyo)* **1986**, *34*, 633–642, doi:10.1248/cpb.34.633.

133. Tanaka, T.; Nonaka, G.-I.; Nishioka, I. Tannins and Related Compounds. XLII. Isolation and Characterization of Four New Hydrolyzable Tannins, Terflavins A and B, Tergallagin and Tercatain from the Leaves of Terminalia Catappa L. *Chem Pharm Bull (Tokyo)* **1986**, *34*, 1039–1049, doi:10.1248/cpb.34.1039.

134. Kashiwada, Y.; Nonaka, G.I.; Nishioka, I.; Chang, J.J.; Lee, K.H. Antitumor Agents, 129. Tannins and Related Compounds as Selective Cytotoxic Agents. *J Nat Prod* **1992**, *55*, 1033–1043, doi:10.1021/np50086a002.

135. D'Mello, J.P.F.; Duffus, J.H.; Duffus, C.M. *Toxic Substances in Crop Plants*; Royal Society of Chemistry: Cambridge, 1991; ISBN 9780851868639.

136. Ferreira, D.; Bekker, R. Oligomeric Proanthocyanidins: Naturally Occurring O-Heterocycles. *Nat Prod Rep* **1996**, *13*, 411–433, doi:10.1039/np9961300411.

137. Quideau, S.; Deffieux, D.; Douat-Casassus, C.; Pouységu, L. Plant Polyphenols: Chemical Properties, Biological Activities, and Synthesis. *Angewandte Chemie - International Edition* **2011**, *50*, 586–621, doi:10.1002/anie.201000044.

138. Menaa, F.; Menaa, A.; Tréton, J. Polyphenols against Skin Aging. In *Polyphenols in Human Health and Disease*; Academic Press, 2014; Vol. 1, pp. 819–830 ISBN 9780123984562.

139. Argyropoulou, A.; Aligiannis, N.; Trougakos, I.P.; Skaltsounis, A.L. Natural Compounds with Anti-Ageing Activity. *Nat Prod Rep* **2013**, *30*, 1412–1437, doi:10.1039/C3NP70031C.

140. Cavinato, M.; Waltenberger, B.; Baraldo, G.; Grade, C.V.C.; Stuppner, H.; Jansen-Dürr, P. Plant Extracts and Natural Compounds Used against UVB-Induced Photoaging. *Biogerontology* **2017**, *18*, 499–516, doi:10.1007/S10522-017-9715-7/FIGURES/3.

141. de Lima Cherubim, D.J.; Buzanello Martins, C.V.; Oliveira Fariña, L.; da Silva de Lucca, R.A. Polyphenols as Natural Antioxidants in Cosmetics Applications. *J Cosmet Dermatol* **2020**, *19*, 33–37, doi:10.1111/JOCD.13093.

142. Michalak, M. Plant-Derived Antioxidants: Significance in Skin Health and the Ageing Process. *International Journal of Molecular Sciences 2022, Vol. 23, Page 585* **2022**, *23*, 585, doi:10.3390/IJMS23020585.

143. Tundis, R.; Loizzo, M.R.; Bonesi, M.; Menichini, F. Potential Role of Natural Compounds Against Skin Aging.

144. Michalak, M.; Pierzak, M.; Kręcisz, B.; Suliga, E. Bioactive Compounds for Skin Health: A Review. *Nutrients 2021, Vol. 13, Page 203* **2021**, *13*, 203, doi:10.3390/NU13010203.

145. Melo, L.F.M. de; Aquino-Martins, V.G. de Q.; Silva, A.P. da; Oliveira Rocha, H.A.; Scortecci, K.C. Biological and Pharmacological Aspects of Tannins and Potential Biotechnological Applications. *Food Chem* **2023**, *414*, 135645, doi:10.1016/J.FOODCHEM.2023.135645.

146. Ryeom, G.G.M.; Bang, W.J.; Kim, Y.B.; Lee, G.E. Gallotannin Improves the Photoaged-Related Proteins by Extracellular Signal-Regulated Kinases/c-Jun N-Terminal Kinases Signaling Pathway in Human Epidermal Keratinocyte Cells. *J Med Food* **2018**, *21*, 785–792, doi:10.1089/JMF.2017.4096.

147. Bae, J.Y.; Choi, J.S.; Choi, Y.J.; Shin, S.Y.; Kang, S.W.; Han, S.J.; Kang, Y.H. (−)Epigallocatechin Gallate Hampers Collagen Destruction and Collagenase Activation in Ultraviolet-B-Irradiated Human Dermal Fibroblasts: Involvement of Mitogen-Activated Protein Kinase. *Food and Chemical Toxicology* **2008**, *46*, 1298–1307, doi:10.1016/J.FCT.2007.09.112.

148. Kwon, D.J.; Bae, Y.S.; Ju, S.M.; Goh, A.R.; Youn, G.S.; Choi, S.Y.; Park, J. Casuarinin Suppresses TARC/CCL17 and MDC/CCL22 Production via Blockade of NF-KB and STAT1 Activation in HaCaT Cells. *Biochem Biophys Res Commun* **2012**, *417*, 1254–1259, doi:10.1016/J.BBRC.2011.12.119.

149. Parasaram, V.; Nosoudi, N.; Chowdhury, A.; Vyavahare, N. Pentagalloyl Glucose Increases Elastin Deposition, Decreases Reactive Oxygen Species and Matrix Metalloproteinase Activity in Pulmonary Fibroblasts under Inflammatory Conditions. *Biochem Biophys Res Commun* **2018**, *499*, 24–29, doi:10.1016/J.BBRC.2018.03.100.

150. Park, H.J.; Kim, H.J.; Kwon, H.J.; Lee, J.Y.; Cho, B.K.; Lee, W.J.; Yang, Y.; Cho, D.H. UVB-Induced Interleukin-18 Production Is Downregulated by Tannic Acids in Human HaCaT Keratinocytes. *Exp Dermatol* **2006**, *15*, 589–595, doi:10.1111/J.1600-0625.2006.00449.X.

151. Aires, A.; Carvalho, R.; Saavedra, M.J. Valorization of Solid Wastes from Chestnut Industry Processing: Extraction and Optimization of Polyphenols, Tannins and Ellagitannins and Its Potential for Adhesives, Cosmetic and Pharmaceutical Industry. *Waste Management* **2016**, *48*, 457–464, doi:10.1016/J.WASMAN.2015.11.019.

152. Jimenez, F.; Mitts, T.F.; Liu, K.; Wang, Y.; Hinek, A. Ellagic and Tannic Acids Protect Newly Synthesized Elastic Fibers from Premature Enzymatic Degradation in Dermal Fibroblast Cultures. *J Invest Dermatol* **2006**, *126*, 1272–1280, doi:10.1038/SJ.JID.5700285.

153. Jimenez, F.; Mitts, T.F.; Liu, K.; Wang, Y.; Hinek, A. Ellagic and Tannic Acids Protect Newly Synthesized Elastic Fibers from Premature Enzymatic Degradation in Dermal Fibroblast Cultures. *Journal of Investigative Dermatology* **2006**, *126*, 1272–1280, doi:10.1038/SJ.JID.5700285.

154. Khanbabaee, K.; Ree, T. van Tannins: Classification and Definition. *Nat Prod Rep* **2001**, *18*, 641–649, doi:10.1039/B101061L.

155. Sanjust, E.; Rinaldi, A.C. Cytinus under the Microscope: Disclosing the Secrets of a Parasitic Plant. *Plants* **2021**, *10*, 146, doi:10.3390/plants10010146.

156. Vega, C. de; Thorogood, C.J.; Albaladejo, R.G.; Rakotonasolo, F.; Hobbhahn, N.; Martos, F.; Burgoyne, P.M.; Johnson, S.D. Evolutionary and Ecological Insights from Cytinus: A Plant within a Plant. *Plants, People, Planet* **2023**, doi:10.1002/PPP3.10409.

157. Thorogood, C.J.; Teixeira-Costa, L.; Ceccantini, G.; Davis, C.; Hiscock, S.J. Endoparasitic Plants and Fungi Show Evolutionary Convergence across Phylogenetic Divisions. *New Phytologist* **2021**, *232*, 1159–1167, doi:10.1111/NPH.17556.

158. Maisetta, G.; Batoni, G.; Caboni, P.; Esin, S.; Rinaldi, A.C.; Zucca, P. Tannin Profile, Antioxidant Properties, and Antimicrobial Activity of Extracts from Two Mediterranean Species of Parasitic Plant Cytinus. *BMC Complement Altern Med* **2019**, *19*, 82, doi:10.1186/s12906-019-2487-7.

159. Zucca, P.; Pintus, M.; Manzo, G.; Nieddu, M.; Steri, D.; Rinaldi, A.C. Antimicrobial, Antioxidant and Anti-Tyrosinase Properties of Extracts of the Mediterranean Parasitic Plant Cytinus Hypocistis. *BMC Res Notes* **2015**, *8*, 562, doi:10.1186/s13104-015-1546-5.

160. de Vega, C.; Berjano, R.; Arista, M.; Ortiz, P.L.; Talavera, S.; Stuessy, T.F. Genetic Races Associated with the Genera and Sections of Host Species in the Holoparasitic Plant Cytinus (Cytinaceae) in the Western Mediterranean Basin. *New Phytologist* **2008**, *178*, 875–887, doi:10.1111/j.1469-8137.2008.02423.x.

161. Westwood, J.H.; Yoder, J.I.; Timko, M.P.; dePamphilis, C.W. The Evolution of Parasitism in Plants. *Trends Plant Sci* **2010**, *15*, 227–235, doi:10.1016/j.tplants.2010.01.004.

162. Rubiales, D.; Heide-Jørgensen, H.S. Parasitic Plants. In *Encyclopedia of Life Sciences*; John Wiley & Sons, Ltd: Chichester, UK, 2011 ISBN 0412371200.

163. Smith, J.D.; Mescher, M.C.; De Moraes, C.M. Implications of Bioactive Solute Transfer from Hosts to Parasitic Plants. *Curr Opin Plant Biol* **2013**, *16*, 464–472, doi:10.1016/j.pbi.2013.06.016.

164. Bouman, F.; Meijer, W. Comparative Structure of Ovules and Seeds in Rafflesiaceae. *Plant Systematics and Evolution* **1994**, *193*, 187–212, doi:10.1007/BF00983550.

165. De Vega, C.; Ortiz, P.L.; Arista, M.; Talavera, S. The Endophytic System of Mediterranean Cytinus (Cytinaceae) Developing on Five Host Cistaceae Species. *Ann Bot* **2007**, *100*, 1209–1217, doi:10.1093/aob/mcm217.

166. De Vega, C.; Herrera, C.M.; Dötterl, S. Floral Volatiles Play a Key Role in Specialized Ant Pollination. *Perspect Plant Ecol Evol Syst* **2014**, *16*, 32–42, doi:10.1016/J.PPEES.2013.11.002.

167. De Vega, C.; Arista, M.; Ortiz, P.L.; Herrera, C.M.; Talavera, S. The Ant-Pollination System of Cytinus Hypocistis (Cytinaceae), a Mediterranean Root Holoparasite. *Ann Bot* **2009**, *103*, 1065–1075, doi:10.1093/AOB/MCP049.

168. Martos, F.; Hobbhahn, N.; de Vega, C.; Johnson, S.D. Phylogeography and Host-Shift Speciation in the Vampirecups, an Enigmatic Clade of Endophytic Holoparasitic Plants. *J Biogeogr* **2023**, *00*, 1–14, doi:10.1111/JBI.14692.

169. Henderson, L.D.J. *Greek Wild Flowers and Plant Lore in Ancient Greece. (Translated and Augmented by William T. Stearn and Eldwyth Ruth Stearn)*; Cambridge University Press, 1993; Vol. 50;.

170. Tardío, J.; Pardo-De-Santayana, M.; Morales, R. Ethnobotanical Review of Wild Edible Plants in Spain. *Botanical Journal of the Linnean Society* **2006**, *152*, 27–71, doi:10.1111/J.1095-8339.2006.00549.X.

171. Pardo-de-Santayana, M.; Tardío, J.; Blanco, E.; Carvalho, A.M.; Lastra, J.J.; San Miguel, E.; Morales, R. Traditional Knowledge of Wild Edible Plants Used in the Northwest of the Iberian Peninsula (Spain and Portugal): A Comparative Study. *J Ethnobiol Ethnomed* **2007**, *3*, 1–11, doi:10.1186/1746-4269-3-27/TABLES/4.

172. Magiatis, P.; Pratsinis, H.; Kalpoutzakis, E.; Konstantinidou, A.; Davaris, P.; Skaltsounis, A.-L. Hydrolyzable Tannins, the Active Constituents of Three Greek Cytinus Taxa against Several Tumor Cell Lines. *Biol Pharm Bull* **2001**, *24*, 707–709, doi:10.1248/bpb.24.707.

173. Fürstenwerth, H.; Schildknecht, H. Die Farbstoffe von Cytinus Hypocistis, I. Isoterchebin, Der Gelbe Farbstoff Des Zistrosenwürgers Cytinus Hypocistis (Rafflesiaceae, Schmarotzerblumengewächse). *Justus Liebigs Ann Chem* **1976**, *1976*, 112–123, doi:10.1002/JLAC.197619760111.

174. Chiocchio, I.; Mandrone, M.; Sanna, C.; Maxia, A.; Tacchini, M.; Poli, F. Screening of a Hundred Plant Extracts as Tyrosinase and Elastase Inhibitors, Two Enzymatic Targets of Cosmetic Interest. *Ind Crops Prod* **2018**, *122*, 498–505, doi:10.1016/J.INDCROP.2018.06.029.

175. Carvalho, A.M.; Barata, A.M. The Consumption of Wild Edible Plants. In *Wild Plants, Mushrooms and Nuts: Functional Food Properties and Applications*; John Wiley & Sons, Ltd, 2016; pp. 159–198 ISBN 9781118944653.

176. Torija-Isasa, M.E.; Matallana-González, M.C. A Historical Perspective of Wild Plant Foods in the Mediterranean Area. *Mediterranean Wild Edible Plants: Ethnobotany and Food Composition Tables* **2016**, 3–13, doi:10.1007/978-1-4939-3329-7_1/COVER.

177. Łuczaj, Ł.; Pieroni, A.; Tardío, J.; Pardo-De-Santayana, M.; Sõukand, R.; Svanberg, I.; Kalle, R. Wild Food Plant Use in 21st Century Europe: The Disappearance of Old Traditions and the Search for New Cuisines Involving Wild Edibles. *Acta Societatis Botanicorum Poloniae* **2012**, *81*, 359–370, doi:10.5586/ASBP.2012.031.

178. Nebel, S.; Pieroni, A.; Heinrich, M. Ta Chòrta: Wild Edible Greens Used in the Graecanic Area in Calabria, Southern Italy. *Appetite* **2006**, *47*, 333–342, doi:10.1016/J.APPET.2006.05.010.

179. Jman Redzic, S. Wild Edible Plants and Their Traditional Use in the Human Nutrition in Bosnia-Herzegovina. *Ecol Food Nutr* **2006**, *45*, 189–232, doi:10.1080/03670240600648963.

180. Tardío, J.; Pardo-De-Santayana, M.; Morales, R. Ethnobotanical Review of Wild Edible Plants in Spain. *Botanical Journal of the Linnean Society* **2006**, *152*, 27–71, doi:10.1111/J.1095-8339.2006.00549.X.

181. Carvalho, A.M.; Morales, R. Persistence of Wild Food and Wild Medicinal Plant Knowledge in a Northeastern Region of Portugal. In *Ethnobotany in the New Europe: People, Health and Wild Plant Resources*; Berghahn Books, 2010; Vol. 14, pp. 147–171 ISBN 9781845458140.

182. Těšitel, J. Functional Biology of Parasitic Plants: A Review. *Plant Ecology and Evolution 149(1): 5-20* **2016**, *149*, 5–20, doi:10.5091/PLECEVO.2016.1097.

183. Rubiales, D. Parasitic Plants, Wild Relatives and the Nature of Resistance. *New Phytologist* **2003**, *160*, 459–461, doi:10.1046/J.1469-8137.2003.00929.X.

184. De Vega, C.; Ortiz, P.L.; Arista, M.; Talavera, S. The Endophytic System of Mediterranean Cytinus (Cytinaceae) Developing on Five Host Cistaceae Species. *Ann Bot* **2007**, *100*, 1209–1217, doi:10.1093/AOB/MCM217.

185. Mlcek, J.; Rop, O. Fresh Edible Flowers of Ornamental Plants – A New Source of Nutraceutical Foods. *Trends Food Sci Technol* **2011**, *22*, 561–569, doi:10.1016/J.TIFS.2011.04.006.

186. Nicolson, S.W.; Thornburg, R.W. Nectar Chemistry. *Nectaries and Nectar* **2007**, 215–264, doi:10.1007/978-1-4020-5937-7_5/COVER.

187. Fernandes, Â.; Barros, L.; Martins, A.; Herbert, P.; Ferreira, I.C.F.R. Nutritional Characterisation of Pleurotus Ostreatus (Jacq. Ex Fr.) P. Kumm. Produced Using Paper Scraps as Substrate. *Food Chem* **2015**, *169*, 396–400, doi:10.1016/J.FOODCHEM.2014.08.027.

188. Pinela, J.; Barros, L.; Carvalho, A.M.; Ferreira, I.C.F.R. Influence of the Drying Method in the Antioxidant Potential and Chemical Composition of Four Shrubby Flowering Plants from the Tribe Genisteae (Fabaceae). *Food and Chemical Toxicology* **2011**, *49*, 2983–2989, doi:10.1016/J.FCT.2011.07.054.

189. Fernandes, Â.; Barreira, J.C.M.; Antonio, A.L.; Santos, P.M.P.; Martins, A.; Oliveira, M.B.P.P.; Ferreira, I.C.F.R. Study of Chemical Changes and Antioxidant Activity Variation Induced by Gamma-Irradiation on Wild Mushrooms: Comparative Study through Principal Component Analysis. *Food Research International* **2013**, *54*, 18–25, doi:10.1016/J.FOODRES.2013.06.011.

190. Boden, G.; Sargrad, K.; Homko, C.; Mozzoli, M.; Stein, T.P. Effect of a Low-Carbohydrate Diet on Appetite, Blood Glucose Levels, and Insulin Resistance in Obese Patients with Type 2 Diabetes. *Ann Intern Med* **2005**, *142*, doi:10.7326/0003-4819-142-6-200503150-00006.

191. Fernandes, L.; Casal, S.; Pereira, J.A.; Saraiva, J.A.; Ramalhosa, E. Edible Flowers: A Review of the Nutritional, Antioxidant, Antimicrobial Properties and Effects on Human Health. *Journal of Food Composition and Analysis* **2017**, *60*, 38–50, doi:10.1016/J.JFCA.2017.03.017.

192. Lunn, J.; Theobald, H.E. The Health Effects of Dietary Unsaturated Fatty Acids. *Nutr Bull* **2006**, *31*, 178–224, doi:10.1111/J.1467-3010.2006.00571.X.

193. Fernandes, L.; Ramalhosa, E.; Pereira, J.A.; Saraiva, J.A.; Casal, S. The Unexplored Potential of Edible Flowers Lipids. *Agriculture 2018, Vol. 8, Page 146* **2018**, *8*, 146, doi:10.3390/AGRICULTURE8100146.

194. Ness, A. Diet, Nutrition and the Prevention of Chronic Diseases. WHO Technical Report Series 916. Report of a Joint WHO/FSA Expert Consultation. *Int J Epidemiol* **2004**, *33*, 914–915, doi:10.1093/IJE/DYH209.

195. Carvalho, I.S.; Teixeira, M.C.; Brodelius, M. Fatty Acids Profile of Selected Artemisia Spp. Plants: Health Promotion. *LWT - Food Science and Technology* **2011**, *44*, 293–298, doi:10.1016/J.LWT.2010.05.033.

196. Ricchi, M.; Odoardi, M.R.; Carulli, L.; Anzivino, C.; Ballestri, S.; Pinetti, A.; Fantoni, L.I.; Marra, F.; Bertolotti, M.; Banni, S.; et al. Differential Effect of Oleic and Palmitic Acid on Lipid Accumulation and Apoptosis in Cultured Hepatocytes. *J Gastroenterol Hepatol* **2009**, *24*, 830–840, doi:10.1111/J.1440-1746.2008.05733.X.

197. French, M.A.; Sundram, K.; Clandinin, M.T. Cholesterolaemic Effect of Palmitic Acid in Relation to Other Dietary Fatty Acids. *Asia Pac J Clin Nutr* **2002**, *11*, S401–S407, doi:10.1046/J.1440-6047.11.S.7.3.X.

198. Terés, S.; Barceló-Coblijn, G.; Benet, M.; Álvarez, R.; Bressani, R.; Halver, J.E.; Escribá, P. V. Oleic Acid Content Is Responsible for the Reduction in Blood Pressure Induced by Olive Oil. *Proceedings of the National Academy of Sciences* **2008**, *105*, 13811–13816, doi:10.1073/PNAS.0807500105.

199. Simopoulos, A.P. Essential Fatty Acids in Health and Chronic Disease. *Am J Clin Nutr* **1999**, *70*, doi:10.1093/AJCN/70.3.560S.

200. Balunas, M.J.; Kinghorn, A.D. Drug Discovery from Medicinal Plants. *Life Sci* **2005**, *78*, 431–441, doi:10.1016/J.LFS.2005.09.012.

201. Thomford, N.E.; Senthebane, D.A.; Rowe, A.; Munro, D.; Seele, P.; Maroyi, A.; Dzobo, K. Natural Products for Drug Discovery in the 21st Century: Innovations for Novel Drug Discovery. *International Journal of Molecular Sciences 2018, Vol. 19, Page 1578* **2018**, *19*, 1578, doi:10.3390/IJMS19061578.

202. Nurzyńska-Wierdak, R. Phenolic Compounds from New Natural Sources—Plant Genotype and Ontogenetic Variation. *Molecules* **2023**, *28*, doi:10.3390/MOLECULES28041731.

203. Okuda, T.; Ito, H. Tannins of Constant Structure in Medicinal and Food Plants—Hydrolyzable Tannins and Polyphenols Related to Tannins. *Molecules* **2011**, *16*, 2191–2217, doi:10.3390/molecules16032191.

204. Zolghadri, S.; Bahrami, A.; Hassan Khan, M.T.; Munoz-Munoz, J.; Garcia-Molina, F.; Garcia-Canovas, F.; Saboury, A.A. A Comprehensive Review on Tyrosinase Inhibitors. *J Enzyme Inhib Med Chem* **2019**, *34*, 279, doi:10.1080/14756366.2018.1545767.

205. Silva, A.R.; Fernandes, Â.; García, P.A.; Barros, L.; Ferreira, I.C.F.R. Cytinus Hypocistis (L.) L. Subsp. Macranthus Wettst.: Nutritional Characterization. *Molecules* **2019**, *24*, 1111, doi:10.3390/molecules24061111.

206. Bessada, S.M.F.; Barreira, J.C.M.; Barros, L.; Ferreira, I.C.F.R.; Oliveira, M.B.P.P. Phenolic Profile and Antioxidant Activity of Coleostephus Myconis (L.) Rchb.f.: An Underexploited and Highly Disseminated Species. *Ind Crops Prod* **2016**, *89*, 45–51, doi:10.1016/j.indcrop.2016.04.065.

207. Guimarães, R.; Barros, L.; Dueñas, M.; Calhelha, R.C.; Carvalho, A.M.; Santos-Buelga, C.; Queiroz, M.J.R.P.; Ferreira, I.C.F.R. Nutrients, Phytochemicals and Bioactivity of Wild Roman Chamomile: A Comparison between the Herb and Its Preparations. *Food Chem* **2013**, *136*, 718–725, doi:10.1016/j.foodchem.2012.08.025.

208. Souilem, F.; Fernandes, Â.; Calhelha, R.C.; Barreira, J.C.M.; Barros, L.; Skhiri, F.; Martins, A.; Ferreira, I.C.F.R. Wild Mushrooms and Their Mycelia as Sources of Bioactive Compounds: Antioxidant, Anti-Inflammatory and Cytotoxic Properties. *Food Chem* **2017**, *230*, 40–48, doi:10.1016/j.foodchem.2017.03.026.

209. Lockowandt, L.; Pinela, J.; Roriz, C.L.; Pereira, C.; Abreu, R.M.V.; Calhelha, R.C.; Alves, M.J.; Barros, L.; Bredol, M.; Ferreira, I.C.F.R. Chemical Features and Bioactivities of Cornflower (Centaurea Cyanus L.) Capitula: The Blue Flowers and the Unexplored Non-Edible Part. *Ind Crops Prod* **2019**, *128*, 496–503, doi:10.1016/J.INDCROP.2018.11.059.

210. Spínola, V.; Castilho, P.C. Evaluation of Asteraceae Herbal Extracts in the Management of Diabetes and Obesity. Contribution of Caffeoylquinic Acids on the Inhibition of Digestive Enzymes Activity and Formation of Advanced Glycation End-Products (in Vitro). *Phytochemistry* **2017**, *143*, 29–35, doi:10.1016/J.PHYTOCHEM.2017.07.006.

211. Les, F.; Venditti, A.; Cásedas, G.; Frezza, C.; Guiso, M.; Sciubba, F.; Serafini, M.; Bianco, A.; Valero, M.S.; López, V. Everlasting Flower (Helichrysum Stoechas Moench) as a Potential Source of Bioactive Molecules with Antiproliferative, Antioxidant, Antidiabetic and Neuroprotective Properties. *Ind Crops Prod* **2017**, *108*, 295–302, doi:10.1016/J.INDCROP.2017.06.043.

212. Chen, C.H.; Chan, H.C.; Chu, Y.T.; Ho, H.Y.; Chen, P.Y.; Lee, T.H.; Lee, C.K. Antioxidant Activity of Some Plant Extracts Towards Xanthine Oxidase, Lipoxygenase and Tyrosinase. *Molecules 2009, Vol. 14, Pages 2947-2958* **2009**, *14*, 2947–2958, doi:10.3390/MOLECULES14082947.

213. Madureira, J.; Dias, M.I.; Pinela, J.; Calhelha, R.C.; Barros, L.; Santos-Buelga, C.; Margaça, F.M.A.; Ferreira, I.C.F.R.; Cabo Verde, S. The Use of Gamma Radiation for Extractability Improvement of Bioactive Compounds in Olive Oil Wastes. *Science of The Total Environment* **2020**, *727*, 138706, doi:10.1016/j.scitotenv.2020.138706.

214. Sokovicẋ, M.; Glamočlija, J.; Marin, P.D.; Brkić, D.; Van Griensven, L.J.L.D. Antibacterial Effects of the Essential Oils of Commonly Consumed Medicinal Herbs Using an In Vitro Model. *Molecules 2010, Vol. 15, Pages 7532-7546* **2010**, *15*, 7532–7546, doi:10.3390/MOLECULES15117532.

215. Carocho, M.; Barros, L.; Bento, A.; Santos-Buelga, C.; Morales, P.; Ferreira, I.C.F.R. Castanea Sativa Mill. Flowers amongst the Most Powerful Antioxidant Matrices: A Phytochemical Approach in Decoctions and Infusions. *Biomed Res Int* **2014**, *2014*, 1–7, doi:10.1155/2014/232956.

216. Tan, H.P.; Ling, S.K.; Chuah, C.H. Characterisation of Galloylated Cyanogenic Glucosides and Hydrolysable Tannins from Leaves of Phyllagathis Rotundifolia by LC-ESI-MS/MS. *Phytochemical Analysis* **2011**, *22*, 516–525, doi:10.1002/pca.1312.

217. Mena, P.; Calani, L.; Dall'Asta, C.; Galaverna, G.; García-Viguera, C.; Bruni, R.; Crozier, A.; Del Rio, D. Rapid and Comprehensive Evaluation of (Poly)Phenolic Compounds in Pomegranate (Punica Granatum L.) Juice by UHPLC-MSn. *Molecules* **2012**, *17*, 14821–14840, doi:10.3390/molecules171214821.

218. Owen, R.W.; Haubner, R.; Hull, W.E.; Erben, G.; Spiegelhalder, B.; Bartsch, H.; Haber, B. Isolation and Structure Elucidation of the Major Individual Polyphenols in Carob Fibre. *Food and Chemical Toxicology* **2003**, *41*, 1727–1738, doi:10.1016/S0278-6915(03)00200-X.

219. Calani, L.; Beghè, D.; Mena, P.; Del Rio, D.; Bruni, R.; Fabbri, A.; Dall'Asta, C.; Galaverna, G. Ultra-HPLC-MSn (Poly)Phenolic Profiling and Chemometric Analysis of Juices from Ancient Punica Granatum L. Cultivars: A Nontargeted Approach. *J Agric Food Chem* **2013**, *61*, 5600–5609, doi:10.1021/jf400387c.

220. Sentandreu, E.; Cerdán-Calero, M.; Sendra, J.M. Phenolic Profile Characterization of Pomegranate (Punica Granatum) Juice by High-Performance Liquid Chromatography with Diode Array Detection Coupled to an Electrospray Ion Trap Mass Analyzer. *Journal of Food Composition and Analysis* **2013**, *30*, 32–40, doi:10.1016/j.jfca.2013.01.003.

221. Wyrepkowski, C.C.; Da Costa, D.L.M.G.; Sinhorin, A.P.; Vilegas, W.; De Grandis, R.A.; Resende, F.A.; Varanda, E.A.; Dos Santos, L.C. Characterization and Quantification of the Compounds of the Ethanolic Extract from Caesalpinia Ferrea Stem Bark and Evaluation of Their Mutagenic Activity. *Molecules 2014, Vol. 19, Pages 16039-16057* **2014**, *19*, 16039–16057, doi:10.3390/MOLECULES191016039.

222. Hofmann, T.; Nebehaj, E.; Albert, L. Antioxidant Properties and Detailed Polyphenol Profiling of European Hornbeam (Carpinus Betulus L.) Leaves by Multiple Antioxidant Capacity Assays and High-Performance Liquid Chromatography/Multistage Electrospray Mass Spectrometry. *Ind Crops Prod* **2016**, *87*, 340–349, doi:10.1016/j.indcrop.2016.04.037.

223. Liberal, J.; Costa, G.; Carmo, A.; Vitorino, R.; Marques, C.; Domingues, M.R.; Domingues, P.; Gonçalves, A.C.; Alves, R.; Sarmento-Ribeiro, A.B.; et al. Chemical Characterization and Cytotoxic Potential of an Ellagitannin-Enriched Fraction from Fragaria Vesca Leaves. *Arabian Journal of Chemistry* **2019**, *12*, 3652–3666, doi:10.1016/J.ARABJC.2015.11.014.

224. Salminen J-P; Ossipov, V.; Loponen, J.; Haukioja, E.; Pihlaja, K. Characterisation of Hydrolysable Tannins from Leaves of Betula Pubescens by High-Performance Liquid Chromatography-Mass Spectrometry. *J Chromatogr A* **1999**, *864*, 283–291.

225. Hofmann, T.; Nebehaj, E.; Albert, L. Antioxidant Properties and Detailed Polyphenol Profiling of European Hornbeam (Carpinus Betulus L.) Leaves by Multiple Antioxidant Capacity Assays and High-Performance Liquid Chromatography/Multistage Electrospray Mass Spectrometry. *Ind Crops Prod* **2016**, *87*, 340–349, doi:10.1016/J.INDCROP.2016.04.037.

226. Lichota, A.; Gwozdzinski, K. Anticancer Activity of Natural Compounds from Plant and Marine Environment. *Int J Mol Sci* **2018**, *19*, doi:10.3390/IJMS19113533.

227. Pohanka, M.; Snopkova, S.; Havlickova, K.; Bostik, P.; Sinkorova, Z.; Fusek, J.; Kuca, K.; Pikula, J. Macrophage-Assisted Inflammation and Pharmacological Regulation of the Cholinergic Anti-Inflammatory Pathway. *Curr Med Chem* **2011**, *18*, 539–551.

228. Guo, Y.; Sakulnarmrat, K.; Konczak, I. Anti-Inflammatory Potential of Native Australian Herbs Polyphenols. *Toxicol Rep* **2014**, *1*, 385–390, doi:10.1016/J.TOXREP.2014.06.011.

229. Sultana, R.; Perluigi, M.; Butterfield, D.A. Lipid Peroxidation Triggers Neurodegeneration: A Redox Proteomics View into the Alzheimer Disease Brain. *Free Radic Biol Med* **2013**, *62*, 157–169, doi:10.1016/j.freeradbiomed.2012.09.027.

230. Silva, A.R.; Finimundy, T.C.; Barros, L.; Ferreira, I.C.F.R. Exogenous Antioxidants Derived from Plants, Fungi, and Other Taxa. In *Handbook of Antioxidant Methodology: Approaches to Activity Determination*; 2021; Vol. Chapter 6, pp. 203–245.

231. Cordiano, R.; Di Gioacchino, M.; Mangifesta, R.; Panzera, C.; Gangemi, S.; Minciullo, P.L. Malondialdehyde as a Potential Oxidative Stress Marker for Allergy-Oriented Diseases: An Update. *Molecules 2023, Vol. 28, Page 5979* **2023**, *28*, 5979, doi:10.3390/MOLECULES28165979.

232. Gulcin, İ. Antioxidants and Antioxidant Methods: An Updated Overview. *Arch Toxicol* **2020**, *94*, 651–715, doi:10.1007/s00204-020-02689-3.

233. Yin, Z.; Zhang, W.; Feng, F.; Zhang, Y.; Kang, W. α-Glucosidase Inhibitors Isolated from Medicinal Plants. *Food Science and Human Wellness* **2014**, *3*, 136–174, doi:10.1016/J.FSHW.2014.11.003.

234. Dirir, A.M.; Daou, M.; Yousef, A.F.; Yousef, L.F. A Review of Alpha-Glucosidase Inhibitors from Plants as Potential Candidates for the Treatment of Type-2 Diabetes. *Phytochemistry Reviews 2021 21:4* **2021**, *21*, 1049–1079, doi:10.1007/S11101-021-09773-1.

235. Zaidi, K.U.; Ali, A.S.; Ali, S.A.; Naaz, I. Microbial Tyrosinases: Promising Enzymes for Pharmaceutical, Food Bioprocessing, and Environmental Industry. *Biochem Res Int* **2014**, *2014*, doi:10.1155/2014/854687.

236. Draelos, Z.D. Skin Lightening Preparations and the Hydroquinone Controversy. *Dermatol Ther* **2007**, *20*, 308–313, doi:10.1111/j.1529-8019.2007.00144.x.

237. Draelos, Z.D. Skin Lightening Preparations and the Hydroquinone Controversy. *Dermatol Ther* **2007**, *20*, 308–313, doi:10.1111/j.1529-8019.2007.00144.x.

238. Rozas, O.; Contreras, D.; Mondaca, M.A.; Pérez-Moya, M.; Mansilla, H.D. Experimental Design of Fenton and Photo-Fenton Reactions for the Treatment of Ampicillin Solutions. *J Hazard Mater* **2010**, *177*, 1025–1030, doi:10.1016/J.JHAZMAT.2010.01.023.

239. Leonardi, M.; Furtado, A.N.M.; Comandini, O.; Geml, J.; Rinaldi, A.C. Halimium as an Ectomycorrhizal Symbiont: New Records and an Appreciation of Known Fungal Diversity. *Mycol Prog* **2020**, *19*, 1495–1509, doi:10.1007/s11557-020-01641-0.

240. Silva, A.R.; Pinela, J.; Dias, M.I.; Calhelha, R.C.; Alves, M.J.; Mocan, A.; García, P.A.; Barros, L.; Ferreira, I.C.F.R. Exploring the Phytochemical Profile of Cytinus Hypocistis (L.) L. as a Source of

Health-Promoting Biomolecules behind Its in Vitro Bioactive and Enzyme Inhibitory Properties. *Food and Chemical Toxicology* **2020**, *136*, 111071, doi:10.1016/j.fct.2019.111071.

241. Heleno, S.A.; Ferreira, I.C.F.R.; Esteves, A.P.; Ćirić, A.; Glamočlija, J.; Martins, A.; Soković, M.; Queiroz, M.J.R.P. Antimicrobial and Demelanizing Activity of Ganoderma Lucidum Extract, p-Hydroxybenzoic and Cinnamic Acids and Their Synthetic Acetylated Glucuronide Methyl Esters. *Food and Chemical Toxicology* **2013**, *58*, 95–100, doi:10.1016/j.fct.2013.04.025.

242. Ayuso, M.; Pinela, J.; Dias, M.I.; Barros, L.; Ivanov, M.; Calhelha, R.C.; Soković, M.; Ramil-Rego, P.; Barreal, M.E.; Gallego, P.P.; et al. Phenolic Composition and Biological Activities of the in Vitro Cultured Endangered Eryngium Viviparum J. Gay. *Ind Crops Prod* **2020**, *148*, 112325, doi:10.1016/j.indcrop.2020.112325.

243. Chihoub, W.; Dias, M.I.; Barros, L.; Calhelha, R.C.; Alves, M.J.; Harzallah-Skhiri, F.; Ferreira, I.C.F.R. Valorisation of the Green Waste Parts from Turnip, Radish and Wild Cardoon: Nutritional Value, Phenolic Profile and Bioactivity Evaluation. *Food Research International* **2019**, *126*, 108651, doi:10.1016/j.foodres.2019.108651.

244. Heffels, P.; Müller, L.; Schieber, A.; Weber, F. Profiling of Iridoid Glycosides in Vaccinium Species by UHPLC-MS. *Food Research International* **2017**, *100*, 462–468, doi:10.1016/j.foodres.2016.11.018.

245. García-Pérez, P.; Ayuso, M.; Lozano-Milo, E.; Pereira, C.; Dias, M.I.; Ivanov, M.; Calhelha, R.C.; Soković, M.; Ferreira, I.C.F.R.; Barros, L.; et al. Phenolic Profiling and in Vitro Bioactivities of Three Medicinal Bryophyllum Plants. *Ind Crops Prod* **2021**, *162*, 113241, doi:10.1016/j.indcrop.2021.113241.

246. Du, X.-G.; Wang, W.; Zhang, Q.-Y.; Cheng, J.; Avula, B.; Khan, I.A.; Guo, D.-A. Identification of Xanthones from Swertia Punicea Using High-Performance Liquid Chromatography Coupled with Electrospray Ionization Tandem Mass Spectrometry. *Rapid Communications in Mass Spectrometry* **2012**, *26*, 2913–2923, doi:10.1002/RCM.6419.

247. Falcão, S.I.; Vale, N.; Gomes, P.; Domingues, M.R.M.; Freire, C.; Cardoso, S.M.; Vilas-Boas, M. Phenolic Profiling of Portuguese Propolis by LC-MS Spectrometry: Uncommon Propolis Rich in Flavonoid Glycosides. *Phytochemical Analysis* **2013**, *24*, 309–318, doi:10.1002/pca.2412.

248. Bastos, C.; Barros, L.; Dueñas, M.; Calhelha, R.C.; Queiroz, M.J.R.P.; Santos-Buelga, C.; Ferreira, I.C.F.R. Chemical Characterisation and Bioactive Properties of Prunus Avium L.: The Widely Studied Fruits and the Unexplored Stems. *Food Chem* **2015**, *173*, 1045–1053, doi:10.1016/j.foodchem.2014.10.145.

249. Rodríguez-Medina, I.C.; Beltrán-Debón, R.; Molina, V.M.; Alonso-Villaverde, C.; Joven, J.; Menéndez, J.A.; Segura-Carretero, A.; Fernández-Gutiérrez, A. Direct Characterization of Aqueous Extract of Hibiscus Sabdariffa Using HPLC with Diode Array Detection Coupled to ESI and Ion Trap MS. *J Sep Sci* **2009**, *32*, 3441–3448, doi:10.1002/jssc.200900298.

250. Gori, A.; Ferrini, F.; Marzano, M.; Tattini, M.; Centritto, M.; Baratto, M.; Pogni, R.; Brunetti, C. Characterisation and Antioxidant Activity of Crude Extract and Polyphenolic Rich Fractions from C. Incanus Leaves. *Int J Mol Sci* **2016**, *17*, 1344, doi:10.3390/ijms17081344.

251. Guimarães, R.; Barros, L.; Dueñas, M.; Calhelha, R.C.; Carvalho, A.M.; Santos-Buelga, C.; Queiroz, M.J.R.P.; Ferreira, I.C.F.R. Infusion and Decoction of Wild German Chamomile: Bioactivity and Characterization of Organic Acids and Phenolic Compounds. *Food Chem* **2013**, *136*, 947–954, doi:10.1016/j.foodchem.2012.09.007.

252. Bouziane, A.; Bakchiche, B.; Dias, M.; Barros, L.; Ferreira, I.; AlSalamat, H.; Bardaweel, S. Phenolic Compounds and Bioactivity of Cytisus Villosus Pourr. *Molecules* **2018**, *23*, 1994, doi:10.3390/molecules23081994.

253. Guimarães, R.; Barros, L.; Dueñas, M.; Carvalho, A.M.; Queiroz, M.J.R.P.; Santos-Buelga, C.; Ferreira, I.C.F.R. Characterisation of Phenolic Compounds in Wild Fruits from Northeastern Portugal. *Food Chem* **2013**, *141*, 3721–3730, doi:10.1016/J.FOODCHEM.2013.06.071.

254. Barros, L.; Alves, C.T.; Dueñas, M.; Silva, S.; Oliveira, R.; Carvalho, A.M.; Henriques, M.; Santos-Buelga, C.; Ferreira, I.C.F.R. Characterization of Phenolic Compounds in Wild Medicinal Flowers from Portugal by HPLC-DAD-ESI/MS and Evaluation of Antifungal Properties. *Ind Crops Prod* **2013**, *44*, 104–110, doi:10.1016/j.indcrop.2012.11.003.

255. Simirgiotis, M.J.; Theoduloz, C.; Caligari, P.D.S.; Schmeda-Hirschmann, G. Comparison of Phenolic Composition and Antioxidant Properties of Two Native Chilean and One Domestic Strawberry Genotypes. *Food Chem* **2009**, *113*, 377–385, doi:10.1016/j.foodchem.2008.07.043.

256. Giusti, M.M.; Wrolstad, R.E. Acylated Anthocyanins from Edible Sources and Their Applications in Food Systems. *Biochem Eng J* **2003**, *14*, 217–225, doi:10.1016/S1369-703X(02)00221-8.

257. Teixeira, N.; Nabais, P.; de Freitas, V.; Lopes, J.A.; Melo, M.J. In-Depth Phenolic Characterization of Iron Gall Inks by Deconstructing Representative Iberian Recipes. *Sci Rep* **2021**, *11*, 8811, doi:10.1038/s41598-021-87969-3.

258. Silva, V.; Falco, V.; Dias, M.I.; Barros, L.; Silva, A.; Capita, R.; Alonso-Calleja, C.; Amaral, J.S.; Igrejas, G.; Ferreira, I.C.F.R.; et al. Evaluation of the Phenolic Profile of Castanea Sativa Mill. By-Products and Their Antioxidant and Antimicrobial Activity against Multiresistant Bacteria. *Antioxidants* **2020**, *9*, 87, doi:10.3390/ANTIOX9010087.

259. Soong, Y.Y.; Barlow, P.J. Isolation and Structure Elucidation of Phenolic Compounds from Longan (Dimocarpus Longan Lour.) Seed by High-Performance Liquid Chromatography-Electrospray Ionization Mass Spectrometry. *J Chromatogr A* **2005**, *1085*, 270–277, doi:10.1016/j.chroma.2005.06.042.

260. Kerbab, K.; Sansone, F.; Zaiter, L.; Esposito, T.; Celano, R.; Franceschelli, S.; Pecoraro, M.; Benayache, F.; Rastrelli, L.; Picerno, P.; et al. Halimium Halimifolium: From the Chemical and Functional Characterization to a Nutraceutical Ingredient Design. *Planta Med* **2019**, *85*, 1024–1033, doi:10.1055/a-0953-6007.

261. Pinela, J.; Prieto, M.A.; Barreiro, M.F.; Carvalho, A.M.; Oliveira, M.B.P.P.; Curran, T.P.; Ferreira, I.C.F.R. Valorisation of Tomato Wastes for Development of Nutrient-Rich Antioxidant Ingredients: A Sustainable Approach towards the Needs of the Today's Society. *Innovative Food Science and Emerging Technologies* **2017**, *41*, 160–171, doi:10.1016/j.ifset.2017.02.004.

262. Mandim, F.; Petropoulos, S.A.; Giannoulis, K.D.; Dias, M.I.; Fernandes, Â.; Pinela, J.; Kostic, M.; Soković, M.; Barros, L.; Santos-Buelga, C.; et al. Seasonal Variation of Bioactive Properties and Phenolic Composition of Cynara Cardunculus Var. Altilis. *Food Research International* **2020**, *134*, 109281, doi:10.1016/j.foodres.2020.109281.

263. Mandim, F.; Petropoulos, S.A.; Fernandes, Â.; Santos-Buelga, C.; Ferreira, I.C.F.R.; Barros, L. Chemical Composition of Cynara Cardunculus L. Var. Altilis Heads: The Impact of Harvesting Time. *Agronomy* **2020**, *10*, 1088, doi:10.3390/agronomy10081088.

264. Gomes, T.; Delgado, T.; Ferreira, A.; Pereira, J.A.; Baptista, P.; Casal, S.; Ramalhosa, E. Application of Response Surface Methodology for Obtaining Lettuce (Lactuca Sativa L.) by-Products Extracts with High Antioxidative Properties. *Ind Crops Prod* **2013**, *44*, 622–629, doi:10.1016/j.indcrop.2012.09.011.

265. Caesar, L.K.; Cech, N.B. Synergy and Antagonism in Natural Product Extracts: When 1 + 1 Does Not Equal 2. *Nat Prod Rep* **2019**, *36*, 869–888, doi:10.1039/C9NP00011A.

266. Rebaya, A.; Belghith, S.I.; Baghdikian, B.; Leddet, V.M.; Mabrouki, F.; Olivier, E.; Cherif, J.K.; Ayadi, M.T. Total Phenolic, Total Flavonoid, Tannin Content, and Antioxidant Capacity of Halimium Halimifolium (Cistaceae). *J Appl Pharm Sci* **2015**, *5*, 052–057, doi:10.7324/JAPS.2015.50110.

267. Mukherjee, P.K.; Biswas, R.; Sharma, A.; Banerjee, S.; Biswas, S.; Katiyar, C.K. Validation of Medicinal Herbs for Anti-Tyrosinase Potential. *J Herb Med* **2018**, *14*, 1–16.

268. Zyad, A.; Leouifoudi, I.; Tilaoui, M.; Mouse, H.A.; Khouchani, M.; Jaafari, A. Natural Products as Cytotoxic Agents in Chemotherapy against Cancer. In *Cytotoxicity*; InTech, 2018.

269. Silva, A.R.; Taofiq, O.; Ferreira, I.C.F.R.; Barros, L. Hypericum Genus Cosmeceutical Application – A Decade Comprehensive Review on Its Multifunctional Biological Properties. *Ind Crops Prod* **2021**, *159*, doi:10.1016/j.indcrop.2020.113053.

270. Nunes, C. dos R.; Barreto Arantes, M.; Menezes de Faria Pereira, S.; Leandro da Cruz, L.; de Souza Passos, M.; Pereira de Moraes, L.; Vieira, I.J.C.; Barros de Oliveira, D. Plants as Sources of Anti-Inflammatory Agents. *Molecules* **2020**, *25*, 3726, doi:10.3390/molecules25163726.

271. Cheesman, M.J.; Ilanko, A.; Blonk, B.; Cock, I.E. Developing New Antimicrobial Therapies: Are Synergistic Combinations of Plant Extracts/Compounds with Conventional Antibiotics the Solution? *Pharmacogn Rev* **2017**, *11*, 57–72, doi:10.4103/phrev.phrev_21_17.

272. Srivastava, J.; Chandra, H.; Nautiyal, A.R.; Kalra, S.J.S. Antimicrobial Resistance (AMR) and Plant-Derived Antimicrobials (PDAms) as an Alternative Drug Line to Control Infections. *3 Biotech* **2014**, *4*, 451–460, doi:10.1007/s13205-013-0180-y.

273. Falcão, L.; Araújo, M.E.M. Vegetable Tannins Used in the Manufacture of Historic Leathers. *Molecules* **2018**, *23*, doi:10.3390/molecules23051081.

274. Molino, S.; Pilar Francino, M.; Ángel Rufián Henares, J. Why Is It Important to Understand the Nature and Chemistry of Tannins to Exploit Their Potential as Nutraceuticals? *Food Research International* **2023**, *173*, 113329, doi:10.1016/J.FOODRES.2023.113329.

275. Silva, A.R.; Pinela, J.; Dias, M.I.; Calhelha, R.C.; Alves, M.J.; Mocan, A.; García, P.A.; Barros, L.; Ferreira, I.C.F.R. Exploring the Phytochemical Profile of *Cytinus Hypocistis* (L.) L. as a Source of Health-Promoting Biomolecules behind Its in Vitro Bioactive and Enzyme Inhibitory Properties. *Food and Chemical Toxicology* **2020**, *136*.

276. Albuquerque, B.R.; Pinela, J.; Barros, L.; Oliveira, M.B.P.P.; Ferreira, I.C.F.R. Anthocyanin-Rich Extract of Jabuticaba Epicarp as a Natural Colorant: Optimization of Heat- and Ultrasound-Assisted Extractions and Application in a Bakery Product. *Food Chem* **2020**, *316*, 126364, doi:10.1016/j.foodchem.2020.126364.

277. Rocchetti, G.; Blasi, F.; Montesano, D.; Ghisoni, S.; Marcotullio, M.C.; Sabatini, S.; Cossignani, L.; Lucini, L. Impact of Conventional/Non-Conventional Extraction Methods on the Untargeted Phenolic Profile of Moringa Oleifera Leaves. *Food Research International* **2019**, *115*, 319–327, doi:10.1016/j.foodres.2018.11.046.

278. Barba, F.J.; Putnik, P.; Bursać Kovačević, D.; Poojary, M.M.; Roohinejad, S.; Lorenzo, J.M.; Koubaa, M. Impact of Conventional and Non-Conventional Processing on Prickly Pear (Opuntia Spp.) and Their Derived Products: From Preservation of Beverages to Valorization of by-Products. *Trends Food Sci Technol* **2017**, *67*, 260–270, doi:10.1016/j.tifs.2017.07.012.

279. Castro-López, C.; Ventura-Sobrevilla, J.M.; González-Hernández, M.D.; Rojas, R.; Ascacio-Valdés, J.A.; Aguilar, C.N.; Martínez-Ávila, G.C.G. Impact of Extraction Techniques on Antioxidant Capacities and Phytochemical Composition of Polyphenol-Rich Extracts. *Food Chem* **2017**, *237*, 1139–1148.

280. Fraga-Corral, M.; García-Oliveira, P.; Pereira, A.G.; Lourenço-Lopes, C.; Jimenez-Lopez, C.; Prieto, M.A.; Simal-Gandara, J. Technological Application of Tannin-Based Extracts. *Molecules* **2020**, *25*, 614, doi:10.3390/molecules25030614.

281. Mueller-Harvey, I. Analysis of Hydrolysable Tannins. *Anim Feed Sci Technol* **2001**, *91*, 3–20, doi:10.1016/S0377-8401(01)00227-9.

282. Taofiq, O.; Silva, A.R.; Costa, C.; Ferreira, I.; Nunes, J.; Prieto, M.A.; Simal-Gandara, J.; Barros, L.; Ferreira, I.C.F.R. Optimization of Ergosterol Extraction from: Pleurotus Mushrooms Using Response Surface Methodology. *Food Funct* **2020**, *11*, 5887–5897, doi:10.1039/d0fo00301h.

283. Rocha, R.; Pinela, J.; Abreu, R.M.V.; Añibarro-Ortega, M.; Pires, T.C.S.P.; Saldanha, A.L.; Alves, M.J.; Nogueira, A.; Ferreira, I.C.F.R.; Barros, L. Extraction of Anthocyanins from Red Raspberry for Natural Food Colorants Development: Processes Optimization and In Vitro Bioactivity. *Processes* **2020**, *8*, 1447, doi:10.3390/pr8111447.

284. Gomes, T.; Delgado, T.; Ferreira, A.; Pereira, J.A.; Baptista, P.; Casal, S.; Ramalhosa, E. Application of Response Surface Methodology for Obtaining Lettuce (Lactuca Sativa L.) by-Products Extracts with High Antioxidative Properties. *Ind Crops Prod* **2013**, *44*, 622–629, doi:10.1016/j.indcrop.2012.09.011.

285. Sahoo, P.; Barman, T.Kr. ANN Modelling of Fractal Dimension in Machining. In *Mechatronics and Manufacturing Engineering*; Elsevier, 2012; pp. 159–226.

286. Vieira, V.; Prieto, M.A.; Barros, L.; Coutinho, J.A.P.; Ferreira, O.; Ferreira, I.C.F.R. Optimization and Comparison of Maceration and Microwave Extraction Systems for the Production of Phenolic Compounds from *Juglans Regia* L. for the Valorization of Walnut Leaves. *Ind Crops Prod* **2017**, *107*, 341–352.

287. Sousa, JordanaN.; Pedroso, NathaliaB.; Borges, LeonardoL.; A., G.; Paula, JoseR.; Conceicao, EdemilsonC. Optimization of Ultrasound-Assisted Extraction of Polyphenols, Tannins and Epigallocatechin Gallate from Barks of Stryphnodendron Adstringens (Mart.) Coville Bark Extracts. *Pharmacogn Mag* **2014**, *10*, 318, doi:10.4103/0973-1296.133287.

288. Diouf, P.N.; Stevanovic, T.; Boutin, Y. The Effect of Extraction Process on Polyphenol Content, Triterpene Composition and Bioactivity of Yellow Birch (Betula Alleghaniensis Britton) Extracts. *Ind Crops Prod* **2009**, *30*, 297–303, doi:10.1016/j.indcrop.2009.05.008.

289. Carrera, C.; Ruiz-Rodríguez, A.; Palma, M.; Barroso, C.G. Ultrasound Assisted Extraction of Phenolic Compounds from Grapes. *Anal Chim Acta* **2012**, *732*, 100–104, doi:10.1016/j.aca.2011.11.032.

290. Dahmoune, F.; Spigno, G.; Moussi, K.; Remini, H.; Cherbal, A.; Madani, K. Pistacia Lentiscus Leaves as a Source of Phenolic Compounds: Microwave-Assisted Extraction Optimized and Compared with Ultrasound-Assisted and Conventional Solvent Extraction. *Ind Crops Prod* **2014**, *61*, 31–40, doi:10.1016/j.indcrop.2014.06.035.

291. Chemat, F.; Rombaut, N.; Meullemiestre, A.; Turk, M.; Perino, S.; Fabiano-Tixier, A.-S.; Abert-Vian, M. Review of Green Food Processing Techniques. Preservation, Transformation, and Extraction. *Innovative Food Science & Emerging Technologies* **2017**, *41*, 357–377, doi:10.1016/J.IFSET.2017.04.016.

292. Shirmohammadli, Y.; Efhamisisi, D.; Pizzi, A. Tannins as a Sustainable Raw Material for Green Chemistry: A Review. *Ind Crops Prod* **2018**, *126*, 316–332, doi:10.1016/j.indcrop.2018.10.034.

293. Silva, A.R.; Pinela, J.; Dias, M.I.; Calhelha, R.C.; Alves, M.J.; Mocan, A.; García, P.A.; Barros, L.; Ferreira, I.C.F.R. Exploring the Phytochemical Profile of *Cytinus Hypocistis* (L.) L. as a Source of Health-Promoting Biomolecules behind Its in Vitro Bioactive and Enzyme Inhibitory Properties. *Food and Chemical Toxicology* **2020**, *136*.

294. Albuquerque, B.R.; Prieto, M.A.; Vazquez, J.A.; Barreiro, M.F.; Barros, L.; Ferreira, I.C.F.R. Recovery of Bioactive Compounds from Arbutus Unedo L. Fruits: Comparative Optimization Study of Maceration/Microwave/Ultrasound Extraction Techniques. *Food Research International* **2018**, *109*, 455–471, doi:10.1016/j.foodres.2018.04.061.

295. Leichtweis, M.G.; Pereira, C.; Prieto, M.A.; Barreiro, M.F.; Beraldi, I.J.; Barros, L.; Ferreira, I.C.F.R. Ultrasound as a Rapid and Low-Cost Extraction Procedure to Obtain Anthocyanin-Based Colorants from *Prunus Spinosa* L. Fruit Epicarp: Comparative Study with Conventional Heat-Based Extraction. *Molecules* **2019**, *24*, 1–17.

296. Iberahim, N.; Sethupathi, S.; Goh, C.L.; Bashir, M.J.K.; Ahmad, W. Optimization of Activated Palm Oil Sludge Biochar Preparation for Sulphur Dioxide Adsorption. *J Environ Manage* **2019**, *248*, doi:10.1016/j.jenvman.2019.109302.

297. Pinela, J.; Prieto, M.A.; Barros, L.; Carvalho, A.M.; Oliveira, M.B.P.P.; Saraiva, J.A.; Ferreira, I.C.F.R. Cold Extraction of Phenolic Compounds from Watercress by High Hydrostatic Pressure: Process Modelling and Optimization. *Sep Purif Technol* **2018**, *192*, 501–512.

298. Pinela, J.; Prieto, M.A.; Pereira, E.; Jabeur, I.; Barreiro, M.F.; Barros, L.; Ferreira, I.C.F.R. Optimization of Heat- and Ultrasound-Assisted Extraction of Anthocyanins from Hibiscus Sabdariffa Calyces for Natural Food Colorants. *Food Chem* **2019**, *275*, 309–321, doi:10.1016/j.foodchem.2018.09.118.

299. Osorio-Tobón, J.F. Recent Advances and Comparisons of Conventional and Alternative Extraction Techniques of Phenolic Compounds. *J Food Sci Technol* 2020, *57*, 4299–4315.

300. Liang, X.; Jiang, Y.; Guo, Z.; Fang, S. Separation, UPLC-QTOF-MS/MS Analysis, and Antioxidant Activity of Hydrolyzable Tannins from Water Caltrop (Trapa Quadrispinosa) Pericarps. *LWT* **2020**, *133*, 110010, doi:10.1016/j.lwt.2020.110010.

301. Veiga, M.; Costa, E.M.; Silva, S.; Pintado, M. Impact of Plant Extracts upon Human Health: A Review. *Crit Rev Food Sci Nutr* **2020**, *60*, 873–886, doi:10.1080/10408398.2018.1540969.

302. Briskin, D.P. Medicinal Plants and Phytomedicines. Linking Plant Biochemistry and Physiology to Human Health. *Plant Physiol* **2000**, *124*, 507–514, doi:10.1104/PP.124.2.507.

303. Ma, X.H.; Zheng, C.J.; Han, L.Y.; Xie, B.; Jia, J.; Cao, Z.W.; Li, Y.X.; Chen, Y.Z. Synergistic Therapeutic Actions of Herbal Ingredients and Their Mechanisms from Molecular Interaction and Network Perspectives. *Drug Discov Today* **2009**, *14*, 579–588, doi:10.1016/J.DRUDIS.2009.03.012.

304. Tiwari, V. Molecular Insight into the Therapeutic Potential of Phytoconstituents Targeting Protein Conformation and Their Expression. *Phytomedicine* **2019**, *52*, 225–237, doi:10.1016/J.PHYMED.2018.09.214.

305. Enke, C.G.; Nagels, L.J. Undetected Components in Natural Mixtures: How Many? What Concentrations? Do They Account for Chemical Noise? What Is Needed to Detect Them? *Anal Chem* **2011**, *83*, 2539–2546, doi:10.1021/AC102818A/SUPPL_FILE/AC102818A_SI_001.PDF.

306. Caesar, L.K.; Cech, N.B. Synergy and Antagonism in Natural Product Extracts: When 1 + 1 Does Not Equal 2. *Nat Prod Rep* **2019**, *36*, 869, doi:10.1039/C9NP00011A.

307. Rahman, S.; Ul Haq, F.; Ali, A.; Khan, M.N.; Shah, S.M.Z.; Adhikhari, A.; El-Seedi, H.R.; Musharraf, S.G. Combining Untargeted and Targeted Metabolomics Approaches for the Standardization of Polyherbal Formulations through UPLC–MS/MS. *Metabolomics* **2019**, *15*, 1–11, doi:10.1007/S11306-019-1582-6/TABLES/3.

308. Khan, I.A. Issues Related to Botanicals. *Life Sci* **2006**, *78*, 2033–2038, doi:10.1016/J.LFS.2005.12.019.

309. Widyawati, T.; Yusoff, N.A.; Bello, I.; Asmawi, M.Z.; Ahmad, M. Bioactivity-Guided Fractionation and Identification of Antidiabetic Compound of Syzygium Polyanthum (Wight.)'s

Leaf Extract in Streptozotocin-Induced Diabetic Rat Model. *Molecules* **2022**, *27*, doi:10.3390/MOLECULES27206814.

310. Najmi, A.; Javed, S.A.; Al Bratty, M.; Alhazmi, H.A. Modern Approaches in the Discovery and Development of Plant-Based Natural Products and Their Analogues as Potential Therapeutic Agents. *Molecules* **2022**, *27*, doi:10.3390/MOLECULES27020349.

311. Nothias, L.F.; Nothias-Esposito, M.; Da Silva, R.; Wang, M.; Protsyuk, I.; Zhang, Z.; Sarvepalli, A.; Leyssen, P.; Touboul, D.; Costa, J.; et al. Bioactivity-Based Molecular Networking for the Discovery of Drug Leads in Natural Product Bioassay-Guided Fractionation. *J Nat Prod* **2018**, *81*, 758–767, doi:10.1021/ACS.JNATPROD.7B00737/SUPPL_FILE/NP7B00737_SI_001.PDF.

312. Kellogg, J.J.; Todd, D.A.; Egan, J.M.; Raja, H.A.; Oberlies, N.H.; Kvalheim, O.M.; Cech, N.B. Biochemometrics for Natural Products Research: Comparison of Data Analysis Approaches and Application to Identification of Bioactive Compounds. *J Nat Prod* **2016**, *79*, 376–386, doi:10.1021/ACS.JNATPROD.5B01014/SUPPL_FILE/NP5B01014_SI_001.PDF.

313. Zengin, G.; Cádiz-Gurrea, M. de la L.; Fernández-Ochoa, Á.; Leyva-Jiménez, F.J.; Carretero, A.S.; Momotko, M.; Yildiztugay, E.; Karatas, R.; Jugreet, S.; Mahomoodally, M.F.; et al. Selectivity Tuning by Natural Deep Eutectic Solvents (NADESs) for Extraction of Bioactive Compounds from Cytinus Hypocistis-Studies of Antioxidative, Enzyme-Inhibitive Properties and LC-MS Profiles. *Molecules* **2022**, *27*, doi:10.3390/MOLECULES27185788.

314. Silva, A.R.; Pinela, J.; García, P.A.; Ferreira, I.C.F.R.; Barros, L. Cytinus Hypocistis (L.) L.: Optimised Heat/Ultrasound-Assisted Extraction of Tannins by Response Surface Methodology. *Sep Purif Technol* **2021**, *276*, 119358, doi:10.1016/j.seppur.2021.119358.

315. *Test No. 432: In Vitro 3T3 NRU Phototoxicity Test*; OECD Guidelines for the Testing of Chemicals, Section 4; OECD, 2019; ISBN 9789264071162.

316. Liao, W.; Ning, Z.; Chen, L.; Wei, Q.; Yuan, E.; Yang, J.; Ren, J. Intracellular Antioxidant Detoxifying Effects of Diosmetin on 2,2-Azobis(2-Amidinopropane) Dihydrochloride (AAPH)-Induced Oxidative Stress through Inhibition of Reactive Oxygen Species Generation. *J Agric Food Chem* **2014**, *62*, 8648–8654, doi:10.1021/JF502359X/ASSET/IMAGES/MEDIUM/JF-2014-02359X_0002.GIF.

317. Mann, T.; Scherner, C.; Röhm, K.H.; Kolbe, L. Structure-Activity Relationships of Thiazolyl Resorcinols, Potent and Selective Inhibitors of Human Tyrosinase. *Int J Mol Sci* **2018**, *19*, doi:10.3390/IJMS19030690.

318. WINDER, A.J.; HARRIS, H. New Assays for the Tyrosine Hydroxylase and Dopa Oxidase Activities of Tyrosinase. *Eur J Biochem* **1991**, *198*, 317–326, doi:10.1111/J.1432-1033.1991.TB16018.X.

319. Macintyre, L.; Zhang, T.; Viegelmann, C.; Martinez, I.J.; Cheng, C.; Dowdells, C.; Abdelmohsen, U.R.; Gernert, C.; Hentschel, U.; Edrada-Ebel, R.A. Metabolomic Tools for Secondary Metabolite Discovery from Marine Microbial Symbionts. *Marine Drugs 2014, Vol. 12, Pages 3416-3448* **2014**, *12*, 3416–3448, doi:10.3390/MD12063416.

320. Yusoff, Y.M.; Abbott, G.; Young, L.; Edrada-Ebel, R. Metabolomic Profiling of Malaysian and New Zealand Honey Using Concatenated NMR and HRMS Datasets. *Metabolites* **2022**, *12*, 85, doi:10.3390/METABO12010085/S1.

321. Papaccio, F.; D'arino, A.; Caputo, S.; Bellei, B. Focus on the Contribution of Oxidative Stress in Skin Aging. *Antioxidants* **2022**, *11*, doi:10.3390/ANTIOX11061121.

322. Andrade, J.M.; Domínguez-Martín, E.M.; Nicolai, M.; Faustino, C.; Rodrigues, L.M.; Rijo, P. Screening the Dermatological Potential of Plectranthus Species Components: Antioxidant and Inhibitory Capacities over Elastase, Collagenase and Tyrosinase.

https://doi.org/10.1080/14756366.2020.1862099 **2020**, *36*, 257–269, doi:10.1080/14756366.2020.1862099.

323.   Leirós, G.J.; Kusinsky, A.G.; Balañá, M.E.; Hagelin, K. Triolein Reduces MMP-1 Upregulation in Dermal Fibroblasts Generated by ROS Production in UVB-Irradiated Keratinocytes. *J Dermatol Sci* **2017**, *85*, 124–130, doi:10.1016/J.JDERMSCI.2016.11.010.

324.   Salminen, A.; Kaarniranta, K.; Kauppinen, A. Photoaging: UV Radiation-Induced Inflammation and Immunosuppression Accelerate the Aging Process in the Skin. *Inflammation Research 2022 71:7* **2022**, *71*, 817–831, doi:10.1007/S00011-022-01598-8.

325.   Kim, K.; Park, H.; Lim, K.M. Phototoxicity: Its Mechanism and Animal Alternative Test Methods. *Toxicol Res* **2015**, *31*, 97, doi:10.5487/TR.2015.31.2.097.

326.   Honzel, D.; Carter, S.G.; Redman, K.A.; Schauss, A.G.; Endres, J.R.; Jensen, G.S. Live Cell Assays for the Assessment of Antioxidant Activities of Plant Extracts. *Antioxidants 2021, Vol. 10, Page 944* **2021**, *10*, 944, doi:10.3390/ANTIOX10060944.

327.   Correa, V.G.; Garcia-Manieri, J.A.A.; Silva, A.R.; Backes, E.; Corrêa, R.C.G.; Barros, L.; Bracht, A.; Peralta, R.M. Exploring the α-Amylase-Inhibitory Properties of Tannin-Rich Extracts of Cytinus Hypocistis on Starch Digestion. *Food Research International* **2023**, *173*, 113260, doi:10.1016/J.FOODRES.2023.113260.

328.   Silva, A.R.; Ayuso, M.; Pereira, C.; Dias, M.I.; Kostić, M.; Calhelha, R.C.; Soković, M.; García, P.A.; Ferreira, I.C.F.R.; Barros, L. Evaluation of Parasite and Host Phenolic Composition and Bioactivities – The Practical Case of Cytinus Hypocistis (L.) L. and Halimium Lasianthum (Lam.) Greuter. *Ind Crops Prod* **2022**, *176*, 114343, doi:10.1016/J.INDCROP.2021.114343.

329.   Lin, T. chen; Nonaka, G. ichiro; Nishioka, I.; Ho, F. chi Tannins and Related Compounds. CII. : Structures of Terchebulin, an Ellagitannin Having a Novel Tetraphenylcarboxylic Acid(Terchebulic Acid)Moiety, and Biogenetically Related Tannins from Terminalia Chebula RETZ. *Chem Pharm Bull (Tokyo)* **1990**, *38*, 3004–3008, doi:10.1248/CPB.38.3004.

330.   Tanaka, T.; Nonaka, G.I.; Nishioka, I. Tannins and Related Compounds. XLII. : Isolation and Characterization of Four New Hydrolyzable Tannins, Terflavins A and B, Tergallagin and Tercatain from the Leaves of Terminalia Catappa L. *Chem Pharm Bull (Tokyo)* **1986**, *34*, 1039–1049, doi:10.1248/CPB.34.1039.

331.   Okuda, T.; Yoshida, T.; Ashida, M.; Yazaki, K. Tannis of Casuarina and Stachyurus Species. Part 1. Structures of Pendunculagin, Casuarictin, Strictinin, Casuarinin, Casuariin, and Stachyurin. *J Chem Soc Perkin 1* **1983**, *0*, 1765–1772, doi:10.1039/P19830001765.

332.   Feldman, K.S.; Sahasrabudhe, K. Ellagitannin Chemistry. Syntheses of Tellimagrandin II and a Dehydrodigalloyl Ether-Containing Dimeric Gallotannin Analogue of Coriariin A. *J Org Chem* **1999**, *64*, 209–216, doi:10.1021/jo9816966.

333.   Okuda, T.; Yoshida, T.; Kuwahara, M.; Memon, U.; Shingu, T. Tannins of Rosaceous Medicinal Plants. I. Structures of Potentillin, Agrimonic Acids A and B, and Agrimoniin, a Dimeric Ellagitannin. *Chem Pharm Bull (Tokyo)* **1984**, *32*, 2165–2173, doi:10.1248/CPB.32.2165.

334.   Tamura, S.; Yang, G.M.; Yasueda, N.; Matsuura, Y.; Komoda, Y.; Murakami, N. Tellimagrandin I, HCV Invasion Inhibitor from Rosae Rugosae Flos. *Bioorg Med Chem Lett* **2010**, *20*, 1598–1600, doi:10.1016/J.BMCL.2010.01.084.

335.   Okuda, T.; Yoshida, T.; Kuwahara, M.; Memon, M.U.; Shingu, T. Agrimoniin and Potentillin, an Ellagitannin Dimer and Monomer Having an α-Glucose Core. *J Chem Soc Chem Commun* **1982**, 163–164, doi:10.1039/C39820000163.

336.   Nonaka, G. ichiro; Ishimatsu, M.; Ageta, M.; Nishioka, I. Tannins and Related Compounds. LXXVI. : Isolation and Characterization of Cercidinins A and B and Cuspinin, Unusual 2, 3-(R)-

Hexahydroxydiphenoyl Glucoses from Cercidiphyllum Japonicum and Castanopsis Cuspidata Var. Sieboldii. *Chem Pharm Bull (Tokyo)* **1989**, *37*, 50–53, doi:10.1248/CPB.37.50.

337.   Yamaguchi, S.; Hirokane, T.; Yoshida, T.; Tanaka, T.; Hatano, T.; Ito, H.; Nonaka, G.I.; Yamada, H. Roxbin B Is Cuspinin: Structural Revision and Total Synthesis. *Journal of Organic Chemistry* **2013**, *78*, 5410–5417, doi:10.1021/JO400562K/SUPPL_FILE/JO400562K_SI_001.PDF.

338.   Immel, S.; Khanbabaee, K. Atropdiastereoisomers of Ellagitannin Model Compounds: Configuration, Conformation, and Relative Stability of d-Glucose Diphenoyl Derivatives. *Tetrahedron Asymmetry* **2000**, *11*, 2495–2507, doi:10.1016/S0957-4166(00)00179-8.

339.   Hrenn, A.; Steinbrecher, T.; Labahn, A.; Schwager, J.; Schempp, C.M.; Merfort, I. Plant Phenolics Inhibit Neutrophil Elastase. *Planta Med* **2006**, *72*, 1127–1131, doi:10.1055/S-2006-946700/ID/2/BIB.

340.   Ebrahim, H.Y.; Mady, M.S.; Atya, H.B.; Ali, S.A.; Elsayed, H.E.; Moharram, F.A. Melaleuca Rugulosa (Link) Craven Tannins: Appraisal of Anti-Inflammatory, Radical Scavenging Activities, and Molecular Modeling Studies. *J Ethnopharmacol* **2022**, *298*, 115596, doi:10.1016/J.JEP.2022.115596.

341.   Yin, J.; Kim, H.H.; Hwang, I.H.; Kim, D.H.; Lee, M.W. Anti-Inflammatory Effects of Phenolic Compounds Isolated from Quercus Mongolica Fisch. Ex Ledeb. on UVB-Irradiated Human Skin Cells. *Molecules 2019, Vol. 24, Page 3094* **2019**, *24*, 3094, doi:10.3390/MOLECULES24173094.

342.   Afaq, F.; Mukhtar, H. Botanical Antioxidants in the Prevention of Photocarcinogenesis and Photoaging. *Exp Dermatol* **2006**, *15*, 678–684, doi:10.1111/J.1600-0625.2006.00466.X.

SUPPLEMENTARY MATERIAL

Table S5.1. Optimal processing conditions that maximize the HAE and UAE extraction of tannins from *C. hypocistis*, model-predicted and experimental response values.

	OPTIMAL HAE CONDITIONS			**OPTIMUM RESPONSE**	
	t (min)	*T* (°C)	*S* (ethanol %, *v/v*)	Model-predicted	Experimental
For each response variable					
Y_1	27.3	45.5	0.0	67±1% (*w/w*)	-
Y_2	104.0	51.3	65.9	36.4±0.9 mg/g E	-
Y_3	79.0	83.0	69.9	39.5±0.9 mg/g E	-
Y_4	62.5	48.7	83.7	76±1 mg/g E	-
Y_5	57.8	60.0	95.9	30.9±0.8 mg/g E	-
Y_6	89.9	50.7	96.1	40±1 mg/g E	-
Y_7	29.3	44.1	82.5	27.3±0.6 mg/g E	-
Y_8	70.8	48.0	85.4	16.6±0.6 mg/g E	-
Y_9	65.7	52.1	98.8	245±3 mg/g E	-
Considering all response variables					
Y_1				53±1% (*w/w*)	54±1% (*w/w*)[*]
Y_2				29.5±0.7 mg/g E	11.4±0.5 mg/g E
Y_3				26.4±0.7 mg/g E	24±1 mg/g E[*]
Y_4				60±1 mg/g E	65±7 mg/g E[*]
Y_5	95.1	46.4	74.3	24.0±0.4 mg/g E	41±2 mg/g E
Y_6				29.5±0.9 mg/g E	24.5±0.6 mg/g E[*]
Y_7				19±0.4 mg/g E	27.4±0.6 mg/g E
Y_8				13.2±0.4 mg/g E	8.5±0.4 mg/g E
Y_9				203±3 mg/g E	200±4 mg/g E[*]
	OPTIMAL UAE CONDITIONS			**OPTIMUM RESPONSE**	
	t (min)	*P* (W)	*S* (ethanol %, *v/v*)	Model-predicted	Experimental
For each response variable					
Y_1	28.4	456.0	22.7	69±1% (*w/w*)	-
Y_2	9.3	217.8	71.1	27.8±0.4 mg/g E	-
Y_3	17.4	289.1	64.4	26.9±0.5 mg/g E	-
Y_4	19.8	274.9	76.2	48.0±0.5 mg/g E	-
Y_5	15.7	240.2	70.9	21.1±0.4 mg/g E	-
Y_6	19.1	184.8	76.0	26.7±0.5 mg/g E	-
Y_7	18.3	231.4	74.2	16.6±0.3 mg/g E	-
Y_8	18.8	208.6	77.0	10.9±0.2 mg/g E	-
Y_9	19.5	405.1	72.4	176±2 mg/g E	-
Considering all response variables					
Y_1				53±1% (*w/w*)	52±2% (*w/w*)[*]
Y_2				26.5±0.5 mg/g E	11.0±0.5 mg/g E
Y_3				24.9±0.8 mg/g E	21.8±0.4 mg/g E[*]
Y_4				46±1 mg/g E	60±3 mg/g E
Y_5	18.7	327.4	69.3	21.2±0.8 mg/g E	36±2 mg/g E
Y_6				23.5±0.6 mg/g E	17.1±0.8 mg/g E
Y_7				15.6±0.4 mg/g E	25±1 mg/g E
Y_8				9.9±0.3 mg/g E	8.2±0.4 mg/g E[*]
Y_9				173±2 mg/g E	178±8 mg/g E[*]

Response variables: Y_1: extraction yield (extract weight); Y_2: tetragalloyl-glucoside II; Y_3: tetragalloyl-glucoside III; Y_4: pentagalloyl-glucoside; Y_5: galloyl-bis-HHDP-glucose II; Y_6: digalloyl-bis-HHDP-glucose II; Y_7: trigalloyl-bis-HHDP-glucose I; Y_8: trigalloyl-bis-HHDP-glucose II; and Y_9: total tannins. [*]Good agreement between experimental and model-predicted values.

S6.1. Crude extracts, fractions, and subfractions preparation

Plant extraction was conducted as described in a previous publication [314] to maximise the following conditions: **(C₁)** extraction yield (extract dry weight, %, w/w); **(C₂)** mg of tannins (total) per g of extract; and **(C₃)** optimum response considering conditions C_1 and C_2. Samples (1g) from the three years were mixed with a hydroethanolic solution (*v/v*) and extracted in an ice bath: **(C₁)** 22.7% (*v/v*) for 28.4 minutes at 456.0 W.; **(C₂)** 72.4% (*v/v*) for 19.5 minutes at 327.4 W; and **(C₃)** 69.3% (*v/v*) for 18.7 minutes at 327.4 W. All extracts were lyophilised and stored at room temperature before use. The dried extracts were redissolved in a 20% (*v/v*) hydroethanolic solution and centrifuged; the resulting supernatants were utilised for further experiments.

Fractionation of the hydroethanolic extracts exhibiting the best (extracts C_1, C_2, and C_3 from the 1st year) and worst (extract C_3 from the 2nd year) anti-elastase activity was performed using an HP20 reverse-phase column. Portions of the extracts (2 g) were loaded onto the top of the adsorbent bed (250 g) in an open glass column (30 cm × 3 cm). The samples were eluted with a mobile phase (5500 mL) and collected in 500 mL fractions as follows: 100% dH2O; 90:10; 80:20; 70:30; 60:40; 50:50; 40:60; 30:70; 20:80; 10:90; 100% EtOH, resulting in 11×500 mL for each extract. Each fraction was individually concentrated using a rotary evaporator and freeze-dried using an Epsilon 2-4 LSCplus freeze dryer. The dried powder was dissolved in a 20% (v/v) hydroethanolic solution at a final concentration of 1 mg/mL, centrifuged, and the resulting supernatant was utilised for further experiments.

Fraction 19 (year 1; extraction condition C_2), collected at 50:50 dH2O:EtOH, was chosen for further purification using medium-pressure liquid chromatography (MPLC). A portion of Fraction 19 (100 mg) was reconstituted in 2 mL of 20% MeOH and centrifuged. The supernatant was packed into an empty dry loader cartridge (Alltech, Carnforth, UK) to be transferred to a Grace Davison Reveleris® flash chromatography system (Alltech, Carnforth, UK) equipped with a dual-UV wavelength detector that was set at 254 and 280nm, an ELSD, and an automatic fraction collector. The flow rate was set at 12mL/min in isocratic conditions with 75:15 HCOOH:MeOH for 5 min, then increasing to 100%

MeOH over 50 min and holding for 5 min. This process yielded subfractions F19.1 (9 mg) and F19.9 (45 mg); F19.1 was obtained as a fine dark powder, while F19.9 was a fine yellow powder.

S6.2. Cell lines and culture conditions

Human foreskin fibroblasts (HFF-1; SCRC-1041) and mouse embryonic fibroblasts (BALB/3T3 clone A31; CCL-163) were purchased from ATCC (Manassas, VA, USA). The human immortalised non-tumorigenic keratinocyte cell line (HaCaT; number: 300493) was acquired from CLS Cell Lines Service (Germany). HFF-1, BALB/3T3, and HaCaT cell lines were grown in Dulbecco's modified Eagle's medium (DMEM; ATCC; 30-2002) supplemented with 10% calf bovine serum iron-fortified (ATCC-30-2030), 2mM L-glutamine (ATCC-30-2214), and a Penicillin-Streptomycin-Amphotericin B solution (100 U/mL penicillin and 100 μg/mL streptomycin, and 0.25 μg/mL amphotericin B; (ATCC-PCS-999-002). All cells were maintained in T75 flasks (5% CO_2; 37 °C) and routinely passaged at 80–90% confluence using trypsin (Gibco; 25200-056). Cells were passaged every three days with a maximal passage number of 27. Cell viability was assessed using the trypan blue dye (Gibco; 15250061) exclusion assay.

Table S6.1. Cytotoxic, phototoxic, antioxidant, and enzyme inhibitory properties of *C. hypocistis* optimum extracts.

	Year 1			Year 2			Year 3		
	C_1	C_2	C_3	C_1	C_2	C_3	C_1	C_2	C_3
	Cytotoxic activity (IC$_{50}$, µg/mL)								
HaCaT	265.8 ± 8.3	250.1 ± 4.9	317.2 ± 11.5	317 ± 8	306.2 ± 9.6	309.4 ± 11.9	332 ± 12	322.8 ± 13.2	289.4 ± 11.8
HFF-1	>400	>400	>400	>400	337.3 ± 17.2	>400	282 ± 5	242.4 ± 7.5	258.1 ± 10.6
BALB/3T3	3T3 Neutral Red Uptake (NRU) phototoxicity activity								
PIF	1.0	1.5	1.0	1.4	1.0	0.8	1.7	1.6	1.4
MPE	0.04	0.13	0.11	0.01	0.03	0.05	-0.08	0.10	0.01
	Cellular antioxidant activity (IC$_{50}$, µg/mL)								
HaCaT	43.5 ± 4.3	29.0 ± 2.8	20.8 ± 1.2	30.9 ± 2.3	32.7 ± 4.0	33.3 ± 5.7	46.7 ± 3.6	21.8 ± 1.5	21.5 ± 1.3
HFF-1	53.5 ± 4.1	28.2 ± 4.9	38.5 ± 3.7	36.1 ± 5.8	25.7 ± 3.7	23.9 ± 2.8	33.2 ± 3.5	23.7 ± 3.0	22.8 ± 4.4
Bacterial collagenase	Anti-collagenase activity (IC$_{50}$, µg/mL)								
	48.2 ± 3.7	28.7 ± 2.9	33.7 ± 4.2	18.4 ± 2.6	12.4 ± 1.5	11.1 ± 0.6	29.5 ± 2.0	13.0 ± 0.7	10.5 ± 0.6
Human elastase	Anti-elastase activity (IC$_{50}$, µg/mL)								
	13.2 ± 2.4	16.5 ± 1.0	21.6 ± 1.0	128.2 ± 3.5	119.7 ± 2.3	128.2 ± 6.8	102.8 ± 4.6	74.3 ± 3.5	109.1 ± 4.7
Human tyrosinase	Anti-tyrosinase activity (IC$_{50}$, µg/mL)								
	11.4 ± 0.1	33.3 ± 0.1	10.2 ± 0.1	15.9 ± 0.1	42.7 ± 0.1	19.6 ± 0.1	36.0 ± 0.1	26.4 ± 0.1	22.8 ± 0.1

HaCaT: human immortalised non-tumorigenic keratinocytes; **HFF-1**: human foreskin fibroblasts; **BALB/3T3**: mouse embryonic fibroblasts; **Extraction conditions** - **C_1**: 22.7% (v/v) for 28.4 minutes at 456.0 W; **C_2**: 72.4% (v/v) for 19.5 minutes at 327.4 W **C_3**: 69.3% (v/v) for 18.7 minutes at 327.4 W; **PIF**: photo irritation factor; **MPE**: mean photo effect; **Non-phototoxicity** (PIF < 2 or MPE < 0.1); **Equivocal phototoxicity** (2 < PIF < 5 or 0.1 < MPE < 0.15); **Phototoxicity** (PIF > 5 or MPE > 0.15). Except for the phototoxic activity presented in terms of PIF and MPE values, the remaining results are shown as IC$_{50}$ mean ± SD.

Table S6.2. Elastase inhibition (%) for the forty-four fractions obtained after fractionation.

Fractions	% Inhibition	SD
1	83,47	1,01
2	86,58	0,79
3	87,69	0,42
4	94,86	0,17
5	96,43	0,49
6	97,36	0,03
7	96,66	0,35
8	91,26	0,13
9	89,80	0,32
10	89,58	0,42
11	82,36	0,94
14	91,02	0,26
15	90,72	0,07
16	92,58	0,26
17	92,51	0,29
18	96,40	0,26
19	97,05	0,19
20	97,26	0,34
21	95,05	0,66
22	85,98	0,44
23	89,84	0,19
24	85,39	0,28
25	90,23	0,20
26	90,92	0,07
27	91,90	0,28
28	92,08	0,42
29	95,70	0,36
30	97,03	0,04
31	96,31	0,24
32	95,45	0,11
33	95,26	0,57
34	90,22	0,13
35	84,00	0,49
60	90,32	0,55
61	89,77	0,11
62	89,34	0,24
63	87,50	0,28
64	87,73	0,98
65	92,00	0,30
66	92,23	0,18
67	88,68	0,26
68	90,53	0,15
69	88,73	0,11
70	86,76	2,87

Fractions in grey: Fractions with elastase inhibition superior to 96%.